Stability of slope material affected by bow thrusters at open quay structures

F.P. Roelse

Master of Science Thesis
March 2014

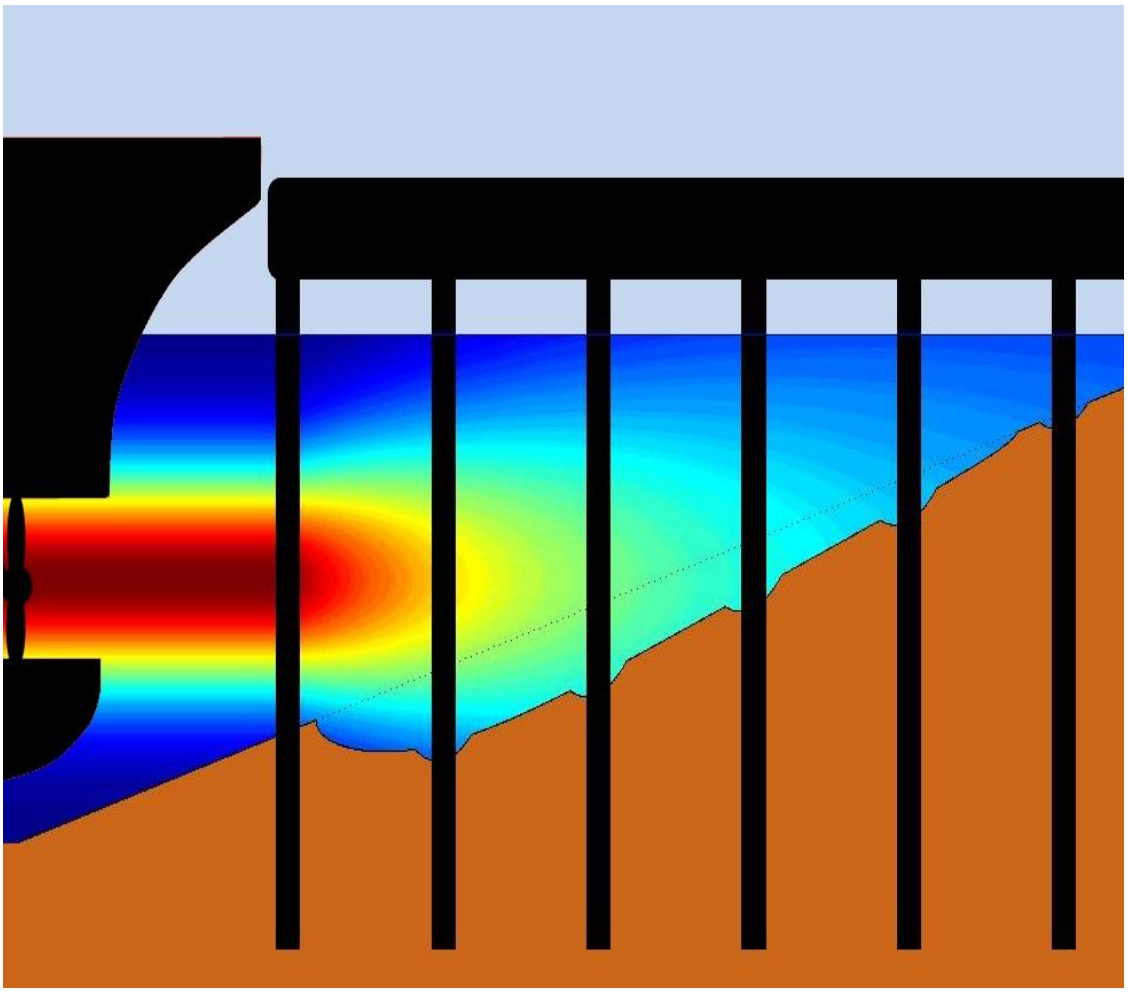

TU Delft Delft University of Technology

Challenge the future

Stability of slope material affected by bow thrusters at open quay structures

By

F.P. Roelse

in partial fulfilment of the requirements for the degree of

Master of Science
in Hydraulic Engineering

at the Delft University of Technology,
to be defended publicly on Wednesday March 5, 2014.

Supervisor:	Prof. ir. T. Vellinga	TU Delft
Thesis committee:	Ir. H.J. Verhagen	TU Delft
	Ir. H.J. Verheij	TU Delft
	Ir. T. Blokland	Municipality of Rotterdam
	Ir. M.G.A. van den Elzen	Grontmij NV

TU Delft Delft University of Technology

Grontmij

Executive summary

In the last decades shipping has increased significantly, resulting in larger ships with an increasing power in bow thrusters. Due to this increasing power, the hydraulic loads at bottom protection near quay structures has also increased, making a traditional bed protection more expensive. Therefore an alternative design method is suggested in which the bottom is not fully protected. As a result, scour could occur. The designer of the super structure should adapt his design on this scour. Consequently the total structure (bed protection and superstructure) could be designed more cost effective compared with the current design method of full bed protection. However, at this moment a method to predict scour at a sloping bed with piles affected by a bow thruster is not available, so it is impossible to apply the alternative design method. The objective of this master thesis is to set up a method to predict the equilibrium scour depth.

In order to set up such a prediction method, a literature study was conducted. This literature study focused on the available knowledge of bow thruster induced currents and the effect of these currents on the instability and erosion of the bed material. The stability and mobility of the bed material depend on the ratio between flow forcing (flow velocities and turbulences) and the bed strength (particle size and density). When this ratio exceeds a critical value the bed is not stable anymore and transport will occur, leading to scour holes.

Not only the thruster jet itself could induce scour formation, also the presence of a pile at the slope could lead to additional scouring. This is caused by the fact that a pile in a flow field causes differences in the flow field (local higher velocities and turbulence intensities). Consequently, extra scour is induced. This scour mechanism is called the pile obstruction mechanism.

The total proposed equation consists of both the pile obstruction mechanism and the jet diffusion mechanism. The equation is validated for a horizontal bed. Due to absence of data for the sloping bed case the equation is not validated for the case of a slope yet. It is recommended to validate the proposed equation for the case of a slope with piles by conducting lab experiments.

Acknowledgements

This report is the results of a research focused on scour at open quay structures for my Master of Science thesis research at the TU Delft. The study was conducted in corporation with NV Grontmij. Existing data gathered by lab experiments were used. The report provides a method to predict the equilibrium scour at an open quay structure with piles. However, the method is not validated yet, so it can only be used as rough estimation instrument.

I would like to thank a number of people who have helped me during this research. First of all I would like to thank the members of the graduation committee; prof. ir. T. Vellinga, ir. H.J. Verhagen, ir. H.J. Verheij, ir. M.G.A. van den Elzen and ir. T. Blokland for their feedback during this research.

Especially, I would like to thank Martijn van den Elzen and Henk Verheij for their frequent guidance during the project. As my daily supervisors, they were willing to help me any time.

At last I would like to thank my colleagues of Grontmij Rotterdam and Grontmij De Bilt for their help, their support and the pleasant cooperation.

Delft, March 2014
Frank Roelse

Content

1 Introduction

In the last decades shipping has changed significantly. The capacity of vessels has increased, resulting in more powerful main propulsion systems and bow thrusters. Consequently, the hydraulic loads on quay structures have increased as well. Open and closed quay structures are built in ports. An example of an open quay structure with piles is presented in Figure 1-1.

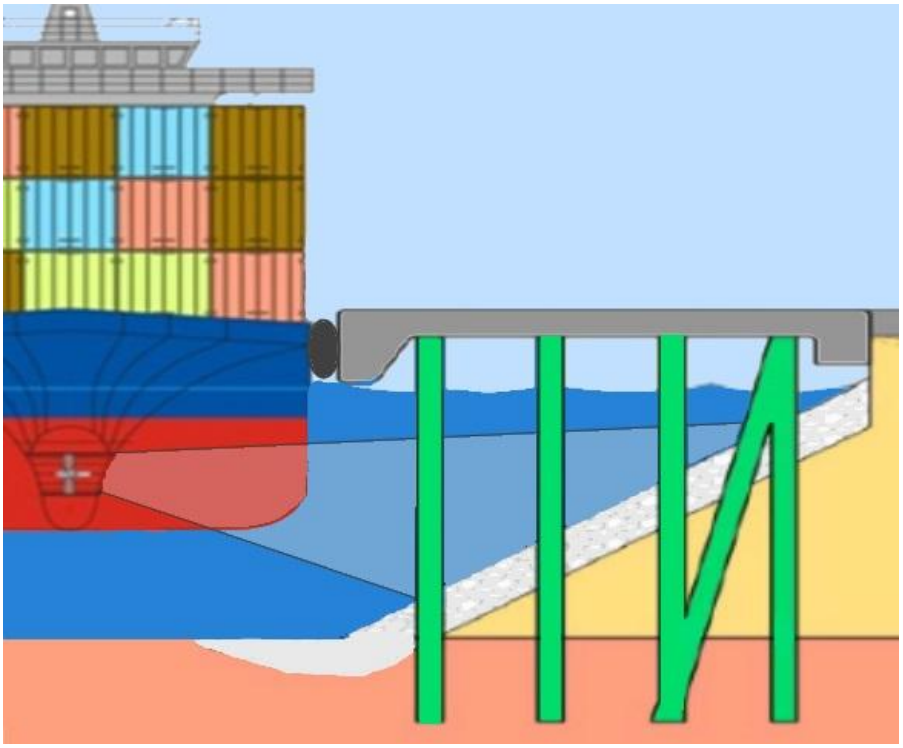

Figure 1-1: schematic overview of an open quay structure

1.1 Problem definition

In practice the slope at an open quay structure is protected against the high hydraulic loads induced by a bow thruster. In (PIANC, 1997) a practical but inaccurate method is described in order to determine the required stone size for a stable slope. An alternative design method is to allow scour, thereby eliminating a costly slope protection. When taking into account the predicted scour during the design phase, the designer could adapt the dimensions of the superstructure in order to ensure a stable design. However, at the moment a reliable method to predict the maximum scour depth is not available. In (PIANC, 2013) a conceptual method is described to estimate scour, but this method is not tested yet. The aim of this master thesis is to set up a design method to predict the maximum scour depth at an open quay structure, in order to help designers to find the most cost effectively design.

1.2 Objective

The objective of this master thesis is to develop a method to predict the equilibrium scour depth. The main research question of the thesis is:

How big is the erosion that occurs on an unprotected or inadequately protected slope with piles due to the hydraulic load of a thruster?

In order to examine the erosion at the slope, it is necessary to determine the hydraulic loads at the slope. Therefore, the following sub question is formulated:

How large are the hydraulic loads induced by a bow thruster on a slope with piles?

When the methods to describe the hydraulic loads are determined, the following question needs to be answered:

How do hydraulic loads induced by a bow thruster current cause scour?

1.3 Background

In (PIANC, 1997) a design guideline is described for an open quay structure. This guideline gives a practical but rather rough method for the determination stone size on slopes under attack of propeller induced currents. However, problems have been encountered with this method because of the increased use and power of the thrusters.

Van Doorn (2012) did his master thesis research about the thruster induced current on a fixed slope with and without piles. Van Doorn (2012) concluded that the hydraulic loads are underestimated based on the current guidelines. The method to define the hydraulic loads at the slope, as described by (Van Doorn, 2012), is used in this thesis.

Chin (1996) conducted research focused on scour at a horizontal sand bed with a pile affected by a jet current. In this research a distinction is made between jet diffusion scour and pile obstruction scour. The jet was located near the bottom of the bed, which caused mainly scour by the jet diffusion mechanism. Other studies are conducted with (propeller) offset jets at a horizontal bed without piles, these studies are be used to examine the jet diffusion mechanism. For the pile obstruction mechanism, methods are developed to predict the scour around a pile on a horizontal bed for uniform flow conditions. These methods are described in (FHWA, 2001) and (Hoffmans *et al.,* 1997).

1.4 Boundary conditions

This thesis does only use ducted bow thruster systems, pump jets are not part of this thesis. Flow field characteristics do change for a free propeller jet compared to a ducted propeller jet, however these changes are not significant. Therefore the method as described in this thesis could also provide a prediction for a free propeller, for example ship main propeller. The method is described for non-cohesive soil types within the sand and gravel range. Other boundary conditions for the new proposed equation are described in chapter 7. Most of these boundary conditions and assumptions are not validated yet, therefore it is recommended to validate the newly proposed equation by conducting lab tests.

2 Literature review

The literature review is divided in different parts. First some general knowledge about bow thrusters and the flow field is described, followed by an overview of bed particle stability and transport. The literature review ends with the present knowledge about scour, this part is described extensively because it is the main topic of this master thesis. Based on the theories as described in the literature review a new scour prediction equation is proposed (chapter 3).

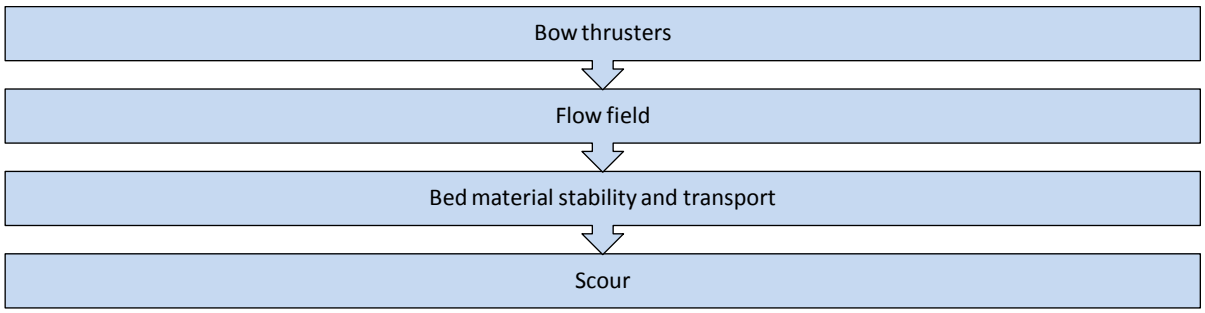

2.1 Bow Thrusters

The most commonly used bow thruster is a propeller. A propeller is characterized by the number of blades (4 or 5 usually), the external diameter, the angel of the blades and the power and thrust delivered at standard regime, the speed and direction of rotation (PIANC, 2013). Propellers are classified into 2 groups: Wageningen B- and K-series, in which the former is non-ducted and the K-series (Kaplan series) is ducted. Ducted propellers are mounted in a tunnel (Figure 2-1), which is usually the case for bow thrusters. These transverse ducted bow thrusters are located near the bow of the ship, placed in single or twin units. In this thesis, research is done into bow thrusters, therefore in the calculations ducted propellers are used. However the calculations for ducted and non-ducted propellers are quite similar. Besides ducted propeller driven bow thrusters, also other types of thrusters exist like pump jets or retractable 360 degree turnable propellers. These types of thrusters are sometimes placed in inland vessels. For sea going vessels, the standard type of bow thruster is the ducted thruster.

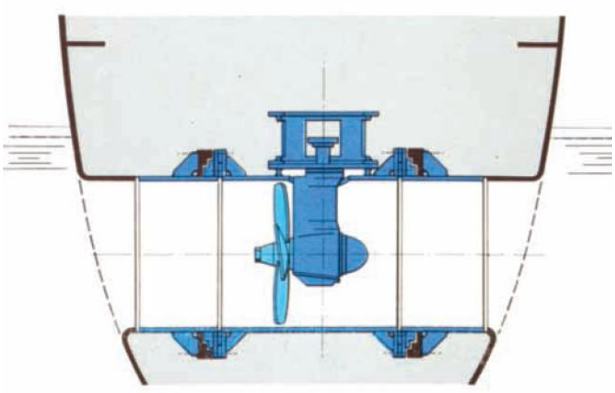

Figure 2-1: Scheme of a tunnel thruster PIANC (2013)

Designers of (open) quay structures need details of the vessels likely to use the facilities, in order to be able to make a design. But it is not always possible to find the significant information about the bow thruster installed in the vessels. Information like propeller diameter, installed power, propeller thrust coefficient and number of revolutions are not always known. However the dimensions of the

vessel are often known. In (Roubos, 2006) and Sievers (referenced in (PIANC, 2013)) data is collected for container vessels in respectively the Rotterdam harbor, the Bremerhaven and Hamburg harbor. For these data relationships are derived between the installed thruster power and the ship's beam, and between the thruster diameter and the ship's beam (PIANC, 2013):

$$P_{thruster} = 87.5 \cdot B_s - 1350 \tag{2.1}$$

$$D_{thruster} = 0.05 \cdot B_s + 0.5 \tag{2.2}$$

Where:

B_s	Ship's beam	[m]
$D_{thruster}$	Bow thruster diameter	[m]
$P_{thruster}$	Bow thruster power	[kW]

Remark: The total installed bow thruster power is calculated, which means that in the case of two thrusters the installed power should be equally divided.

Also for inland shipping similar relations are given by (Verheij, 2010):

$$\begin{gathered} P_{thruster,container} = 2.0 \cdot L_S \cdot T_S - 250 \\ P_{thruster,generalcargo} = 1.75 \cdot L_S \cdot T_S - 150 \\ P_{thruster,tanker} = 0.8 \cdot L_S \cdot T_S + 100 \\ P_{thruster,passengers} = 275 \end{gathered} \tag{2.3}$$

Where:

L_S	Length of the ship	[m]
T_S	Draught of the ship	[m]

According to (Verheij, 2010) an empirical relation between propeller diameter and installed power, for both main propellers and thrusters is given by:

$$D_P = 0.1636 \cdot P^{0.3656} \tag{2.4}$$

For the design of a quay structure, the distance between the thruster and the quay wall or slope is relevant, because the hydraulic forces at the slope depend on this distance. In case of most seagoing container ships the beam of the ship at the bow is less than the maximum beam, therefore the distance between the outflow of a bow thruster is considerable larger compared to the small distance between the amidship section and the quay face (Figure 2-2). In case of inland shipping this difference in distance is not so large. In (Roubos, 2006) it was concluded that for sea going container vessels the outflow point of the duct is typically at a distance $x_{thruster}$ of the quay wall:

$$x_{thruster} \approx 0.5 \cdot B_s \tag{2.5}$$

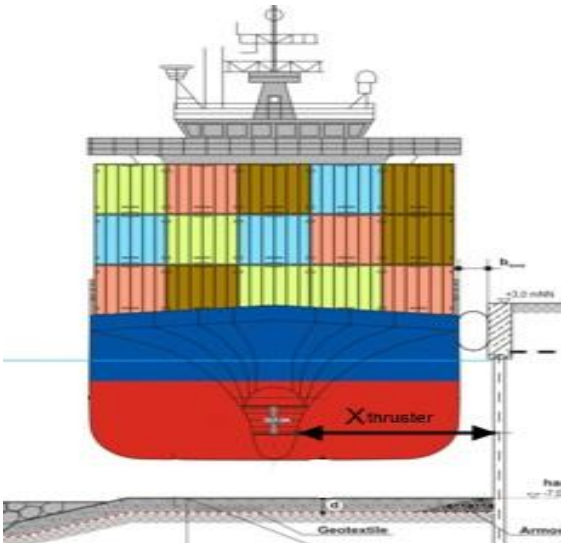

Figure 2-2: Container vessel moored alongside a quay wall with a protected bottom (PIANC(2013))

2.2 Thruster-induced flow field

Many theories have been established to determine the velocity field behind a propeller, the most well known researches are done by (Blaauw & Van de Kaa, 1978), (Verheij, 1985) and (Fuehrer *et al.,* 1977). The propeller jet can be characterized by quantities such as efflux velocity, decay of the maximum axial velocity and the flow field distribution. Most of these theories focus on the average velocities and do not take into account turbulent fluctuations (Van Doorn, 2012). In (PIANC, 2013) two methods are described to calculate the flow field; the Dutch method, based on (Blaauw & Van de Kaa, 1978) and the German method, based on (Fuehrer *et al.,* 1977). When using one of these methods, it is recommended to use this method for the entire calculation, because when mixing the two methods it may result in inaccuracies.

2.2.1 Efflux velocity

The efflux velocity (U_0) is regarded as the mean axial flow velocity just behind the propeller, it can derived by using the axial momentum theory by: (Albertson *et al.,* 1948)

$$U_0 \approx 1.60 \cdot n_p \cdot D_p \cdot \sqrt{K_t} \tag{2.6}$$

Where K_t is the thrust coefficient and n_p is the rotational speed of the propeller. In case the values of K_t or n_p are not known, (Verheij, 1985) gives a method to predict the efflux velocity based on the installed engine power:

$$U_0 \approx 1.15 \cdot \left(\frac{f_p \cdot P}{\rho_w \cdot D_0^2}\right)^{\frac{1}{3}} \tag{2.7}$$

For ducted propellers:
$D_0 \approx 0.85 \cdot D_p$

Where:

ρ_w	Water Density	[kg/m^3]
D_p	Propeller diameter	[m]
f_p	Used percentage of installed engine power	[-]

P	Engine power	[W]

According to (Blaauw & Van de Kaa, 1978) the coefficient of 1.15 in equation 2.7 should be 1.17, however in this thesis 1.15 is applied.

2.2.2 Axial flow velocity

For the calculation of the axial flow velocity two sections are distinguished; the zone of flow establishment and the zone of established flow (Figure 2-3). In the zone of flow establishment the jet is not yet fully developed, the influence of the outer part of the propeller is not yet noticed along the x-axis. As soon as it is the zone of established flow is reached. For propeller jets, this transition is commonly at a distance of around three times the propeller diameter behind the propeller.

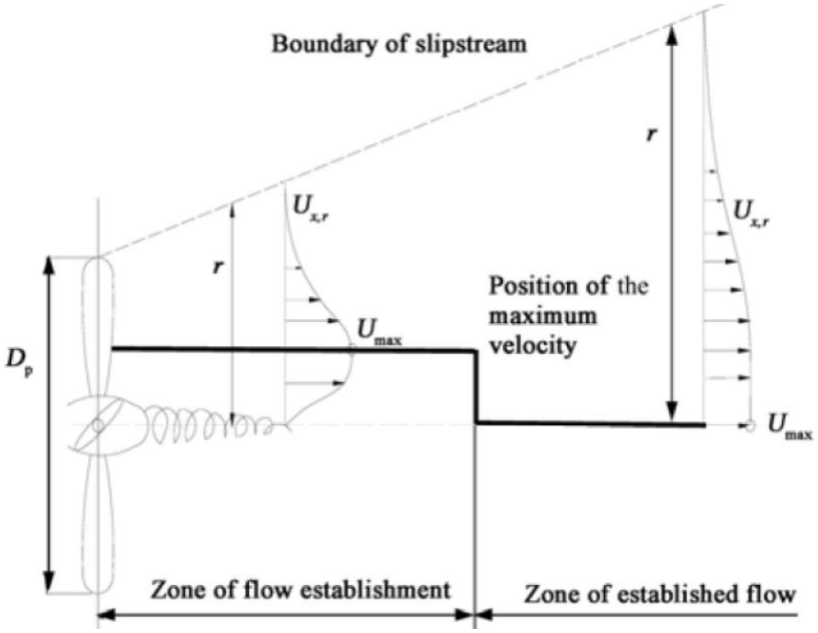

Figure 2-3: Schematic representation of the zone of flow establishment and the zone of established flow (Van Doorn, 2012)

The maximum axial velocity is assumed to be constant in the zone of flow establishment according to (Albertson *et al.,* 1948). In the established flow zone the maximum axial velocity ($U_{x,max}$) decays, the velocities in the centre line are given by:

$$U_{x,max} = U_0 \cdot \frac{1}{2 \cdot C_2} \cdot \left(\frac{x}{D_0}\right)^{-1} \tag{2.8}$$

According to the German method, described in (Römisch K. , 2006), the maximum axis velocity for a non restricted thruster is given by:

$$U_{x,max} = 1.9 \cdot U_0 \cdot \left(\frac{x}{D_p}\right)^{-1.0} \tag{2.9}$$

For $\frac{x}{D_p} > 1.9$.

In case of a flow field restricted by a water level and a bed. The exponent in equation 2.9 changes into -0.6. There is no clear upper boundary for $\frac{x}{D_p}$ given for this method.

For a ducted propeller near a slope (1:3) in the established zone, (Römisch K. , 2006) gives the following axial velocity for $\frac{x}{D_p} > 6$ with an unknown upper boundary for $\frac{x}{D_p}$:

$$U_{x,max} = 2.3 \cdot U_0 \cdot \left(\frac{x}{D_p}\right)^{-0.825} \tag{2.10}$$

According to the Dutch method, (Blaauw & Van de Kaa, 1978) gives the following equation for the maximum velocity in the established zone for a horizontal bed ($\frac{x}{D_p} > 2.8$):

$$U_{x,max} = 2.8 \cdot U_0 \cdot \left(\frac{x}{D_p}\right)^{-1.0} \tag{2.11}$$

More research is done into the decay of the axial flow velocity, but it is not described in this thesis. For more methods (Van Doorn, 2012) is recommended.

2.2.3 Flow distribution

Both the German and the Dutch methods use different flow distributions. In (PIANC, 2013) the following general equation is described to determine the flow velocities at a distance r from the propeller axis and a distance x from the propeller plain in the zone of established flow:

$$U_{x,r} = U_{x,max} \cdot \exp\left(-\frac{1}{2 \cdot C_2^2} \cdot \frac{r^2}{x^2}\right) \tag{2.12}$$

With $C_2 = 0.15$ for the German method (Fuehrer, Römisch, & Engelke, 1977) this results in:

$$U_{x,r} = U_{x,max} \cdot \exp\left[-22.2 \cdot \left(\frac{r}{x}\right)^2\right] \tag{2.13}$$

With $C_2 = 0.18$ for the Dutch method (Blaauw & Van de Kaa, 1978) this results in:

$$U_{x,r} = U_{x,max} \cdot \exp\left[-15.43 \cdot \left(\frac{r}{x}\right)^2\right] \tag{2.14}$$

Given this flow distribution, (Blaauw & Van de Kaa, 1978) calculated the maximum velocity at the horizontal bed ($U_{b,max}$). The derivation of this equation is described in appendix A. The bed velocity in the zone of established flow is:

$$U_{b,max} = f_p \cdot C_5 \cdot \frac{U_0 \cdot D_0}{h_{pb}} \tag{2.15}$$

If f_p=1:

$$U_{b,max} = 0.3 \cdot \frac{U_0 \cdot D_0}{h_{pb}}$$

Where h_{pb} is the distance between propeller axis and the bed.

The German approach gives the following maximum bottom velocity for a horizontal bottom for a main propulsion system (PIANC, 2013).

$$U_{b,max} = E \cdot U_0 \cdot \left(\frac{h_{pb}}{D_p}\right)^{-1.0} \tag{2.16}$$

With E is a coefficient for the type of propulsion system. E=0.71 for a seaborne vessel with a rudder, E=0.42 for a seaborne vessel without a rudder.

For the Dutch method an equation is derived to define the flow velocities just above a slope, this method is based on the velocity distribution as given in equation 2.14. The flow distribution at a slope is given by (Van Doorn, 2012):

$$U_{slope} = \mathrm{f} \cdot A \cdot \left(\frac{D_0}{L} \cdot \frac{L}{x_U}\right)^a \cdot U_0 \cdot \exp\left[-b \cdot \left(\frac{\frac{L}{x_U} - 1}{cot(\alpha)}\right)^2\right]$$

With:

$$\frac{x_{U,max}}{L} = K \cdot \left(\sqrt{1 + \frac{2}{K}} - 1\right) \tag{2.17}$$

And:

$K = \frac{b}{a \cdot (\cot(\alpha))^2}$, $A = 2.8$, $a = 1$ *and* $b = 15.43$

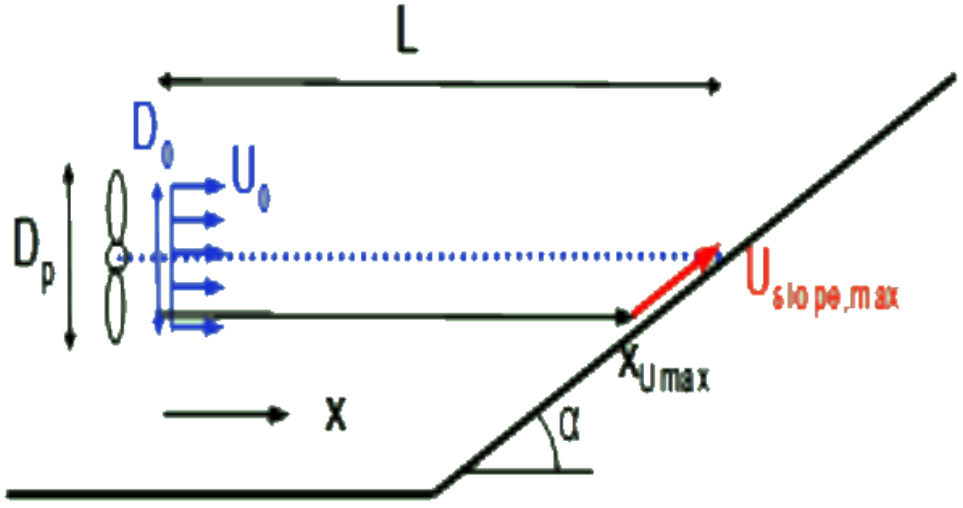

2-4: Schematization of the maximum slope velocity calculation (PIANC, 2013)

This equation is applicable over the entire range of slope angles (α). Therefore it can also be used to determine the bed velocities in case of a horizontal bottom, by assuming a very mild slope (for example 1:10[6]). In Appendix A it is proved that for a very mild slope the calculated maximum slope velocity by using equation 2.17 approaches the calculated maximum bed velocity as calculated by equation 2.15. It is recommended to use equation 2.17 for mild slopes instead of assuming a horizontal bed, because equation 2.17 converges relatively slow to equation 2.15 for decaying slope angles.

In equation 2.17 a correction factor (f) is present, this factor takes into account; the flow confinement, the rougheness of the slope and the presence of piles. Therefore different slope configurations will give different values for f.

In (Van Doorn, 2012) measurements are described of labtests with slopes 1:1.5 and 1:2.5 with different pile configurations and different roughnesses. From these measurements different values of f are derived, however due to errors in the calculations made by van Doorn, the f-values as given should not be used. In further calculations in this report the f-factor is disregarded, because of the unknown quantity. One should always keep in mind this will lead to some inaccuracies in the calculations.

2.2.4 Turbulence

According to (Schiereck G. , 2004) who refers to (Hinze, 1975) the definition of turbulence is: "*Turbulent fluid motion is an irregular motion, but statistically distinct average values can be discerned and can be described by laws of probability*." So the velocity can be written as an average velocity component and a fluctuation:

$$u = \bar{u} + u' \tag{2.18}$$

The intensity of turbulence is defined as the square root of the average of the fluctuations. Turbulence can be expressed in different ways. The relative fluctuation of intensities is a way to express turbulence, it is defined as:

$$r_u = \frac{\sqrt{\overline{u'^2}}}{\bar{u}} \tag{2.19}$$

According to (Verheij, 1985), flow turbulence for a propeller jet consists of a high frequency part and a low frequency part. The high frequency part is caused by the eddy flow and the low frequency is caused by the jet. The high frequency turbulence is damped out first, which results for some distance behind the propeller in a flow pattern where the low-frequent energy is dominating (Van Doorn, 2012). (Schokking, 2002) states that turbulence intensities are largely responsible for the movement of stones. The vortices that are most effective on bed material stability have a diameter of 1.5 respectively 2 times the diameter of the stone.

2.3 Bed material stability and transport

A bed stability assessment can be assessed in two different ways. Described in (Hoan, 2008), (Mosselman, 2000) distinguished two concepts for the assessment of stone stability:

- The stability threshold concept, based on the incipient motion of bed material.
- The stone transport concept, based on the bed load transport or bed material entrainment.

Most of the available stability formulae are based on the concept of incipient motion. A disadvantage of this method is that the threshold of motion is not very well defined. With a low velocity it is possible that a few stones move. When these stones have found a new position they will not move anymore. Therefore this cannot be seen as the threshold of motion for the entire bed. With a higher velocity at some locations stones will move, with an even higher velocity everywhere movement occurs. In the latter situation the system is beyond the threshold of motion, but it is unclear how the

threshold of motion is defined. The threshold of motion is therefore a subjective matter when judged in an experiment. In contrast with the threshold concept, the stability assessment method based on transport leads to a cause-and-effect relationship between flow parameters and bed material transport, and is therefore an objective way of stability assessment.

2.3.1 The stability threshold concept

In practice it is hard to indicate exactly how flow can induce grain movement. But based on the balance of forces on a grain a dimensionless relation between load and strength can be derived:

$$u_c^2 \propto \Delta g d \quad or \quad u_c^2 = K \Delta g d \tag{2.20}$$

Where:

u_c	Critical velocity	[m/s]
Δ	Relative density	[-]
g	Gravitational acceleration	[m/s^2]
d	Characteristic stone diameter (often d_{50} is used)	[m]
K	Constant	[-]

All formulae on grain stability are based on this proportionality. In case the critical value for incipient motion are calculated within this method, the stability of the bed is assessed and therefore the factor K is called the stability parameter. In case of forcing above the critical value, the bed material is not stable anymore. In that case the value of K is called the mobility parameter. There are numerous formulae but the most commonly used are Izbash (paragraph 2.3.1.1) and Shields (paragraph 2.3.1.3).

2.3.1.1 Izbash(1930)

Izbash did research into the stability of stones dumped in a river for the construction of dams. The governing parameter in the Izbash equation is the current velocity. The location of the velocity is not very clear, but it is commonly used when the velocity near the bed is known. There is no depth influence parameter in the Izbash equation. In (Van Doorn, 2012) the original Izbash equation is given by:

$$\beta_{Iz} = \frac{2 \cdot g \cdot \Delta \cdot d_{50}}{\bar{u}_c{}^2} \tag{2.21}$$

With the original Izbash constant: $\beta_{Iz} = 0.7$.

The stability equation was adapted by (Izbash & Khaldre, 1970) described in (CIRIA, 2007) , in this adapted equation a distinction is made between the stability of exposed stones and embedded stones:

$$\begin{aligned} &\text{Exposed stones:} && \frac{u_c^2}{2 \cdot g \cdot \Delta \cdot d_{50}} = 0.7 \\ &\text{Embedded stones:} && \frac{u_c^2}{2 \cdot g \cdot \Delta \cdot d_{50}} = 1.4 \end{aligned} \tag{2.22}$$

Valid for h/d_{50}= 5 to 10

When combining equation 2.21 and 2.22 it can be shown that for the original the Izbash coefficient is given for an embedded situation: $\frac{1}{\beta_{Iz}} = \frac{1}{0.7} = 1.43$. When turbulence fluctuations are included in the original Izbash equation, the averaged velocity has to be rewritten. According to van Doorn, who refers to Verhagen(2001), $\bar{u}^2$ is replaced by $\bar{u}^2 + \overline{u'^2}$. It follows that: $\Delta g d_{50} = \frac{\beta_{Iz}}{2} \cdot (1 + r^2) \cdot \bar{u}^2$. When now is assumed that the stability depends on the maximum flow velocity peaks the following equation is given:

$$\Delta \cdot g \cdot d_{50} = \frac{\beta_{Iz}}{2}(1 + p \cdot r)^2 \cdot \overline{u_c}^2$$

Followed by a new Izbash coefficient. With $\beta_{Iz,new} = \frac{\beta_{Iz}}{(1+p \cdot 0.1)^2}$

In practice a bed protection affected by a thruster current is calculated by the method based on the Izbash equation, this method is described in (Olthof, 2002):

$$d_{50} \geq \beta_{iz,cr} \cdot m_h \cdot \frac{u_{b,max}^2}{2 \cdot g \cdot \Delta} \tag{2.23}$$

With $\beta_{iz,cr}$ is a critical stability coefficient (commonly 2.5-3.0), a value of 2.5 is recommended when some movement is allowed, for no allowable movement a value of 3.0 or higher is recommended. In the coefficient also turbulence can be taken into account, for higher turbulence intensities a higher value of $\beta_{iz,cr}$ is recommended. The slope stability factor (m_h) is used to include the flow direction at the slope according to (CIRIA, 2007):

$$m_h = \frac{\tan(\phi_s)}{\cos(\Theta_u) \cdot \sin(\alpha) + \sqrt{\cos^2(\alpha) \cdot \tan^2(\phi_s) - \sin^2(\Theta_u) \cdot \sin^2(\alpha)}} \tag{2.24}$$

For a flow perpendicular ($\Theta_u = 0$) and upwards to the slope this equation reduces into:

$$m_h = \frac{\sin(\phi_s)}{\sin(\phi_s + \alpha)}$$

Where:

ϕ_s	Angle of repose (for armor slope 40°-42°)	[°]
Θ_u	Angle of flow with respect to the slope.	[°]
α	Slope angle	[°]
p	Factor	[-]
r	Relative turbulence	[-]

2.3.1.2 Pilarczyk

Pilarczyk , described in (CIRIA, 2007), gives a design method for a bed protection at a slope affected by current:

$$\Delta d_{n50} = \phi \cdot \frac{0.035}{\Psi_{cr}} \cdot k_h \cdot k_{sl}^{-1} \cdot \frac{k_t^2 \cdot U^2}{2 \cdot g} \tag{2.25}$$

By rewriting this equation it can be shown that the Pilarczyk equation is comparable to the Shields equation (paragraph 2.3.1.3):

$$\Psi_{cr} = \phi \cdot 0.035 \cdot k_h \cdot k_{sl}^{-1} \cdot \frac{k_t^2 \cdot U^2}{2 \cdot g \cdot \Delta \cdot d_{n50}} \tag{2.26}$$

With:
ϕ is the stability correction factor, it depends on the application and placement:

Placement	Continuous	Edges and transitions
Rip-rap and placed blocks	0.75 to 1	1.5
Mattresses, gabions and washed-in blocks	0.5 to 0.75	0.75 to 1

The critical Shields parameter Ψ_{cr} for different materials and allowable damage:
For rip-rap Pilarczyk advises: Ψ_{cr}=0.035.

k_h is the depth parameter or the velocity profile factor. This factor is necessary to translate the depth-averaged flow velocity into the flow velocity just above the protection. For thrusters and propellers $k_h \approx 1.0$ is recommended and $U = U_{bed}$.

k_{sl} is the slope parameter. k_{sl}^{-1} is equal to m_h-factor given in equation 2.24. The slope parameter, for a flow upwards to the slope, is given by the following formula:

$$k_{sl} = \frac{\sin(\phi_s + \alpha)}{\sin(\phi_s)}$$

k_t is the turbulence factor, Pilarczyk recommends for load due to water (screw) jet a factor between 1.7 and 2.0. But if possible the turbulence factor should be derived from the turbulence intensity by:

$$k_t = \frac{1 + 3r}{1.3}$$

By comparing the recommended turbulence factor with the k_t equation, it can be shown that Pilarczyk uses a relative turbulence (r) for load due to a water jet between 0.4 and 0.53. (Blaauw & Van de Kaa, 1978) found turbulence intensities near the bottom in the range of 0.25 to 0.35. In the measurements by (Van Doorn, 2012), average relative turbulence levels are around 0.3 but with peaks up to 0.5 (Figure 2-5). In (PIANC, 2013), it is noted that when using the Dutch formulae (Blaauw & Van de Kaa, 1978) for near bed velocity, the velocity is underestimated due to the absence of jet confinement. Therefore a compensation in the k_t-factor needs to be implemented when using the Dutch approach for design of the bed protection. When using the Dutch method, a k_t^2-value between 5.2 and 6 is recommended.

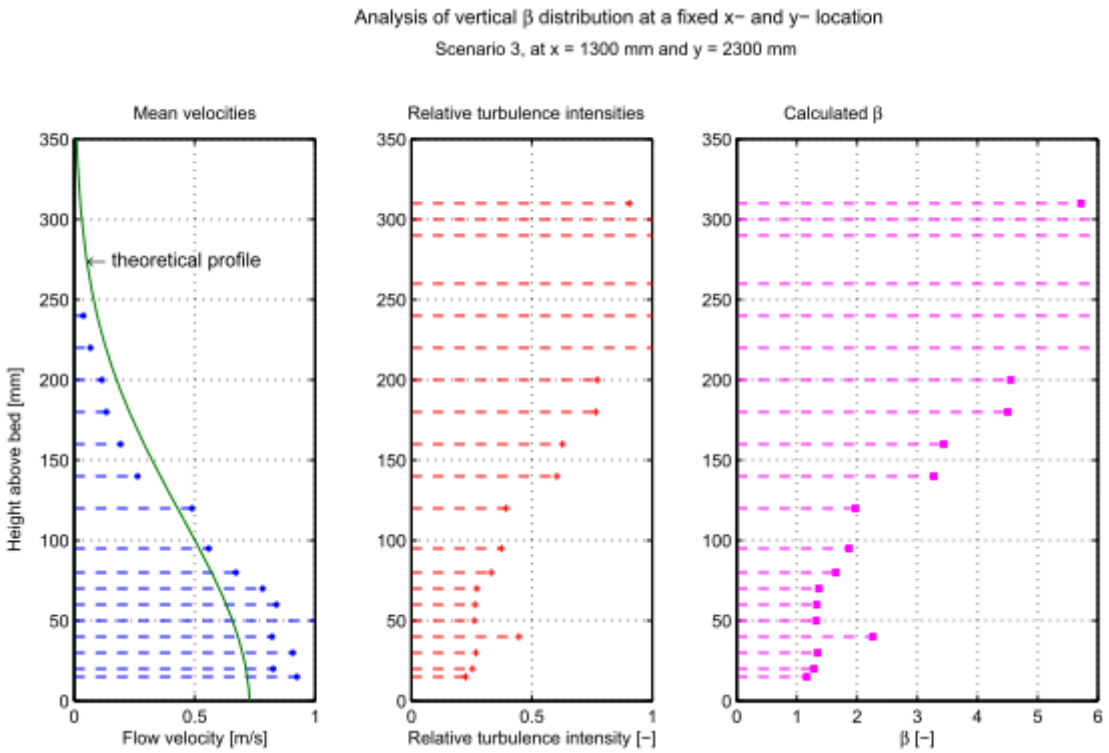

Figure 2-5: measured flow velocities, relative intensities and calculated beta values

When comparing the formula by Pilarczyk with equation 2.23, it can be shown that they are equal for: $\phi = 1$, $\Psi_{cr} = 0.035$, $k_h = 1$, $U = U_{bmax}$ and $\beta_{Iz,cr} = k_t^2$. Therefore when using a $\beta_{Iz,cr}$-factor of 2.5 to 3, this is comparable with a k_t-factor between 1.58 and 1.73, this is a bit lower than the value recommended by Pilarczyk for a screw jet.

2.3.1.3 Shields(1936)

The Shields formula is widely used to determine the required stone size for a bed protection in case of uniform flow. Shields gives a relation between the bed shear stress and the flow forces (Shields, 1936):

$$\Psi_s = \frac{\tau_b}{(\rho_s - \rho_w) \cdot g \cdot d} \tag{2.27}$$

Where:

$$\tau_b = \rho \cdot u_*^2$$

And :

$$u_* = \bar{u} \cdot \frac{\sqrt{g}}{C}$$

This results in:

$$\Psi_s = \frac{u_*^2}{\Delta \cdot g \cdot d} \text{ or } \Psi_s = \frac{\bar{u}^2 \cdot g / C^2}{\Delta \cdot g \cdot d} \tag{2.28}$$

The Chezy-coefficient is a roughness coefficient. It can be related to an equivalent sand roughness according to Nikuradse-Colebrook, for a hydraulical rough situation:

$$C = \frac{\sqrt{g}}{\kappa} \cdot \ln\left(\frac{12R}{k_r}\right) \approx 18 \cdot \log\frac{12R}{k_r}$$

With k_r is an equivalent roughness, for uniform flow it is usually equal to several times the characteristic grain diameter (Schiereck G. , 2004). The critical value of the Shields mobility parameter is particle diameter dependend. In (CIRIA, 2007) a distinction is made between the following different particles:

Cohesive sediments	Silt, $d_{50} < 50\mu m$ and clay, $d_{50} < 5\mu m$
Non-cohesive, fine sediment	Sand, $50\mu m < d_{50} < 2mm$
Non-cohesive, coarse sediment	Gravel, $d_{50} > 2mm$ and stone, $d_{50} > 50mm$

The critical Shields parameter can be predicted by applying the following equation (see also Figure 2-6) :

$$\Psi_{s,cr} = A \cdot D_*^B \qquad (2.29)$$

With D_* is the non dimensional grain size, determined by:

$$D_* = d_{50} \cdot \left(\frac{g\Delta}{\nu^2}\right)^{\frac{1}{3}}$$

Where ν is the kinematic viscosity (for water at $15°C = 1.14 \cdot 10^{-6}, 20°C = 1.00 \cdot 10^{-6}$ m^2/s).

With the coefficients A and B:

Range of D_* (-)	A	B
$1 < D_* < 4$	0.24	-1
$4 < D_* < 10$	0.14	-0.64
$10 < D_* < 20$	0.04	-0.1
$20 < D_* < 150$	0.013	0.29
$D_* > 150$	0.055	0

The plot (Figure 2-6) of the critical shields parameter shows a constant value of the Shields parameter for the dimensionless grain size larger than 150 (particles in the gravel and stone size). For particles in the sand size a small dip appears. This means that for particles in the sand range instability occurs for lower shields parameter than for particles in the gravel and stone range.

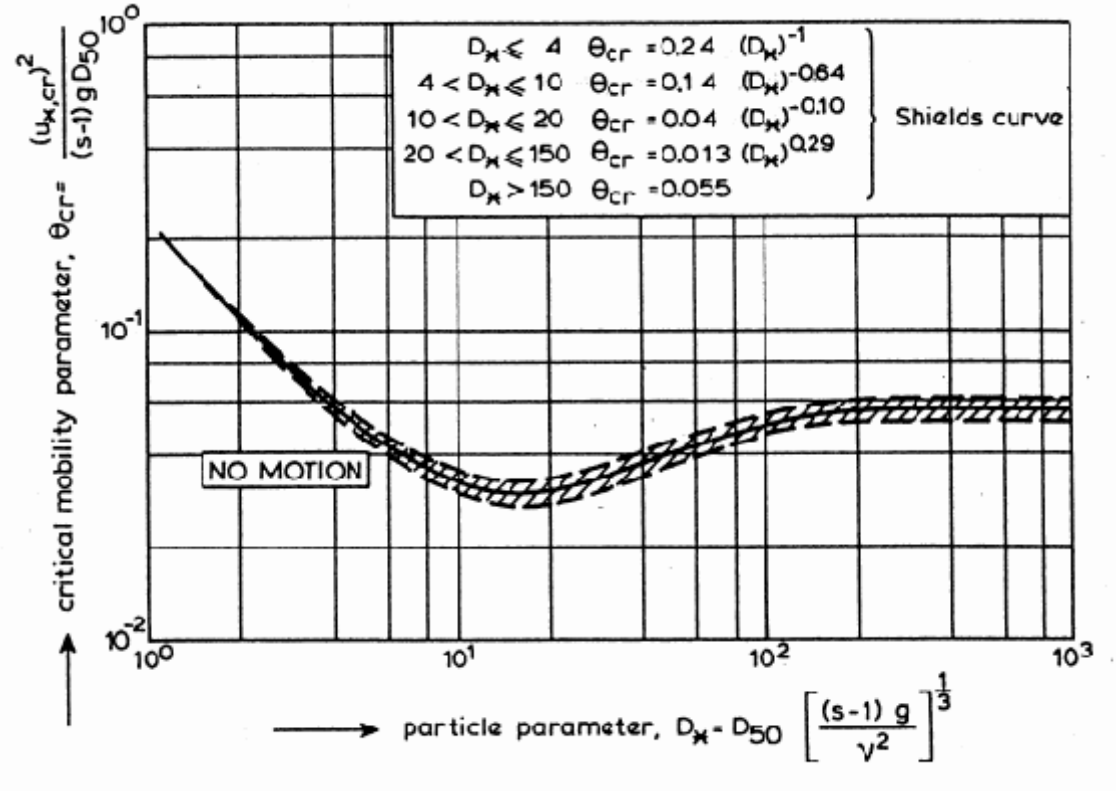

Figure 2-6: critical shear stress according to Shields - van Rijn

Because the mobility parameter by Shields is valid for (stationary) uniform flow, it is not applicable in the case of a thruster jet with relative high turbulence. In a recent approach of (Jongeling & Blom, 2003) and (Hofland, 2005), the profiles of the mean velocity and turbulent kinetic energy in the water column above the bed are used to formulate the forcing-term in the mobility parameter instead of the bed shear stress as used in the Shields approach. In this approach the influence of turbulence is incorporated explicitly.

2.3.1.4 Jongeling (2003)

Jongeling investigated an alternative method to determine the flow force on a granular bed protection behind a sluice for non-uniform flow conditions. The use of the bed shear stress, as provided by Shields (paragraph 2.3.1.3), has been proven insufficient for non-uniform flow conditions, due to the lack of turbulence intensities. The investigation by Jongeling was done with a numerical model. The forcing term in the mobility parameter is based on a depth averaged flow velocity and a turbulence factor averaged over a certain distance from the bottom (hm):

$$\Psi_{WL} = \frac{\langle\left(\bar{u} + \alpha_T\sqrt{k}\right)^2\rangle_{hm}}{\Delta \cdot g \cdot d} \tag{2.30}$$

With:

$$k = \frac{1}{2}(\overline{u'^2} + \overline{v'^2} + \overline{w^2})$$

$\langle \dots \rangle_{hm}$ gives the averaged value of the flow forcing from the bottom till hm above the bed. (Jongeling & Blom, 2003) advises to use $\alpha_T = 6$ and $hm = 5 \cdot d_{n50} + 0.2 \cdot h$ for incipient motion. The critical value: $\Psi_{WL_{crit}} \approx 8$ is recommended.

2.3.1.5 Hofland (2005)

Hofland also used the flow velocity and turbulence intensity as a governing parameter for the mobility parameter in non-uniform flow conditions. This approach is comparable to (Jongeling & Blom, 2003), but in this formula the Bakhmetev mixing length is used as length scale:

$$\Psi_{Lm} = \frac{\max\left[\langle \bar{u} + \alpha_T \sqrt{k} \rangle_{Lm} \cdot \frac{Lm}{z_b}\right]^2}{\Delta \cdot g \cdot d} \tag{2.31}$$

With:

$Lm = \kappa z \sqrt{1 - z_b/h}$ is the Bakhmetev mixing length with κ is the von Kármán constant (=0.4). For incipient motion α_T= 6 is recommended.

2.3.1.6 Hoan (2008)

Also (Hoan, 2008) used the flow and turbulence field as governing forcing parameter. However Hoan did not use the Bakhmetev mixing length, but a length H from the bottom. Besides Hoan added a weight function.

$$\Psi_{Hoan} = \frac{\langle [\bar{u} + \alpha_T \cdot \sigma(u)]^2 \cdot \left(1 - \frac{z_b}{H}\right)^{\beta} \rangle_H}{\Delta \cdot g \cdot d_{n50}} \tag{2.32}$$

With:

Ψ_{Hoan}	Mobility parameter according to Hoan	[-]
$\bar{u}$	Mean velocity at location z	[m/s]
α_T	Turbulence magnification factor	[-]
$\sigma(u)$	$= \sqrt{u'^2}$	[m/s]
$\left(1 - \frac{z_b}{H}\right)^{\beta}$	Weight function	[-]
z_b	Location above bed	[m]
H	Distance above the bed from where the turbulence has negligible influence.	[m]
Δ	Relative density	[-]
g	Gravitational acceleration	[m/s^2]
d_{n50}	Median nominal grain diameter	[m]

At a distance larger than H from the bed the weighting function becomes 0 (Figure 2-8b), this implies that the turbulence and flow velocities in higher regions in the vertical do not influence the mobility of the bed. However Hoan did a sensitivity analyses and found that when using the total water depth (H=h), still a correlation of 0.8 was reached, combined with a α=3 and a β=0.5. Therefore for the test set up of Hoan the following formula is given:

$$\Psi_{Hoan} = \frac{\langle [\bar{u} + 3 \cdot \sigma(u)]^2 \sqrt{1 - \frac{z_b}{h}} \rangle_h}{\Delta \cdot g \cdot d_{n50}} \tag{2.33}$$

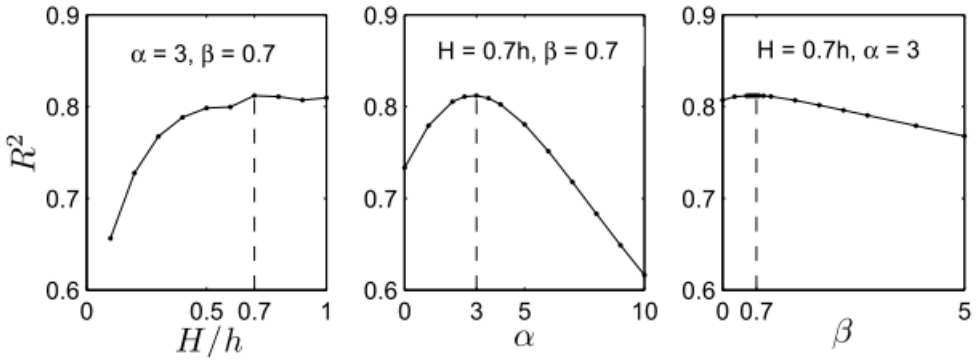

Figure 2-7: Sensitivity analysis for the Hoan tests (Hoan,2008)

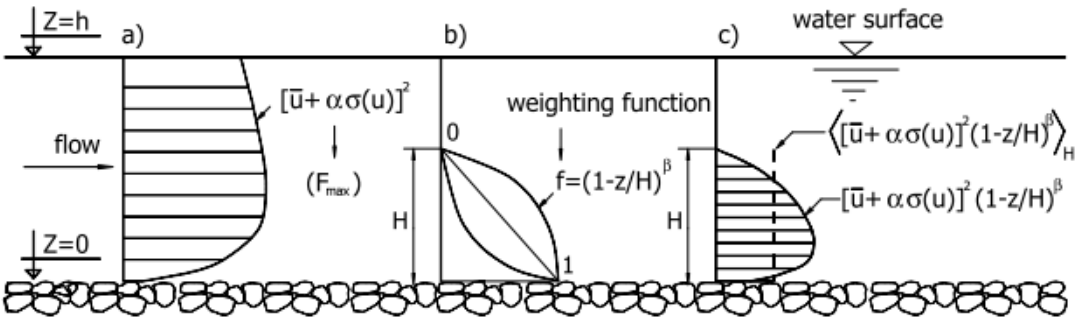

Figure 2-8: distribution of key parameters for the mobility parameter of Hoan. (Hoan, 2008)

By rewriting equation 2.33 it can be used to set up a design equation for the calculation of the bed protection in a non-uniform flow:

$$d_{n50} = \frac{\langle [\bar{u} + \alpha\sigma(u)]^2 \cdot \sqrt{1 + \frac{z}{h}} \rangle_h}{\Delta \cdot g \cdot \Psi_{\text{Hoan,crit}}} \tag{2.34}$$

With $\alpha = 3$ and $\Psi_{Hoan,crit} = 2.9$.

2.3.2 Bed material transport

In paragraph 2.3.1, the stability of bed material was assessed by using incipient motion condition at which the bed material starts to move. This concept is used in the Izbash, Shields, Hoan and Pilarczyk stability equations. The second approach of stability assessment is the transport method, this method is widely used in sediment transport studies. Transport formulae have the following general form:

$$\Phi = f(\Psi - \Psi_c) \tag{2.35}$$

Where Ψ is the mobility parameter and Φ is the transport indicator used to quantify the bed response. Transport formulae are often expressed by a power law relation:

$$\Phi = a(\Psi - \Psi_c)^b \tag{2.36}$$

The dimensionless transport parameter can be expressed in two different ways. First in terms of entrainment. Entrainment takes into account the number of pick-ups (n) per unit time (T) over a certain bed area (A).

$$\Phi_E = \frac{E}{\sqrt{\Delta \cdot \mathrm{g} \cdot \mathrm{d}}} \tag{2.37}$$

With:

$$E = \frac{n \cdot d^3}{A \cdot T}$$

The second method uses the bed load transport which takes into account the number of particles (n) transported through a cross-section (B) per unit time (T) and can be expressed as:

$$\Phi_q = \frac{q_s}{\sqrt{\Delta \cdot \mathrm{g} \cdot \mathrm{d}^3}} \tag{2.38}$$

With:

$$q_s = \frac{n \cdot d^3}{B \cdot T}$$

With:

E	Entrainment rate	[$m^3/m^2/s$]
n	Number of pick-ups per unit time and area	[-]
d	Characteristic particle diameter	[m]
A	Bed area	[m^2]
T	Time	[s]
q_s	Bed load transport per section width	[$m^3/m/s$]
B	Cross-section width	[m]

The entrainment is linked to the bed load transport, a schematization of this proportion is presented in Figure 2-9. The equation is given by:

$$q_s = E \cdot l \tag{2.39}$$

Where l is the particle displacement length. This length can vary due to differences in flow field (for non-uniform flow) and particle characteristics (for non-uniform bed material). The bed load transport depends on the upstream hydraulics; all stones passing a certain section (i.e., the transport) have been entrained upstream of this section. Bed load transport is therefore considered as a non-local parameter. However mobility parameters are local parameters, making $\Psi - \Phi_q$ a relationship of local and non-local parameters. Such a relationship can only be valid for uniform flow where the flow conditions are unchanged along the flow field and for homogeneous bed material.

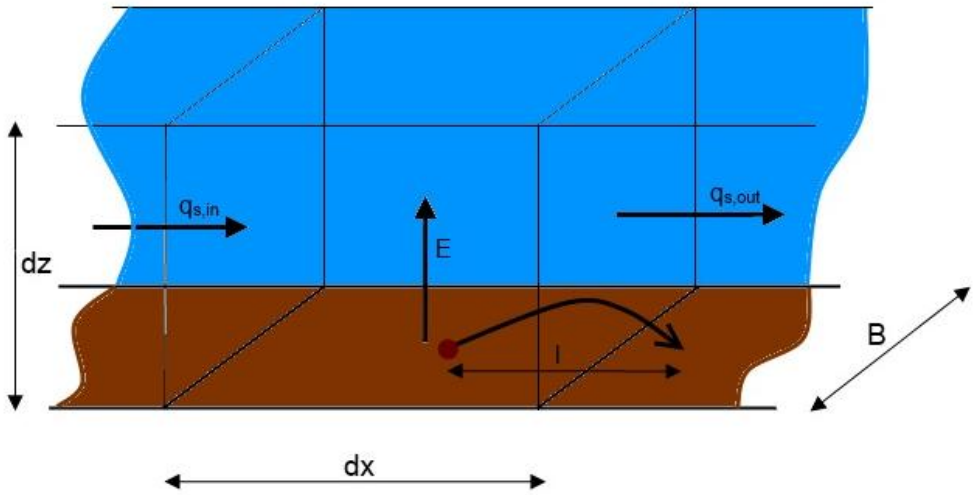

Figure 2-9: Schematization of the entrainment rate and the bed load transport

Because of the non-uniform character of the flow induced by bow thrusters it is difficult to relate bed mobility with the bed load transport method. It is however possible to define the entrainment rates, because $\Psi - \Phi_E$ is a purely local relationship.

2.4 Scour

Scour is caused by local higher mobility parameters, due to this higher mobility local transport could occur, which leads to scour holes. According to (CIRIA, 2007), movement of stones and sediment due to current and or wave action are observed as displacement of individual stones or as scour holes when the bed consists of sand, small stones or gravel. This shows that the relative magnitudes of the movement of coarse and fine particles are of different order. Displacement of individual stones is of the order of several times the stone diameter, while scour depths are at least several orders of magnitude of the grain size. However a clear transition between stone displacement and scour is not given, therefore in this thesis no distinction is made between scour and stone displacement.

Scour occurs in general when the local mobility parameter is larger than the critical mobility parameter, this general physical phenomenon is described in paragraph 2.4.1. In case of an open quay structure with piles affected by a bow thruster jet, the scour could be induced by the propeller

jet itself, this is called the jet diffusion mechanism (paragraph 2.4.2). Furthermore a pile in the flow field induces different flow loads, which could lead to additional scour. The scour induced by the pile is called the pile obstruction mechanism (paragraph 2.4.3).

2.4.1 General scour

In (Hofland, 2005) who refers to (Mosselman 2000) a method is described to link the entrainment rate with the bed degradation. This is done by using the conservation of mass:

$$\frac{\partial z_b}{\partial t} = -\frac{1}{1-\epsilon}(E - D) \tag{2.40}$$

When the deposition (D) of particles is neglected, it is possible to estimate the bed changes on the conservative side. The assumption of negligible deposition is legible because the deposition rate at places with maximum flow forcing is expected to be small (Hofland, 2005). Consequently a relation between the entrainment rate and the degradation of the bed could be made:

$$\Delta z_{b(t_1)} = \frac{1}{1-\epsilon}\int_0^{t_1} E\, dt \tag{2.41}$$

Where the bed is affected by flow forcing from $t = 0$ till $t = t_1$ and $\Delta z_{b(t_1)}$ is the maximum bed degradation at $t = t_1$. During constant flow forcing the entrainment decreases in time, the bed will approach the equilibrium depth. In this thesis the scour formation in time is not taken into account, only the equilibrium scour depth is examined. The objective is to find this equilibrium scour depth by using only the initial flow forcing, because little information is present on the development of the flow forcing during the scouring process. Therefore it is assumed that the initial entrainment rate provides an estimate for the size of the integral as present in equation 2.41 ($E_{initial} \propto \int_0^{t_1} E\, dt$). In equation 2.41 also the porosity of the bed is present, in the data sets that are used in this thesis (appendix B) the bed porosities are unknown, therefore this term is neglected as well. Given these assumptions it is possible to define a relation between the initial entrainment rate and the equilibrium maximum scour depth:

$$\Delta z_{b,max} = h_{sem} \propto E_{initial}$$

The initial entrainment rate can be predicted by using equation 2.36 and 2.37. Therefore it is possible to give a rough estimation for the maximum scour depth for a given initial flow field:

$$h_{sem} = \Delta z_{b,max} \propto E_{initial} \propto a(\Psi_{\text{initial}} - \Psi_c)^b$$

In the past research is done into the relation between initial flow forcing induced by a propeller jet or a free jet and the equilibrium scour depth. Some of these researches are described in the following paragraph.

2.4.2 Jet diffusion scour mechanism

In the past several researches are done into scour formation due to a propeller jet or a free jet forcing. Research by (Yüksel *et al.,* 2005) and (Chin *et al.*, 1996) was done with a jet just above a horizontal bed. In these researches a pile was situated at different locations from the bed (Figure

2-10), but it was concluded that for these set-ups the pile had negligible influence on the scour formation. Therefore the scour is predominately induced by the jet diffusion mechanism.

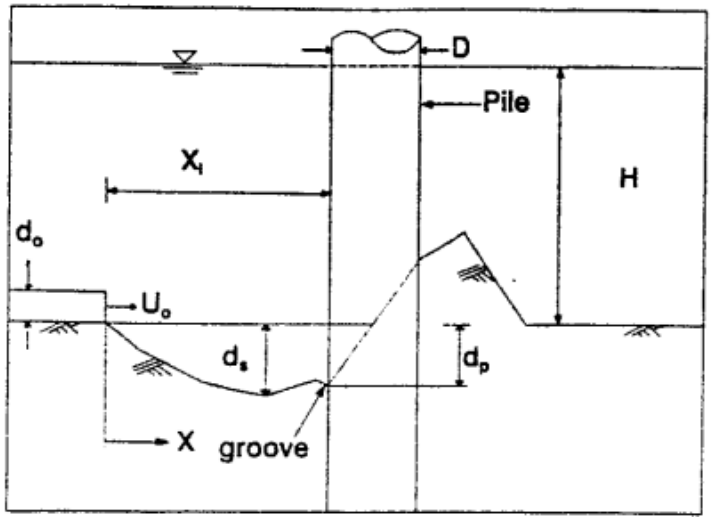

Figure 2-10: Schemetic overview of the test set-up in the tests by Chin et al. (1996), $d_s = h_{sem}$

According to (Yüksel *et al.,* 2005) the maximum equilibrium scour depth (h_{sem}) caused by a jet flow is primarily a function of the densimetric Froude number, in the tests the densimetric Froude number varied from 10 to 29:

$$h_{sem} = 0.29 \cdot Fr_0^{0.9} \cdot D_0 \qquad \text{With: } Fr_0 = \frac{U_0}{\sqrt{g \cdot \Delta \cdot d_{50}}} \tag{2.42}$$

A relation between scour and the densimetric Froude number was also shown by (Chin *et al.*, 1996) ($5 < Fr_0 < 90$):

$$h_{sem} = 0.21 \cdot Fr_0 \cdot D_0 \tag{2.43}$$

The two equations are compared in Figure 2-11.

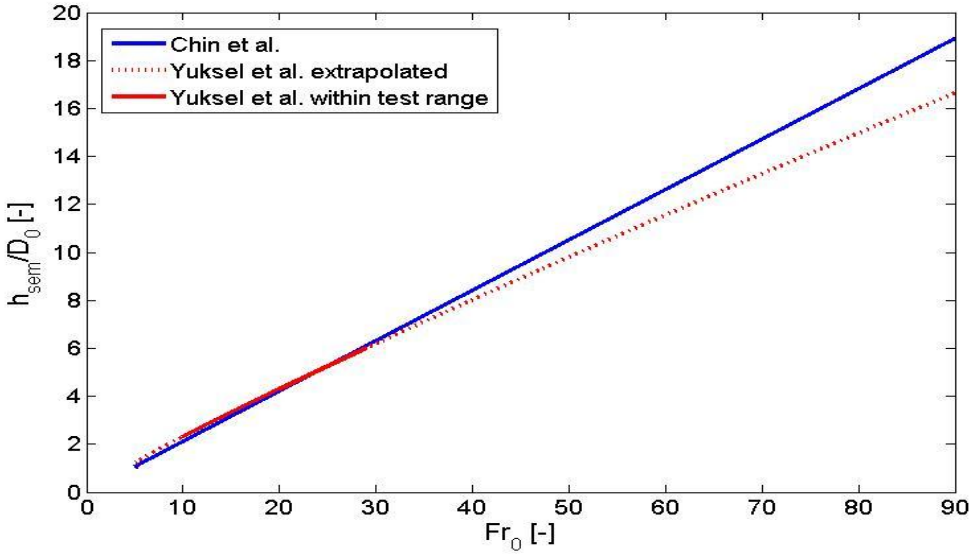

Figure 2-11: Relation between Yüksel (eq. 2.42) and Chin (eq. 2.43)

Research into the jet diffusion mechanism was also done by (Chiew *et al.*, 2012). However the difference between this research compared with the previous two researches is that in this case propellers and jets with an offset (h_{pb}) above a horizontal bed were used (Figure 2-12).

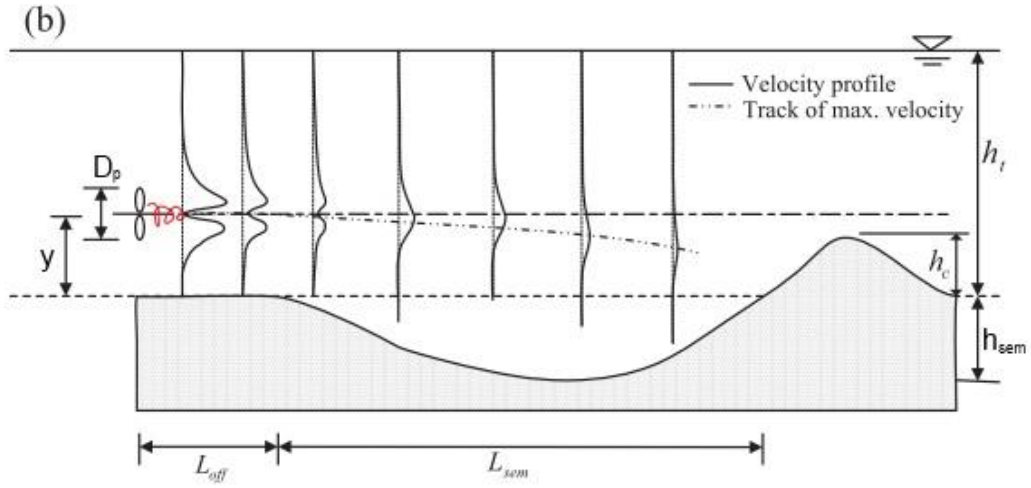

Figure 2-12: Jet induced scour with an offset Chiew et al. 2012, $y = h_{pb}$

This research was a data-analysis of different lab tests done by (Chiew & Lim, 1996), (Karki *et al.*, 2007), (Hamill, 1987) and (Chiew *et al.*, 2012). The data sets contain both propeller jets (Figure 2-12) and pure jets with an offset and densimetric Froude numbers between 5.5 and 60. The following formula for equilibrium scour is given:

$$\frac{h_{sem}}{D_0} = 0.265 \cdot \left(Fr_0 - \left(4.114 \cdot \frac{h_{pb}}{D_0} \right) \right)^{0.955} \cdot \left(\frac{h_{pb}}{D_0} \right)^{-0.022} \tag{2.44}$$

In this equation a critical densimetric Froude number is defined as $\left(4.114 \cdot \frac{h_{pb}}{D_0}\right)$. Furthermore no extra d_{85} or d_{50} is implemented as is the case in the German method as described in equation 2.45. The equation is derived for lab data containing measurements with bed material in the sand range. In Figure 2-13 the results for equation 2.44 are plotted. The equilibrium scour depth increases for increasing densimetric Froude numbers and for decreasing offset.

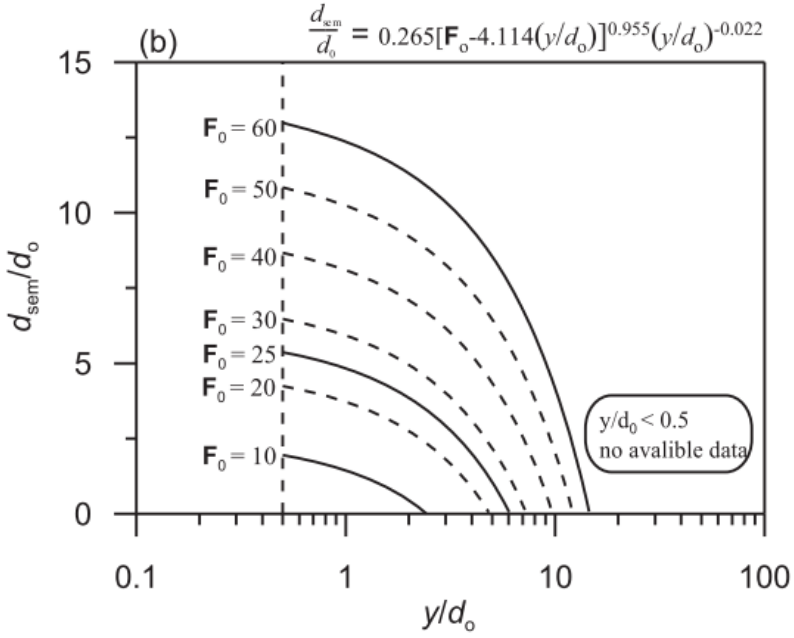

Figure 2-13: Simulated results for equation 2.52 by Chiew e.a. (2012), $y = h_{pb}, d_0 = D_0, d_{sem} = h_{sem}$.

When filling in $\frac{h_{pb}}{D_0}$=0.5, for the case of a propeller just above the bed, it is possible to compare the equation with the scour prediction equations by (Chin *et al,* 1996) and (Yüksel *et al.*, 2005), respectively 2.43 and 2.42.

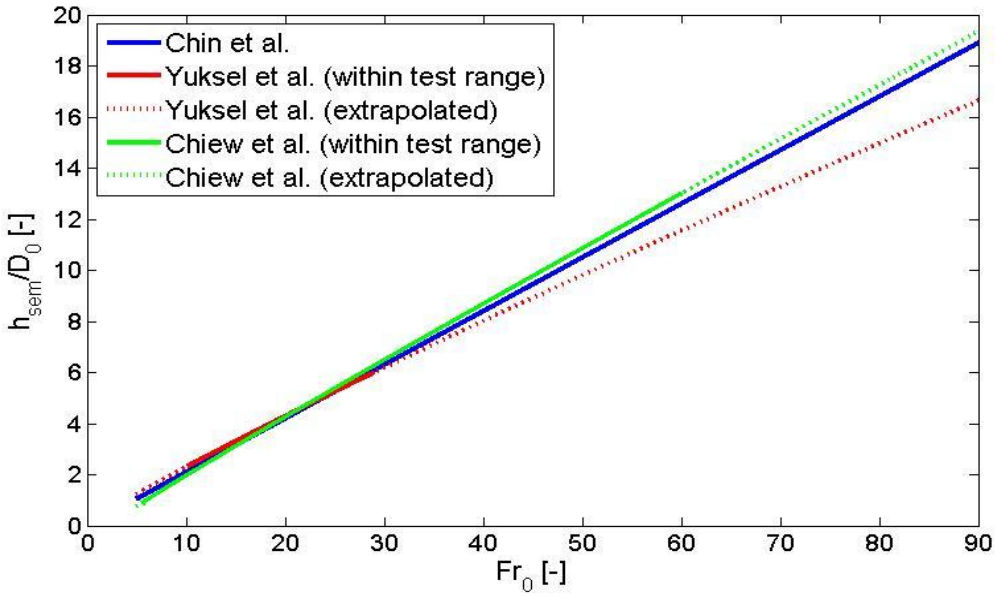

2-14: plot of Chin, Yüksel and Chiew (hpb/D0=0.5)

In (Römisch, 2012) the 'German method' is described to predict scour induced by a ship main propeller for a horizontal bed without piles, in this method also an offset is used:

$$\frac{h_{sem}}{d_{85}} = \frac{h_{pb}}{d_{85}} \cdot C_{ad} \cdot C_{m,r} \cdot \left[a_\alpha \cdot \frac{B}{B_{crit}} - 1 \right]$$

With:

$$C_{ad} = 17 \cdot \left(\frac{h_{pb}}{d_{85}}\right)^{-1} + \left[0.9 \cdot \frac{B}{B_{crit}} - 1\right] \leq 1.0 \text{ (for } 1.1 < \frac{B}{B_{crit}} < 2.2)$$

$$C_{ad} = 1 \text{ (for } \frac{B}{B_{crit}} > 2.2) \text{)} \quad (2.45)$$

$$\text{And: } B = \frac{u_{bed}}{\sqrt{\Delta \cdot g \cdot d_{85}}}$$

$$\text{With: } u_{bed} = E \cdot U_0 \cdot \left(\frac{h_{pb}}{D_p}\right)^{-1.0} \text{ (eq. 2.16)}$$

In this formula, a threshold value for the densimetric Froude number is given (B_{crit}). Also a distance between propeller axis and the bed is implemented, comparable to the method described in equation 2.44. However in this method, the dimensionless distance between the propeller axis and the bed is given by $\frac{h_{pb}}{d_{85}}$ instead of $\frac{h_{pb}}{D_0}$. Also the dimensionless scour depth is in this formula given by $\frac{h_{sem}}{D_{85}}$ instead of $\frac{h_{sem}}{D_0}$ in equation 2.44.

Where:

u_{bed}	Velocity near the bottom	[m/s]
B_{crit}	Critical densimetric Froude number (=1.2 (PIANC, 2013))	[-]
a_α	Angle of scour hole slope correction =0.65 (Römisch K. , 2012)	[-]
$C_{m,r}$	Rudder angle and maneuvering coefficient. For a stationary ship without rudder: $C_{m,r} = 1$	[-]

When combining the bed denismetric Froude number (B) and the formula for the bed velocity according to the German method (eq. 2.16) and assuming $d_{85} \approx 1.3 \cdot d_{50}$ it follows that:

$$B = \frac{u_{bed}}{\sqrt{\Delta \cdot g \cdot d_{85}}} = E \cdot \frac{D_p}{h_{pb}} \cdot \frac{U_0}{\sqrt{\Delta \cdot g \cdot d_{85}}} = E \cdot \frac{D_p}{\sqrt{1.3} \cdot h_{pb}} \cdot Fr_0$$

When combining this term with equation 2.45 the following formula is given:

$$\frac{h_{sem}}{d_{85}} = \frac{h_{pb}}{d_{85}} \cdot C_{ad} \cdot C_{m,r} \cdot \left[a_\alpha \cdot E \cdot \frac{D_p}{h_{pb}} \frac{Fr_0}{B_{crit}} - 1 \right]$$

With: (2.46)

$$C_{ad} = 17 \cdot \left(\frac{h_{pb}}{d_{85}}\right)^{-1} + \left[0.9 \cdot E \cdot \frac{D_p}{h_{pb}} \frac{Fr_0}{B_{crit}} - 1\right] \leq 1.0$$

Equation 2.46 is used to compare the data of the test done by (Drewes *et al.*, 1995) with the data from other tests as described in appendix B.

2.4.3 Pile obstruction mechanism

As described in the previous paragraph scour occurs when the flow forcing is higher than the critical forcing. When a pile is located in the propeller jet it will cause changes in flow field (Figure 2-15) and therefore changes in flow forcing, which could lead to scour around the pile. The flow field around a slender cylindrical pile for uniform flow can be divided into four different characteristics (Van Velzen, 2012). First a down flow in front of the cylinder can be distinguished. This downward flow is caused by the pressure differences in front of the pile, these pressure differences are in turn caused by the vertical differences in horizontal velocities. As a result of the down flow, the approach flow undergoes a three dimensional separation, which causes the boundary layer to roll up into spiral motion around the pile. This spiral motion is called the horseshoe vortex. Furthermore wake vortices are created downstream of the pile. At the sides of the pier the flow accelerates due to converging streamlines.

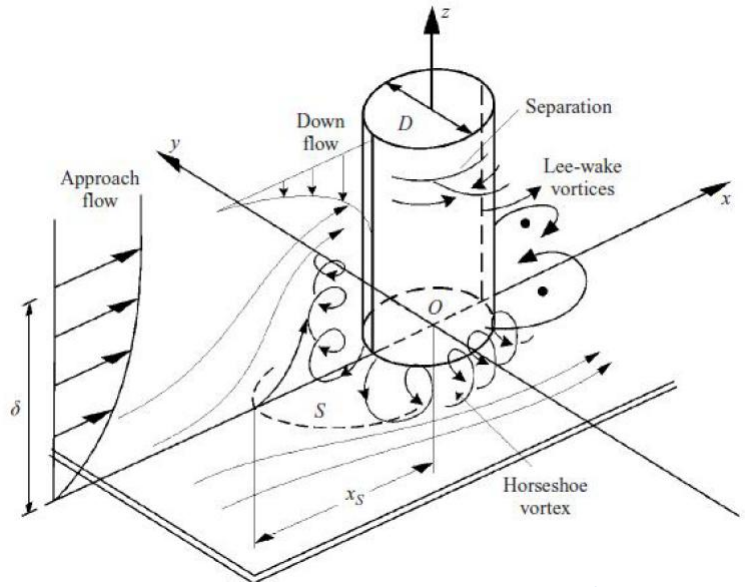

Figure 2-15: Characteristic features of the flow around a pile (Roulund et al. (2005) referenced in Van Velzen (2012))

These changes in flow field can cause local scour. The scour formation will decrease in time, because a recirculation in the scour hole itself takes place. At a certain moment the scour hole reaches an equilibrium depth.

According to (Hoffmans & Verheij, 1997) the following empirical formula for the equilibrium scour depth (based on scour around bridge piers) is given:

$$h_{sem} = 2 \cdot K_i \cdot D \cdot \tanh(\frac{h_0}{D_{pile}}) \tag{2.47}$$

In which $\frac{h_0}{D_{pile}}$ is the flow shallowness. For a relative slender pile: $\frac{h_0}{D_{pile}}$>2-3 equation 2.47 approaches:

$$h_{sem} = 2 \cdot K_i \cdot D_{pile} \tag{2.48}$$

With K_i is the correction factor, this correction factor composes out of a pier velocity-, shape-, orientation-, gradation- and a group factor:

$$K_i = \mathrm{K_u} \cdot K_s \cdot K\omega \cdot K_g \cdot K_{gr} \tag{2.49}$$

With:
K_u = velocity factor, for velocities above the critical velocity $K_u = 1$
K_s = shape factor, for cylindrical piles $K_s = 1$
K_ω = angle of attack factor, for a cylindrical piles this factor is 1
K_g = factor for the influence of bed material gradation. For a single grain size this factor is 1.
K_{gr} = factor for the influence of a group of piles. According to (FWHA, 2001):

$$K_{gr} = 0.57 \cdot \left(1 - \exp\left[-\frac{G}{D_{pile}}\right]\right) + \exp\left[-\frac{0.5G}{D_{pile}}\right] \tag{2.50}$$

With:

h_{sem}	Equilibrium scour depth	[m]
h_0	Initial water depth	[m]
G	Spacing between the piles	[m]
D_{pile}	Pile diameter	[m]

According to the (FWHA, 2001) described in (PIANC, 2013), the local equilibrium scour around bridge piers in rivers can be computed by:

$$\frac{h_{sem}}{h_0} = 2.0 \cdot K_1 \cdot K_2 \cdot K_3 \cdot K_4 \cdot \left(\frac{D_{pile}}{h_0}\right)^{0.65} \cdot Fr^{0.43} \tag{2.51}$$

With:

$$Fr = \frac{U_0}{\sqrt{g h_0}}$$

Where K_1 to K_4 are correction factors and U_0 is the depth averaged velocity. This scour depth equation looks similar to equation 2.47, it depends on the pile diameter and some correction factors are added. However in this equation the Froude number is implemented, therefore the flow velocity is directly included in this formula. Whereas in Equation 2.48 the flow velocity is only implemented in the velocity factor, for flow velocities above a critical value this factor is 1. Consequently for flow velocities above the critical velocity equation 2.48 predicts a constant scour depth, whereas equation 2.52 shows an increasing depth for increasing flow velocities.

With K_1=shape factor (=1 for circular piles), K_2=angle of attack factor (=1 for circular piles), K_3=dune factor, K_4=correction factor for the size of the bed material.

In (Hoffmans & Verheij, 1997) it is stated that the size of bed material in the sand size range has little effect on scour depth. Bed material in the gravel or stone size could influence the depth of the scour hole. In (Melville & Chiew, 1999) is described that the scour depth decreases for increasing sediment coarseness (d_{50}/D_{pile}). The sediment coarseness is incorporated in a correction factor that should be added to the total correction factor:

$$\begin{aligned} K_d &= 0.57 \log\left(2.24 \cdot \tfrac{D_{pile}}{d_{50}}\right) && \text{for } \tfrac{D_{pile}}{d_{50}} < 25 \\ K_d &= 1 && \text{for } \tfrac{D_{pile}}{d_{50}} > 25 \end{aligned} \tag{2.52}$$

3 Newly proposed formula

As described in paragraph 2.4, scour at open quay structures could be induced by two different mechanisms; the jet diffusion mechanism and the pile obstruction mechanism. Therefore in the newly proposed formula for scour prediction these two mechanisms are combined.

3.1 Jet diffusion induced scour

The scour induced by the jet diffusion mechanism depends on the mobility of the bed material at the slope (paragraph 2.4.1). The mobility depends on the forcing at the bed (flow field just above the bed) and the bed strength (stone size). Because of the high turbulence intensities in the jet caused by the bow thruster, it is assumed that the Hoan mobility parameter (equation 2.32) provides the best prediction for the mobility of the bed in case of a bow thruster. For a mobility parameter below a critical value no transport and therefore no scour will occur. Therefore a critical mobility parameter is introduced in the diffusion scour prediction, a critical value is also used in the German method (equation 2.45). Hoan suggests a critical mobility parameter of 2.9. It is assumed that the transport indicator as described in equation 2.36 provides a good method to estimate the jet diffusion induced scour, as described in paragraph 2.4.1. The proposed jet diffusion equation is:

$$\left(\frac{h_{sem}}{D_0}\right)_{jetdiffusion} = \alpha_1 \cdot \left(\Psi_{hoan} - \Psi_{hoan,crit}\right)^{\beta_1} \qquad (3.1)$$

During lab experiments the flow field above the bed could be measured. With this flow field measurements it is possible to determine the Hoan mobility parameter and the critical Hoan mobility parameter. For different values of the Hoan mobility parameter, for example different stone sizes or different flow fields during lab experiments , the scour induced by the jet diffusion scour can be calculated. When the scour depth is measured for different Hoan parameters it is possible to define the values of α_1 and β_1 in equation 3.1.

In practice it is difficult to define the Hoan mobility parameter, because for the calculation detailed information about the flow field above the bed has to be present, which is seldom available. It is however possible to calculate the maximum flow velocity at the slope by applying equation 2.17. This maximum flow velocity at the slope could provide a method to predict the maximum scour depth. Therefore the velocity near the slope is applied to set up a new parameter called the densimetric slope Froude number. This parameter is comparable with the densimetric Froude number Fr_0 as described in paragraph 2.4.2, however not the efflux velocity is used but the velocity near the slope. The densimetric slope Froude number could be calculated by applying the following equation:

$$Fr_{slope} = \frac{U_{slope}}{\sqrt{g \cdot \Delta \cdot d_{50}}} \qquad (3.2)$$

The turbulence intensities are not explicitly taken into account in the densimetric slope Froude number, though because of the set up of the slope velocity calculation turbulence is implicitly implemented due to the fact that the maximum velocities are used in this equation. As in the case of the Hoan mobility parameter, also the densimetric slope Froude number has a critical value for which below this value no transport occurs. The critical value for the slope Froude number can be determined by calculating the critical bed velocity as given in equation 2.23. The following equation for the critical slope Froude number is suggested:

$$Fr^2_{slope,crit} = \frac{U^2_{slope,crit}}{g \cdot \Delta \cdot d_{50}} \approx \frac{\Psi_{cr}}{0.055} \cdot \frac{2}{m_h \cdot \beta_{Iz,crit}} \quad (3.3)$$

With m_h is the slope factor as given in equation 2.24, $\beta_{Iz,crit}$ is the critical Izbash coefficient (between 2.5 and 3). The influence of the bed material size is incorporated within the critical Shields parameter, this parameter can be determined by using equation 2.29. In equation 3.3 the chosen value for the critical Shields parameter is 0.055 because we are interested in movement of the armour stones ($\Psi_{cr} \approx 0.055$) and not in the point at which individual stones become unstable ($\Psi_{cr} \approx 0.035$) (CIRIA, 2007). For bed material within the gravel or stone range (d_{50}>5mm), the critical Shields parameter in case of limited movement is 0.055, consequently the critical densimetric slope Froude number is $\sqrt{\frac{2}{m_h \cdot \beta_{Iz,crit}}}$. For bed material within the sand range the critical densimetric Froude number becomes less, because of the lower critical Shields number (Figure 2-6).

In the Hoan mobility parameter (equation 2.32), the flow forcing is squared and the bed strength contains no square root. Therefore it is assumed that the Hoan mobility parameter is proportional to the densimetric slope Froude number squared:

$$\Psi_{Hoan} \propto Fr^2_{slope}$$

When the Hoan moblity parameter in equation 3.1 is substituted by the densimetric slope Froude number, a more user friendly method is described to estimate the scour induced by the jet diffusion mechanism. The proposed equation is given by:

$$\left(\frac{h_{sem}}{D_0}\right)_{jetdiffusion} = \alpha_2 \cdot \left(Fr^2_{slope,max} - Fr^2_{slope,crit}\right)^{\beta_2} \quad (3.4)$$

The α_2 and β_2 coefficients should be derived by data from tests. In this equation: Fr_{slope}>$Fr_{slope,crit}$.

Other jet diffusion scour prediction formulae (paragraph 2.4.2) use also a densimetric Froude number. This provides an extra confirmation of the possible applicability of the densimetric slope Froude number in the newly proposed equation.

With the distribution of the densimetric slope Froude number along the slope it is possible to define the zone where jet diffusion scour will probably occur. This distribution can be calculated by the distribution of the velocities near the slope, which could be calculated by applying equation 2.17. The method to define these velocities is described in appendix A. Jet diffusion scour occurs at locations where the slope Froude number is larger than the critical slope Froude number. Figure 3-1b shows an example of a slope Froude number distribution for the 1:3 slope as presented in Figure 3-1a. The maximum scour depth will probably occur at the location of maximum slope Froude number. Scour occurs above the highest dotted line in Figure 3-1b, where the densimetric Froude slope number is higher than the critical value. Figure 3-1c shows the resulting scour. The values for α_2 and β_2 that are used in this calculation are respectively 0.3 and 0.5 and are found by data analyses as described in chapter 4.

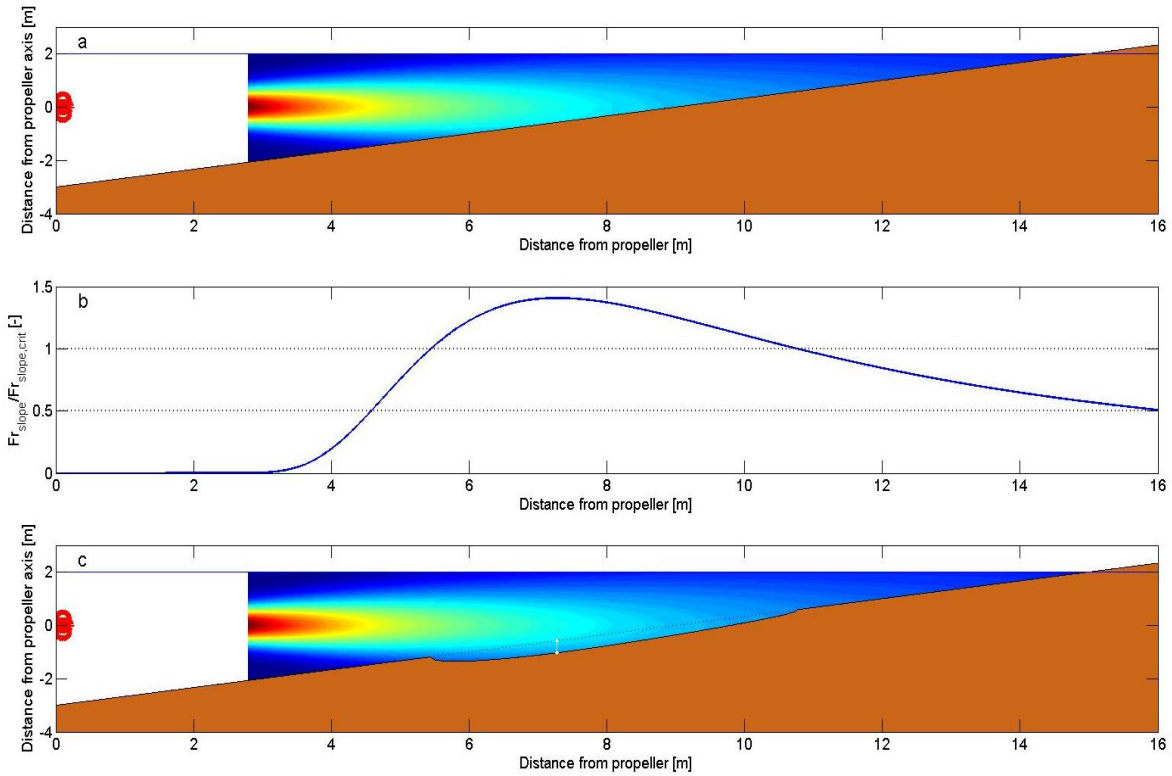

Figure 3-1: Example of the jet diffusion mechanism at a slope (1:3)

3.2 Pile obstruction induced scour

In the past less research is done on scour induced by the pile obstruction mechanism in a jet flow. However there are scour prediction equations for the pile obstruction mechanism in uniform flow cases, for example as described in equation 2.47. Though this method is described for the uniform flow case, it is assumed that it will also give a good first estimate in case of a non-uniform flow field caused by bow thruster. Therefore the proposed equation for scour induced by the pile obstruction mechanism in case of a bow thruster current is given by:

$$\left(\frac{h_{sem}}{D_0}\right)_{pileobstruction} = \gamma \cdot K \cdot \frac{D_{pile}}{D_0} \cdot \tanh\left(\frac{h}{D_{pile}}\right) \tag{3.5}$$

Where K is a coefficient that contains the following correction factors:

$$K = K_{gr} \cdot K_u \cdot K_{shape} \cdot K_g \cdot K_d \tag{3.6}$$

As described in paragraph 2.4.2 a pile group will cause different scour than a single pile, therefore a group factor (K_{gr}) is included in the equation. Below a certain velocity no pile obstruction scour will occur, this critical value is incorporated in the velocity correction factor (K_u):

$$\begin{aligned} K_u &= 0 && \text{for} && U_{slope} < 0.5 \cdot U_{slope,crit} \\ K_u &= 2 \cdot \frac{U_{slope}}{U_{slope,crit}} - 1 && \text{for} && 0.5 \cdot U_{slope,crit} < U_{slope} < U_{slope,crit} \\ K_u &= 1 && \text{for} && U_{slope} > U_{slope,crit} \end{aligned} \tag{3.7}$$

Equation 3.7 shows that the pile obstruction mechanism already occurs for velocities above 0.5 times the critical velocity. Due to the fact that the distribution of the slope velocity has the same distribution as the densimetric slope Froude number, it is also possible to define the velocity correction factor in terms of the densimetric slope Froude number, simply by replacing U_{slope} by Fr_{slope} and $U_{slope,crit}$ by $Fr_{slope,crit}$ in equation 3.7.

In (Hoffmans & Verheij, 1997) γ is 1.5-2.0 for the uniform flow case. In case of a thruster current a different value of γ could occur. This value can be found by data from experiments. As a result of lab data analysis (chapter 4), an estimated value for γ (=1.2) is derived, but because of the lack of sufficient data the validity of that value is questionable.

In equation 2.47 h_0 represents the total water depth of the river. In the case of a bow thruster not the entire water depth has to taken into account, only the water depth that is disturbed by the jet will induce scour and therefore only the width of the jet is taken into account in equation 3.5. The width of the jet is approximated by means of the following equation:

$$for\ x < 5 \cdot waterlevel: h = 0.2x + h_{pb,x}$$
$$for\ x > 5 \cdot waterlevel: h = h_0$$

The jet angle of 1:5 is estimated given the flow field as presented in Figure 3-2, it implies that the propeller jet has an angle of approximately 11 degrees. In case of a free jet this angle is smaller due to the less diffusive character, consequently the calculated jet width is smaller. A schematic view of the calculation of h for a propeller jet is given in Figure 3-2.

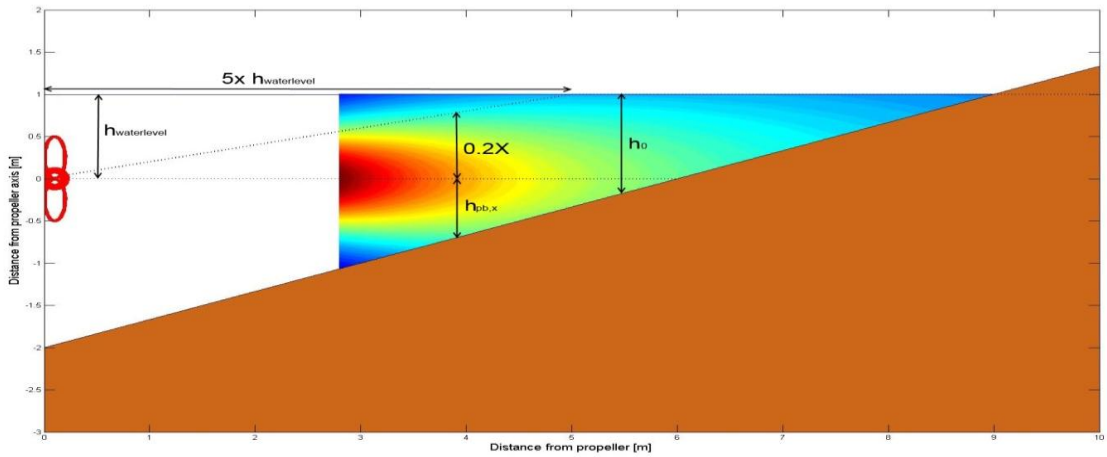

Figure 3-2: schematic view for the calculation of h

In Figure 3-3a a possible set up for a situation where pile obstruction scour could occur is presented. When the pile is located within the range of a Froude slope number higher than 0.5 times the critical Froude slope number, scour induced by the pile obstruction mechanism could occur. In Figure 3-3 a pile is located within the zone where the slope Froude number is between 0.5 and 1 times the critical slope Froude number. A prediction of the maximum scour depth can be calculated by using equation 3.5. The value of the velocity coefficient (K_u) can be calculated by the velocity distribution or the densimetric slope Froude number at the slope, or in this case the horizontal bed. Figure 3-3c shows the resulting scour depth with $\gamma = 1.2$. This scour depth is purely formed by the pile obstruction mechanism because the jet diffusion mechanism does not occur for densimetric slope Froude number below the critical value.

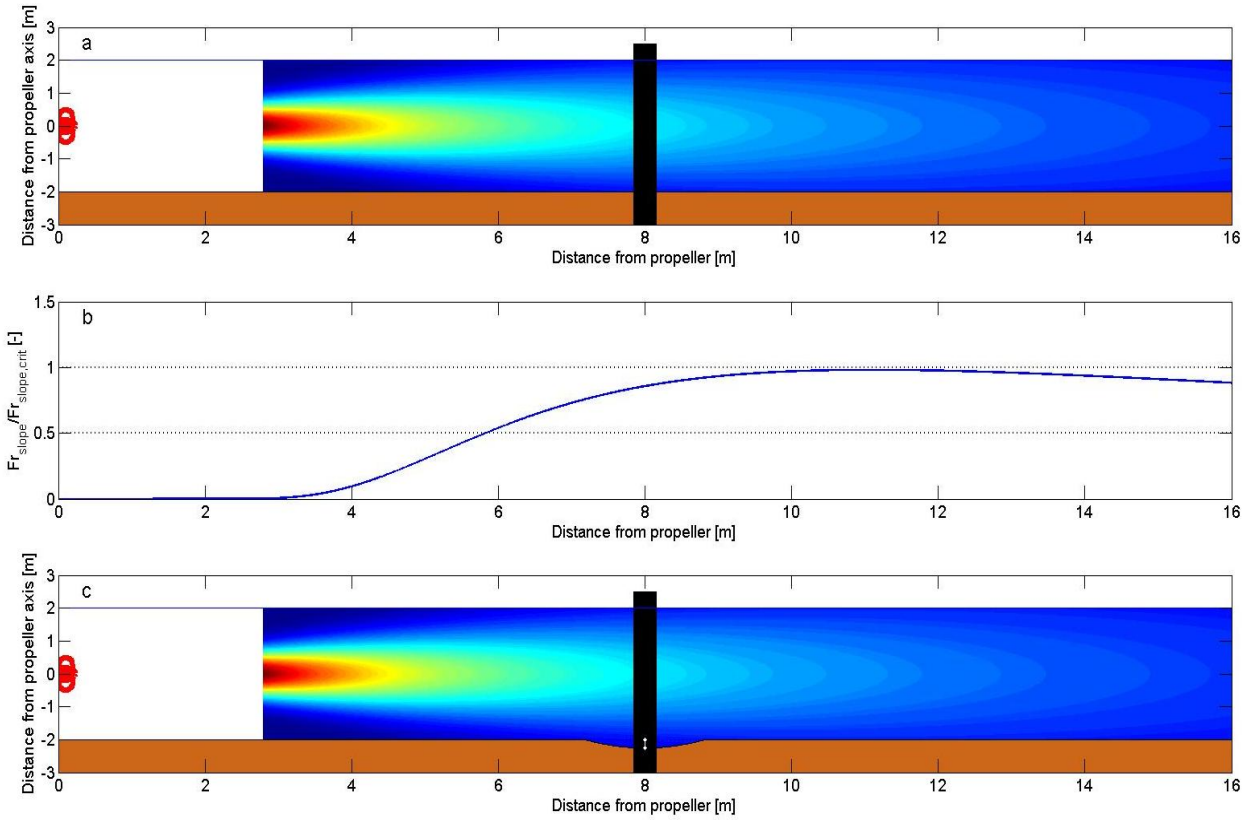

Figure 3-3: example of the pile obstruction mechanism with $x_{pile} = 8m$ and $D_{pile} = 0.3m$ at a horizontal bed

3.3 Combination of the pile obstruction- and the jet diffusion mechanism

The distribution of the slope velocity combined with the location of the piles determines which scour mechanism does occur. When combining the jet diffusion induced scour and the pile obstruction induced scour, a new equation for scour prediction for a slope with piles affected by a bow thruster induced current is set up. In this prediction it is assumed that the jet diffusion mechanism is not influenced by the pile obstruction mechanism and that superposition is allowed. This means that first the scour hole formed by the jet diffusion mechanism is predicted (equation 3.4), subsequently the pile obstruction scour is added (3.5):

$$\frac{h_{sem}}{D_0} = \alpha_2 \cdot \left(Fr_{slope}^2 - Fr_{slope,crit}^2\right)^{\beta_2} + \gamma \cdot K \cdot \frac{D_{pile}}{D_0} \cdot \tanh\left(\frac{h}{D_{pile}}\right) \qquad (3.8)$$

At an open quay structure with piles three different scour scenarios are possible:

- Scenario 0, very low velocities: The maximum slope Froude number is smaller than 0.5 times the critical slope Froude number; both scour mechanism cannot occur. Because of the absence of scour, this scenario is not further described.
- Scenario 1, low flow velocities: The maximum slope Froude number is between 0.5 and 1.0 times the critical slope Froude number; the jet diffusion mechanism will not occur, possibly the pile obstruction mechanism does occur, depending on the location of the pile. This scenario is described in paragraph 3.3.1.
- Scenario 2, eroding flow velocities: The maximum Froude slope number is larger than the critical Froude slope number; the jet diffusion mechanism will cause scour, the pile

obstruction mechanism could occur depending on the location of the pile. In this case both scour mechanism should be combined to predict the scour depth. This scenario is described in paragraph 3.3.2.

3.3.1 Scenario 1: low flow velocities

Because the maximum densimetric slope Froude number is smaller than the critical Froude slope number, the jet diffusion mechanism will not occur. However it is possible that the pile obstruction mechanism does. For a pile located at the slope within the region with a densimetric slope Froude number higher than 0.5 times the critical Froude slope number, pile obstruction induced scour will occur. The jet diffusion part of equation 3.8 falls out and equation 3.5 remains:

$$\frac{h_{sem}}{D_0} = \gamma \cdot K \cdot \frac{D_{pile}}{D_0} \cdot \tanh\left(\frac{h_0}{D_{pile}}\right) \tag{3.5}$$

3.3.2 Scenario 2: eroding flow velocities

In this scenario jet diffusion scour will occur because at a certain region at the slope the slope Froude number is larger than the critical slope Froude number. The maximum scour depth caused by this mechanism can be predicted by using equation 3.4. When a pile is located at the slope also the pile obstruction mechanism could occur. However the contribution of the pile obstruction mechanism on the total maximum scour depth depends on the location of the pile (x_{pile} and y_{pile}). In the following calculations only piles in the propeller axis are taken into account ($y_{pile} = 0$). Three different sub scenarios are distinguished:

- Scenario 2A: the pile is located at a location with $Fr_{slope} < 0.5 \cdot Fr_{slope,crit}$ (red area in Figure 3-4) : no pile induced scour occurs, so the total maximum scour depth is only determined by the jet diffusion scour which will occur in the green area of Figure 3-4. Equation 3.8 reduces into equation 3.4.
- Scenario 2B: the pile is located in the zone with $0.5 \cdot Fr_{slope,crit} < Fr_{slope} < Fr_{slope,crit}$ (yellow area in Figure 3-4): two scour holes are formed, one caused by the jet diffusion mechanism (in the green area of Figure 3-4) and one by the pile obstruction mechanism (in the yellow area of Figure 3-4), these two different scour holes have to be calculated separately by using equation 3.4 and 3.5.
- Scenario 2C: the pile is located inside the zone where $Fr_{slope} > Fr_{slope,crit}$ (green area in Figure 3-4): scour induced by the pile obstruction mechanism is in the zone of jet diffusion scour. Because of the assumption that both mechanisms could occur independently, both mechanisms should be added, first the jet diffusion scour at the location of the pile is calculated. Then the pile obstruction mechanism is added. Equation 3.8 should be used to predict the maximum scour depth.

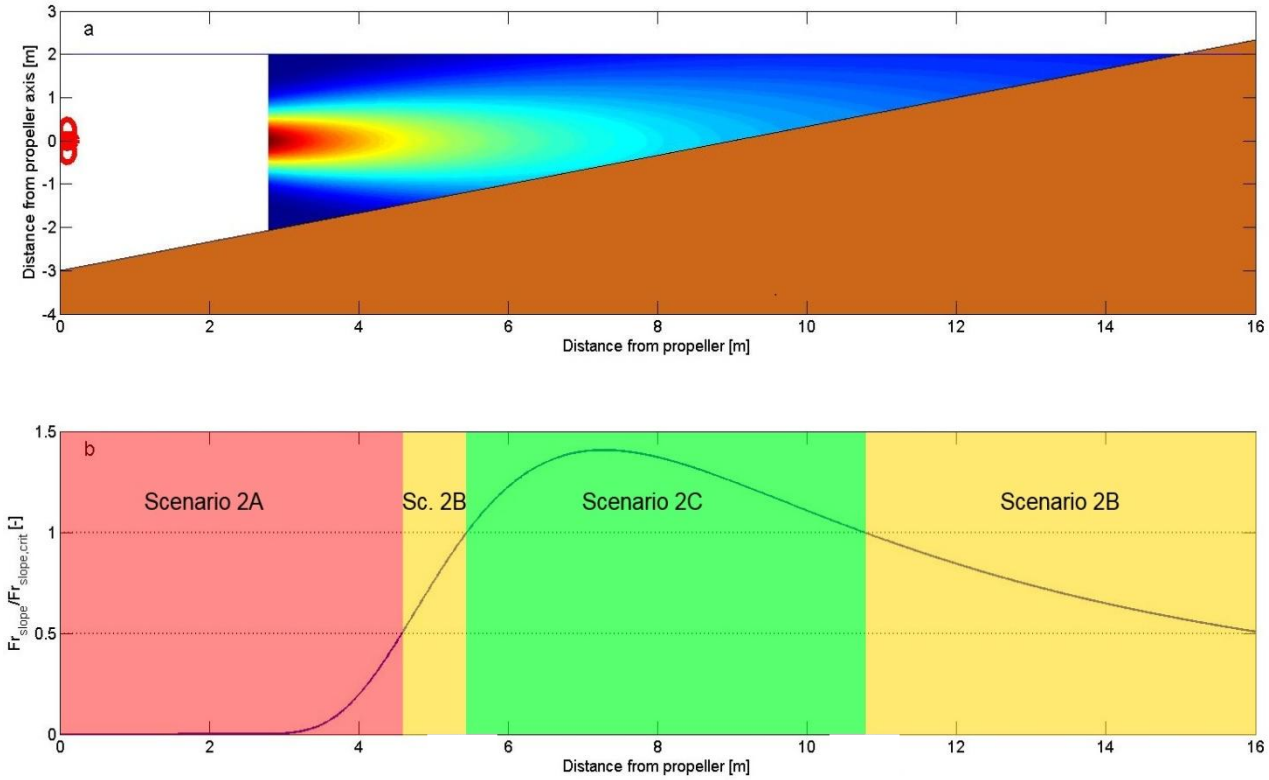

Figure 3-4: Schematization of scenario 2A,2B and 2C

In Figure 3-5 an example of scenario 2C is presented. In the scour hole both scour mechanisms are clearly visible.

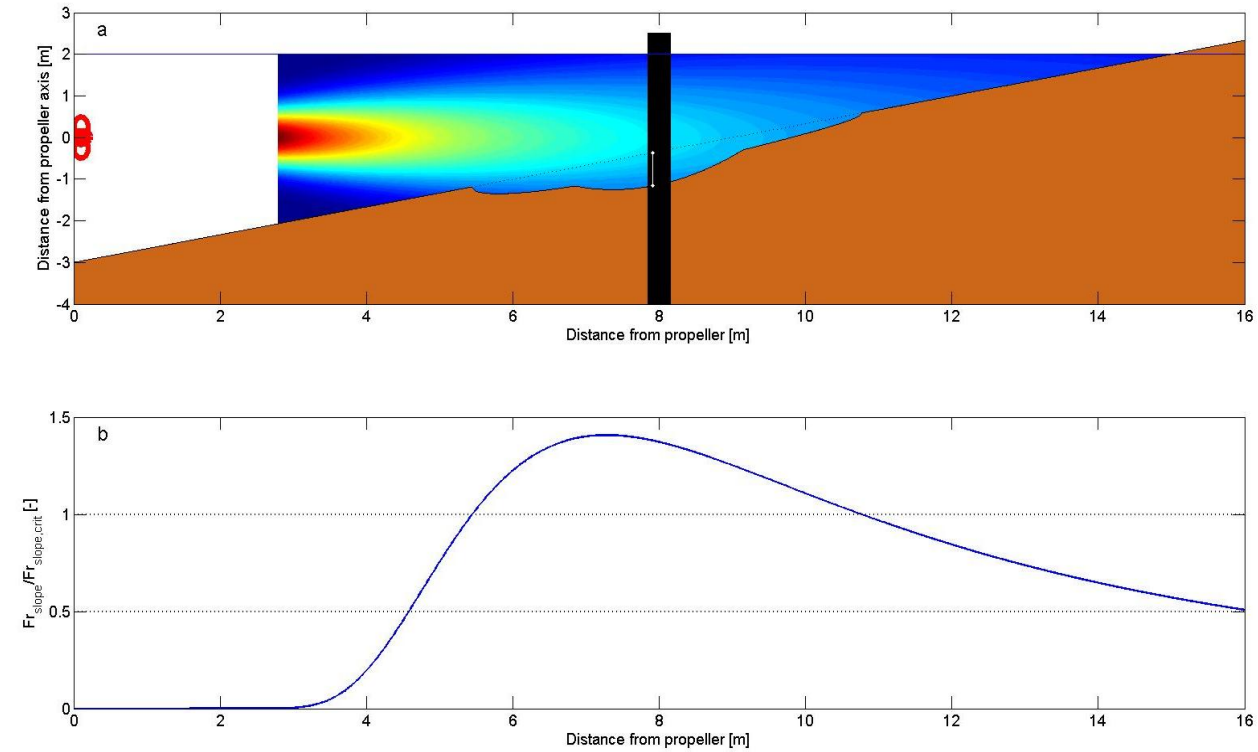

Figure 3-5: example of a scour hole formed by both scour mechanisms combined with $x_{pile} = 8m$ (scenario 2C)

4 Validation of the newly proposed formula

In chapter 3 a new scour prediction equation is described for an open piled quay structure (equation 3.8). In this formula still the coefficients α_2, β_2 and γ have to be determined. This can be done by comparing the new equation with data from lab tests. In this chapter, first the different available researches are described, followed by the validation of the newly proposed formula. Finally the sensitivity of the proposed equation is described.

4.1 Description of the available data sets

The hypothesis formula (equation 3.8) is set up for the case of an open piled quay structure. In the past several lab experiments are conducted for the case of a horizontal bed affected by a propeller wash or a jet. In Table 4-1 the different researches are presented, the shaded cells show the set-up of the different researches. The table shows that no data is available for a sloping bed, therefore the newly proposed formula cannot be validated for the sloping bed case. In the proposed scour prediction equation the bed can be implemented with a slope with a very small slope angle, in that case it is possible to approach a horizontal bed case. By doing this the slope Froude number approaches the horizontal bed Froude number. The critical value of the slope Froude number approaches the critical Froude number for a horizontal bed (with a slope factor equal to 1).

First a validation for the case of a horizontal bed without piles is conducted (paragraph 4.2), followed by a validation in case of a horizontal bed with a single pile (paragraph 4.4). A more extensive overview of the different researches is presented in appendix B.

	Horizontal bed		Sloping bed	
	Without piles	With piles	Without piles	With piles
Karki et al. (2007)	■			
Drewes et al. (1995)	■			
Hong et al. (2012)	■			
Chiew et al. (1995)	■			
Chin et al. (1996)	■	■		
Yüksel et al. (2005)		■		
Hamill (1987)	■			

Table 4-1: Summary of different researches (for an extensive overview of the researches appendix B is recommended)

4.2 Validation for a horizontal bed without piles

Data from 6 different researches are available for the horizontal bed without piles case. The maximum slope Froude number will approach in that case the maximum horizontal bed Froude number. Due to the fact that no piles are concerned in this set-up, the pile obstruction mechanism is dismissed as well. The proposed formula reduces into:

$$\frac{h_{sem}}{D_0} = \alpha_2 \cdot \left(Fr_{bed,max}^2 - Fr_{bed,crit}^2\right)^{\beta_2} \tag{4.1}$$

With:

$$Fr_{bed,max} = \frac{U_{bed,max}}{\sqrt{g \cdot \Delta \cdot d_{50}}} \tag{4.2}$$

And:

$$Fr_{bed,crit} = \sqrt{\frac{\Psi_{cr}}{0.055} \cdot \frac{2}{\beta_{Iz,crit}}} \tag{4.3}$$

With the calculated maximum bed velocity it is possible to compute the maximum bed Froude number. The critical Froude number is calculated with the assumption of a critical Izbash parameter, in this case $\beta_{Iz,crit} = 3$ is assumed. The critical Shields parameter is determined by applying equation 2.29. In the lab test data given by (Chin *et al.,* 1996) the bed material size is not known, however we know that all bed material was in the sand range. Therefore for these tests a critical Shields parameter of 0.03 is assumed.

The maximum bed velocity could be calculated by applying equation 2.17 and assuming a very gentle slope (for example 1:10^6). However when using this very mild slope, the equation approaches the equation for horizontal bed velocity. Therefore for the six different researches first the maximum bed velocity is calculated by using equation 2.15:

$$U_{bed,max} = f_p \cdot 0.3 \cdot \frac{D_0}{h_{pb}} \cdot U_0 \tag{2.15}$$

When combining equation 4.2, 4.3 and 2.15, the data can be implemented by the following equation:

$$\frac{h_{sem}}{D_0} = \alpha_2 \cdot \left(\left(0.3 \cdot \frac{D_0}{h_{pb}} \cdot Fr_0 \right)^2 - \frac{\Psi_{cr}}{0.055} \cdot \frac{2}{3} \right)^{\beta_2} \tag{4.4}$$

In this equation all values except the values of α_2 and β_2 are known, the known parameters are listed in table B.3 of appendix B. By using the curve fitting tool box in Matlab the values of α_2 and β_2 are calculated. By implementing the data of the six different researches $\alpha_2 = 0.54$ and $\beta_2 = 0.39$ gives the best fit, however R^2 is only 0.68. The best fit plot is presented in Figure 4-1. The matlab script for this calculation is presented in appendix D. The 95% confidence bounds are also plotted in Figure 4-1.

The lower 95% confidence bound is given by the following equation:

$$\frac{h_{sem}}{D_0} = 0.63 \cdot \left(\left(0.3 \cdot \frac{D_0}{h_{pb}} \cdot Fr_0 \right)^2 - \frac{\Psi_{cr}}{0.055} \cdot \frac{2}{3} \right)^{0.37} - 1.41$$

The upper 95% confidence bound is given by the following equation:

$$\frac{h_{sem}}{D_0} = 0.52 \cdot \left(\left(0.3 \cdot \frac{D_0}{h_{pb}} \cdot Fr_0 \right)^2 - \frac{\Psi_{cr}}{0.055} \cdot \frac{2}{3} \right)^{0.40} + 1.41$$

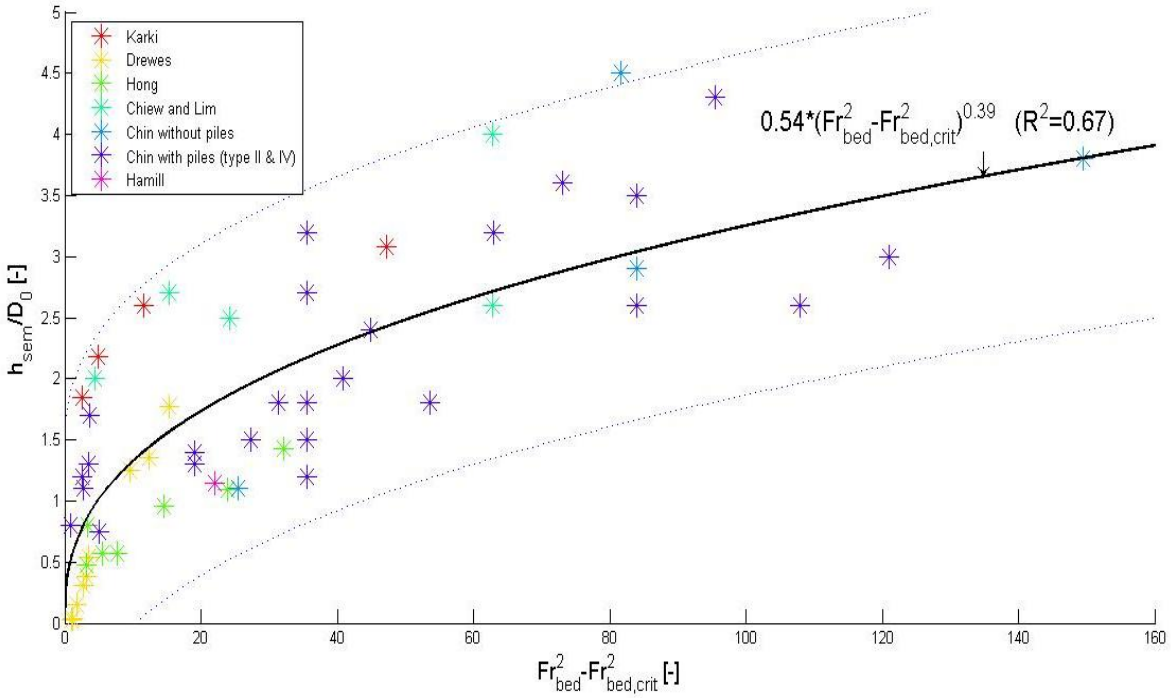

Figure 4-1: Best power law fit for the horizontal bed case without piles (all data points)

In the plot (Figure 4-1) high Fr_{bed} values are used (values of Fr_{bed} up to 17), these high values can only occur for very high bed velocities or small bed material. High Froude values near the bed will induce deep scour holes. In practice very deep holes are probably not desirable and therefore it is assumed that the validation should especially focus on the smaller Froude numbers, for example $Fr_{bed}^2 - Fr_{bed,crit}^2 < 100$.

This master thesis focuses mainly on the propeller induced scour. Therefore also a best fit line is plotted through the propeller data points only (Drewes *et al.*, Hong *et al*. and Hamill). When using only these points, the best fit line is shifted downwards with values of α_2 and β_2 respectively 0.28 and 0.50, furthermore the spreading is less (R^2=0.71) compared with the spreading of all data points. Consequently the 95% confidence bounds are located closer to each other:

Lower boundary:

$$\frac{h_{sem}}{D_0} = 0.39 \cdot \left(\left(0.3 \cdot \frac{D_0}{h_{pb}} \cdot Fr_0 \right)^2 - \frac{\Psi_{cr}}{0.055} \cdot \frac{2}{3} \right)^{0.43} - 0.73$$

Upper boundary:

$$\frac{h_{sem}}{D_0} = 0.23 \cdot \left(\left(0.3 \cdot \frac{D_0}{h_{pb}} \cdot Fr_0 \right)^2 - \frac{\Psi_{cr}}{0.055} \cdot \frac{2}{3} \right)^{0.58} + 0.71$$

The best power law fit and the 95% confidence bounds through the propeller data points are presented in Figure 4-2. In the propeller tests the Fr_{bed} are all below 6, this causes relative small scour depths. Therefore the assumption of only considering the initial bed loads as scour indicator (paragraph 2.4.1) is probably allowed because the changes in the flow field are small in case of a small change in bed level.

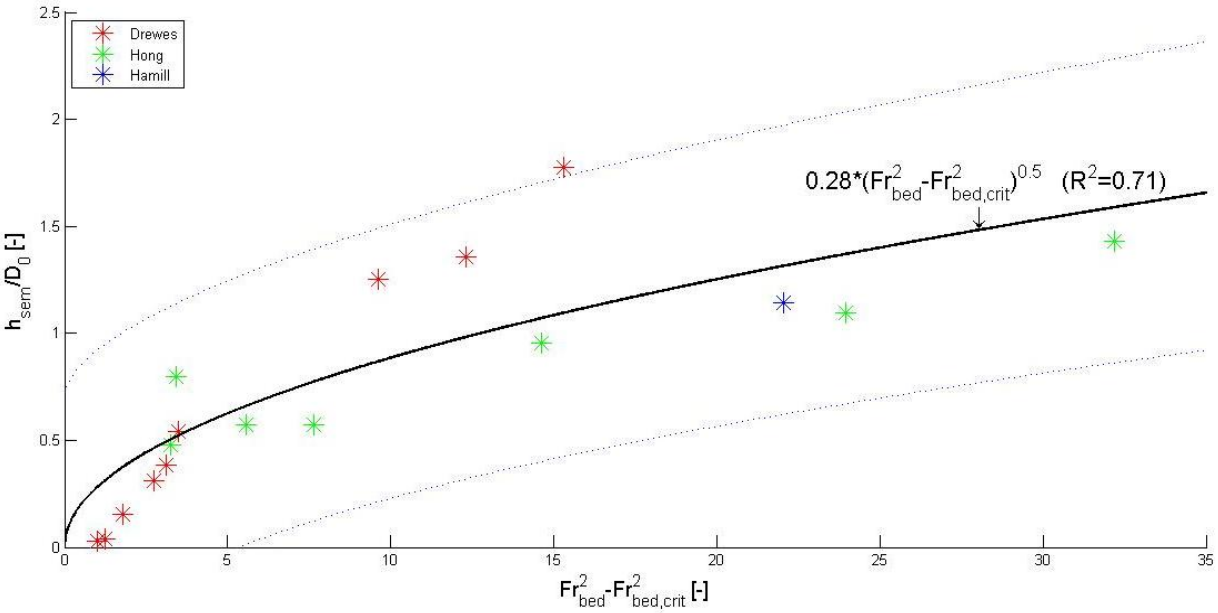

Figure 4-2: Best power law fit for the horizontal bed case without piles (only propeller data points)

For high values of Fr_{bed} the value of $Fr_{bed,crit}$ is negligible because$Fr_{bed}^2 \gg Fr_{bed,crit}^2$.
When the critical value in the proposed equation is neglected, and we fill in the values of $\alpha_2 = 0.28$ and $\beta_2 = 0.50$ it follows that:

$$\frac{h_{sem}}{D_0} = 0.28 \cdot \left(0.3 \cdot \frac{D_0}{h_{pb}} \cdot Fr_0\right)^{1.0}$$

For the case of a propeller just above the bed ($\frac{D_0}{h_{pb}} = 2$), this equation becomes:

$$\frac{h_{sem}}{D_0} = 0.17 \cdot Fr_0$$

This equation is comparable to the equations of (Chin *et al.,* 1996) and (Yüksel *et al.,* 2005). Therefore it is concluded that the proposed equation is valid for the case of a horizontal bed and a propeller just above the bed.

4.3 Comparison with the German and Chiew method

In the proposed equation the jet diameter (D_0) is used to define the dimensionless scour depth. In the German scour prediction method (equation 2.45) the grain size (d_{85}) is used to make the scour dimensionless. When applying the grain size in the proposed equation (equation 3.8) instead of the jet diameter, the data points show a large scatter (Figure 4-3). This scatter shows that in the proposed method the scour could not be made dimensionless by dividing it by the bed material diameter.

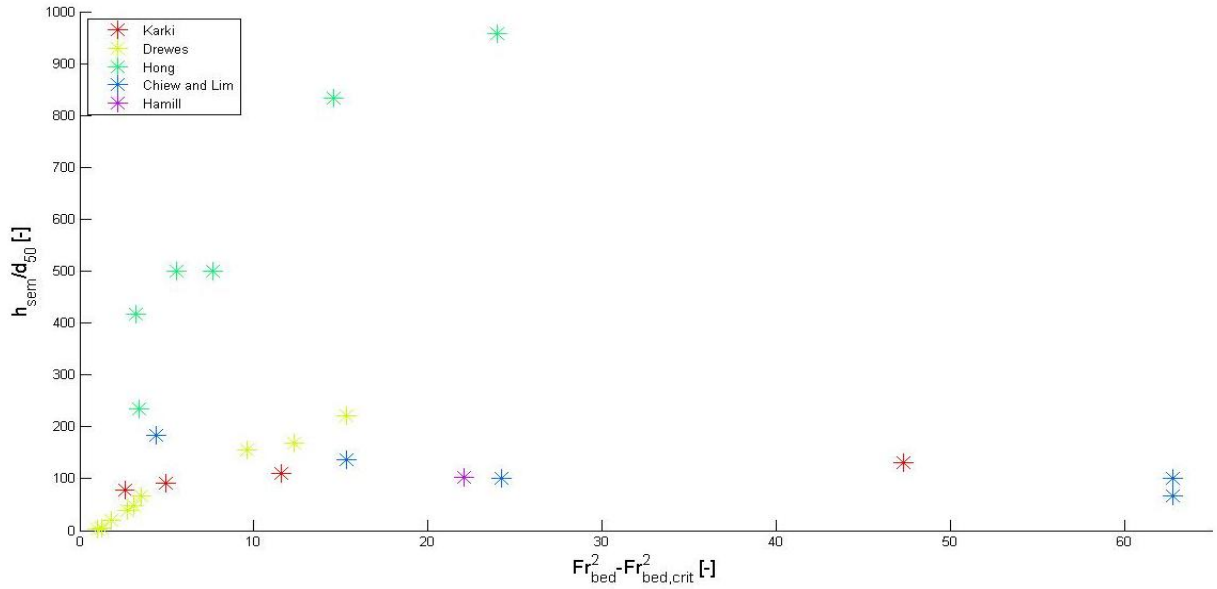

Figure 4-3: scour prediction with dimensionless scour (dividing by d50)

Besides the difference in making the scour depth dimensionless, the German method also uses a different equation set-up, with the densimetric bed Froude number divided by a critical Froude number instead of subtracting the critical Froude number from the densimetric bed Froude number. When the lab experiment scour depths are predicted with both the German method and the newly proposed equation, the results do not show large deviations. The scour prediction method described by (Chiew *et al.*, 2012) (equation 2.44) is also compared with the newly proposed equation and the German method, the results are presented in Figure 4-4. The calculations are described in appendix D.

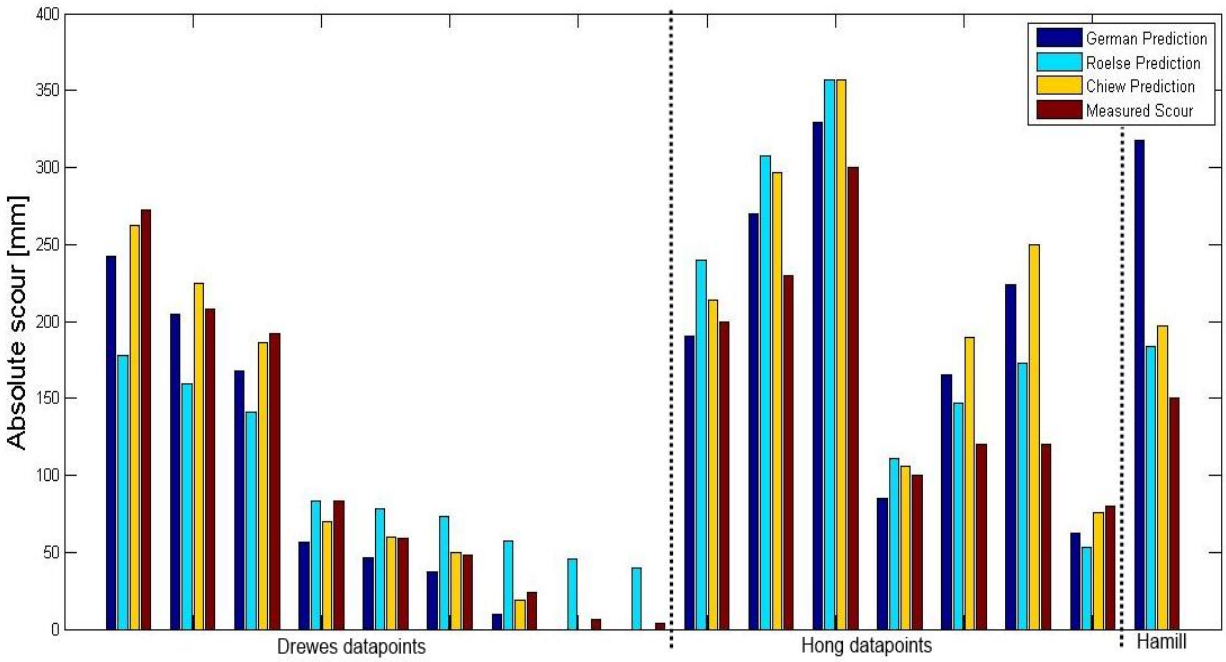

Figure 4-4: comparison of different scour prediction methods

4.4 Validation for a horizontal bed with a single pile

In case of a horizontal bed with a single pile both the jet diffusion mechanism and the pile obstruction mechanism could be present (paragraph 3.3). Two different data sets are available for this case. However because of the lack of information such as pile diameter and distance from the propeller to the pile the dataset of (Chin *et al.*, 1996) could not be used. Therefore only the limited amount of data points given in the (Yüksel *et al.,* 2005) data sets are used to define the value of γ. It is also not possible to define for this dataset the exact location of the pile with respect to the scour hole that is induced by the jet diffusion mechanism. Therefore it is impossible to define the relative contribution of the pile obstruction induced scour on the total maximum scour depth. In this calculation it is assumed that the pile is placed at the location of maximum jet diffusion induced scour, so the total maximum scour depth is calculated by adding the scour depth caused by the pile obstruction diffusion mechanism to the scour depth caused by the jet diffusion mechanism. The value of γ is now calculated by implementing the data from (Yüksel *et al.,* 2005) in the following equation:

$$\frac{h_{sem}}{D_0} = 0.3 \cdot \left(Fr^2_{bed,max} - Fr^2_{bed,crit}\right)^{0.5} + \gamma \cdot K \cdot \frac{D_{pile}}{D_0} \cdot \tanh\left(\frac{h}{D_{pile}}\right) \qquad (4.5)$$

In the case of a single pile the pile group coefficient is equal to 1 and because Yüksel used circular piles and homogeneous sand bed the K-factor reduces to K_u and K_d only. Now it is possible to find the value of γ for different data points. The results for these calculations can be found in appendix D. For all different data points the value of gamma is calculated. The mean value of γ is 1.2.

It is assumed that γ is a constant for all flow velocities, all bed material sizes and all pile diameters. The influence of the slope is assumed to be negligible in the pile obstruction mechanism. In case of different values for α_2 and β_2 the value of γ will also change, because in the calculation the pile obstruction mechanism is defined by subtracting the jet diffusion scour from the total scour.

The values of α_2, β_2 and γ are defined, the total newly proposed equation for the prediction of scour at an open piled quay structure is given by:

$$\frac{h_{sem}}{D_0} = 0.3 \cdot \left(Fr^2_{slope,max} - Fr^2_{slope,crit}\right)^{0.5} + 1.2 \cdot K \cdot \frac{D_{pile}}{D_0} \cdot \tanh\left(\frac{h}{D_{pile}}\right) \qquad (4.6)$$

4.5 Sensitivity analysis of the newly proposed formula

Some assumptions are made to come up with the newly proposed equation (eq. 4.6). These assumptions cause uncertainties and inaccuracies in the scour prediction. In this paragraph the assumptions are described to provide insight in the uncertainties. In chapter 6 a FORM analysis is conducted, this provides insight in the relative contribution to the uncertainties for the different parameters.

4.5.1 Alpha, beta and gamma calculation

There is a lot of scatter in the data for the α_2, β_2 and γ calculation, this will cause a high uncertainty in the use of these coefficients. The extensive overview of inaccuracies in the data sets is described in appendix B.

One assumption made in the validation is the assumed value of the critical Izbash number of 3.0. Another value of $\beta_{Iz,crit}$ will lead to another value of the critical densimetric Froude number. This change will consequently lead to different computed values of α_2 and β_2. However changes in the critical densimetric slope Froude number are only of interest for low values of the densimetric Froude number. Because in the validation of the newly proposed equation also relative high densimetric slope Froude numbers are taken into account, changes in the critical Izbash parameter will not lead to large differences in α_2 and β_2.

Furthermore most data are subtracted from (inaccurate) figures in papers, original measured data points will possibly lead to more accurate data. The best method to reduce the uncertainties is by conducting tests (as described in appendix C), and validate the proposed scour prediction on the data from these tests.

4.5.2 Simplification of the flow field

The flow velocities near the slope are calculated by using the flow distribution by equation 2.17. This flow distribution is based on the flow field of a propeller jet as described by (Blaauw & Van de Kaa, 1978) and not influenced by lateral limitations or bed and water surface influences. However in case of an open quay structure there are restricting boundaries such as the slope and the water surface. Due to the absence of these restricting boundaries in the theoretical calculations, the flow velocities near the slope are underestimated. These underestimated flow velocities cause also underestimated scour depths.

Another simplification of the flow field is caused by the fact that only the initial velocity is used in the scour prediction method. In reality when a scour hole is formed, the flow field will change. This changed flow field causes again different scour patterns etcetera. The flow field development in combination with a developing bed is not taken into account explicitly in this scour prediction.

4.5.3 Equilibrium scour during normative conditions

A main assumption is that the scour is predicted for normative conditions that act for a very long time, so that the maximum equilibrium scour depth is reached. In reality the normative forcing conditions will probably not occur long enough to reach the equilibrium because it is very unlikely that the normative ship will use its bow thrusters during normative conditions (such as water level) for a very long time at the same location. Therefore the predicted maximum equilibrium scour depth will in reality probably never occur.

4.5.4 Absence of deposition in the scour calculation

In the prediction only the scour zone is taken into account, it is unknown where the eroded material is transported to. In reality bed material that is eroded at a certain location, should deposit somewhere else. When deposited material is taken into account, this potentially will reduce the scour depth at certain locations. For design application especially the maximum scour depth is of interest, therefore the situation without deposition calculations can be seen as normative.

4.5.5 Absence of turbulence

At this moment no influence of turbulence is explicitly taken into account for the mobility calculation of the bed material, however turbulence is implicitly incorporated into the equation for the slope

velocities due to the fact that in the flow distribution calculation already the maximum velocities are taken into account. Therefore the implicitly used turbulence leads to a conservative prediction. In order to construct a more accurate method concerning turbulence, it is recommended to use the Hoan mobility parameter, because this parameter will incorporate the influence of the turbulence explicitly. However in practice it is very difficult to use this mobility parameter.

4.5.6 Independency of the jet diffusion- and the pile obstruction mechanism

In the proposed equation it is assumed that the jet diffusion mechanism is not influenced by the presence of piles at the slope. In practice piles will cause changes in the propeller jet and therefore in the jet diffusion scour mechanism. On the other hand, a scour hole caused by the jet diffusion mechanism changes the flow field and has therefore influence on the pile obstruction mechanism.

4.5.7 Absence of 3-dimensional information

In the proposed equation only the scour is calculated for the 2d case, in reality the jet flow has a 3-dimensional character. This can cause sediment transport of bed material in all directions. When assuming the flow distribution as given by equation 2.14 the maximum velocity occurs in the centre line of the jet. At locations further away from the centre line, the flow velocities will decrease, therefore the proposed method, which only takes into account the flow velocities in the propeller axis plane, is normative.

4.5.8 Absence of maximum scour hole slope angle

By executing the proposed equation, no limit is introduced for the maximum slope angle that could occur within the scour hole. In reality the new bed lay out can never have angles larger than the submerged angle of repose of the bed material. When a slope tends to exceed the maximum angle, instabilities occur which will lead to collapsing slopes, causing smaller scour depths because the slope material will fill up the scour hole.

5 Case study

Although there are still a lot of uncertainties within the new scour equation, it can be used as a rough estimation procedure. To examine the applicability of the new developed formula, a case study is conducted. In this study 'Steiger 39' is used as test case. Steiger 39 is a new mooring facility for inland vessels at the 2nd Petroleum haven in Rotterdam (Figure 5-1).

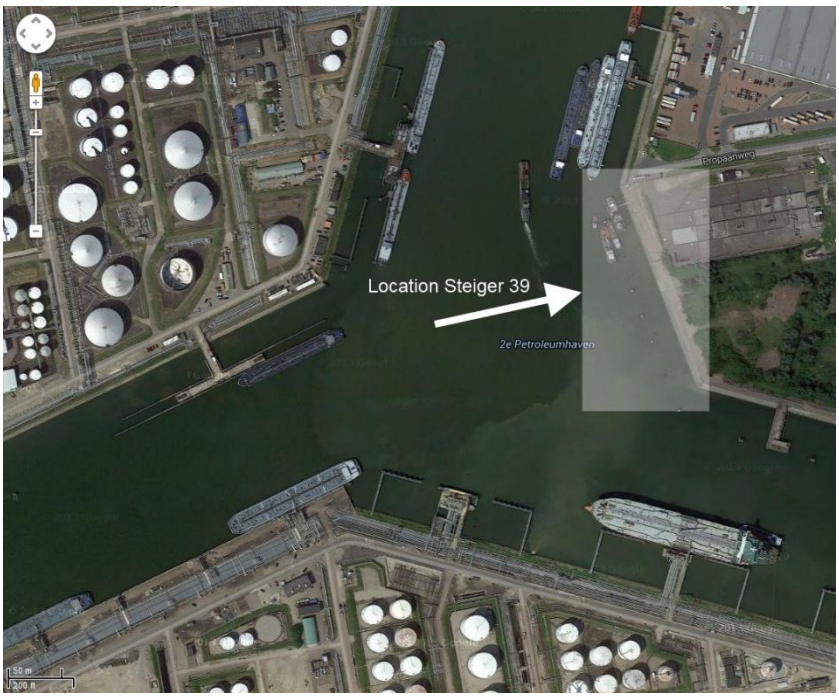

Figure 5-1: 2nd Petroleumhaven with the location of steiger 39 (Google maps)

5.1 Introduction

Havenbedrijf Rotterdam has commissioned in 2012 to demolish the existing mooring place and construct a new mooring structure for inland vessels. The new mooring structure together with the bed protection was designed by Grontmij. During the life cycle cost analysis (LCC) by Grontmij, three different variants were examined:

1. Scour protection at the pile locations and the total slope.
2. Scour protection only around the piles.
3. Unprotected slope.

Variant 3 turned out to be the most cost effective solution (€487*10^3). However this option was not executed due to high uncertainties in the scour prediction calculations. In the final design option 2 (LCC=€554*10^3) was executed. With the newly proposed equation a more accurate scour prediction could be made. Perhaps the new method will lead to lower construction costs and therefore to a more cost effective solution, the new calculation is described in paragraph 5.3.

5.2 Schedule of requirements

The design parameters are described in the schedule of requirements made by Grontmij. This schedule contains both the hydraulic and nautical boundary conditions. In the design drawings the structural layout of the berthing structures are present, such as the slope angle and the position of

the ship with respect to the slope. These drawings are presented in appendix E. For both the original calculations and the new scour prediction equations these data are required.

5.2.1 Hydraulic and nautical boundary conditions

For the design a low water level with a 1% chance of exceeding for all low waters in a year was assumed. This water level will probably occur during 10 to 25 tides per year. Following from the hydro-meteo information at the location of the 1st Eemshaven this design water level is at NAP -0.95m. The minimal guaranteed nautical depth is at NAP -5.65m, however in the design the bottom at the berth location is situated at NAP -6.65m. Therefore the total water depth at design conditions is 5.70m. For the design of the bed protection the inland ship of the CEMT-class Va is normative. Given the draught and the water depth, the keel clearance is approximately 2m. The CEMT-class Va ship has the following characteristics:

Aspect	Value	Unity
Deadweight tonnage	3120	Tons
Water displacement	3900	Tons
Length	110	m
Width	11.45	M
Draught	3.68	m
Height	7.86	m
Maximum mooring velocity	0.25	m/s
Mooring angle	15.0	degree
Main propeller power	1750 (2x875)	kW
Main propeller diameter	1.60	m
Bow thruster power	705	kW
Bow thruster diameter	1.80	m

The diameter of the bow thruster is an important parameter in the scour prediction. In this case the bow thruster is a pumpjet where the propeller outflow opening is located in the bottom of the ship which is probably smaller than the surface of the propeller. Therefore in the calculation the propeller diameter should be smaller. Grontmij uses a propeller diameter of 1.40m during the calculations. For the efflux velocity calculation the original propeller diameter of 1.80m is used. During the case study calculations also the two different propeller diameters are used in order to compare the new calculations with the calculations made by Grontmij.

In the D-sheet pile calculations made by Grontmij (Figure 5-2) it is shown that the upper layer of soil consists of clay. Therefore the proposed equation from this thesis could not be used, because it is only applicable in the case of non-cohesive soils. However when assuming an imaginary stone diameter that has the same critical velocity as given by the Rotterdam harbor authorities for clay (=0.5m/s) it is possible to do the calculations.

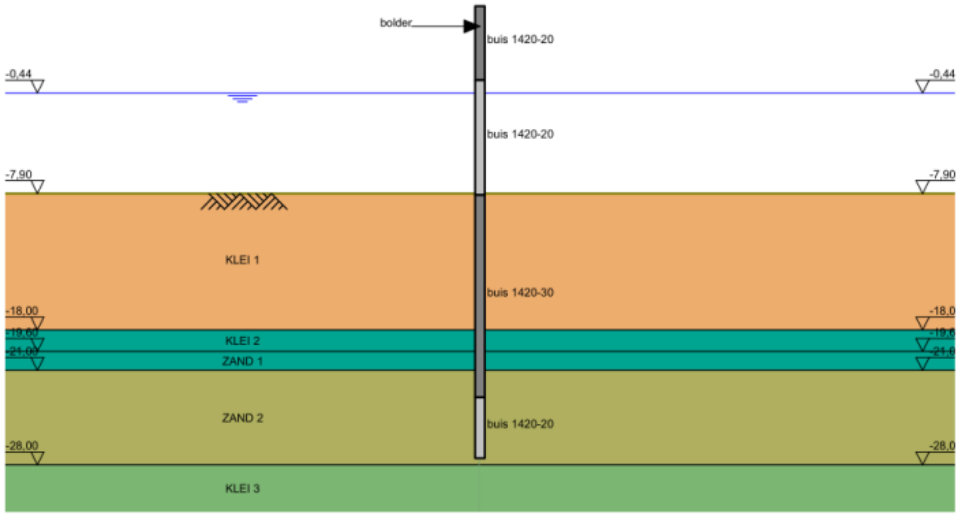

Figure 5-2: soil composition at steiger 39 (source: Grontmij)

5.2.2 Structural layout

The structural layout of steiger 39 is given in the drawings by Grontmij (appendix E).The slope is 1:3. The mooring Dolphin has a diameter of 1420mm and is located at approximately 15m from the intersection of the design water level with the slope. The piles of the gangway have a diameter of 914mm. The ship moors directly against the mooring pile, so the distance between the thruster outflow and the pile is small. Given this layout the distance between bow thruster and slope is approximately 12m. However the distance in the Grontmij calculations is 7.5m.

5.3 Original bed protection calculations

In the bed protection calculation, Grontmij uses the following steps:

1. Calculation of the efflux velocity (equation 2.7)
2. Calculation of the maximum slope velocity (equation 2.17)
3. Calculation of the bed stone size (equation 2.23)

5.3.1 Calculation of the efflux velocity

For the efflux velocity calculation Grontmij uses equation 2.7. But instead of the factor 1.15 the factor 1.17 is used. This results in a efflux velocity of: 6.98m/s.

$$U_0 \approx 1.15 \cdot \left(\frac{f_p \cdot P}{\rho_w \cdot D_0^2} \right)^{\frac{1}{3}} \qquad (2.7)$$

f_p	1
P	705 kW

ρ_w	1025 kg/m^3
D_0	1.8 m

5.3.2 Calculation of the maximum slope velocity

First the location of maximum slope velocity is determined:

$$x_{max} = K \cdot \left(\sqrt{1 + \frac{2}{K}} - 1 \right) \cdot L$$

With: $K = \frac{b}{\alpha_m^2}$

The location of maximum bed velocity is at x_{max}=6.07m. By implementing this location into equation 2.17 it is possible to determine the maximum slope velocity: $U_{slope,max} = 4.13 m/s$.

5.3.3 Calculation of the required stone size

For this calculation equation 2.23 is used. In the equation by Grontmij no slope factor (m_h) is applied, this is a conservative approach because the slope factor will reduce the required stone size.

$$d_{50} > \beta_{Iz,cr} \cdot \frac{u_{slope,max}^2}{2 \cdot g \cdot \Delta} \qquad (2.23)$$

The minimal required stone diameter calculated by this approach is 1.6m. When adding the slope factor ($m_h = 0.75$), the required stone size reduces to 1.2m (still 1-3 ton!). This theoretical computed stone size is assumed to be too large for practical application. Therefore the placed stone grading is much smaller (10-60 kg, d_{50} between 0.26m and 0.31m). The bottom protection is placed over an area of 27m*142m at the open quay structure (see drawings in appendix E). During the life time of the structure some displacements could occur because the stones are according to the calculation not stable during normative conditions, consequently the bed protection is monitored regularly. The scour prediction method estimates a maximum equilibrium scour depth of 1.2m (Figure 5-3) in case of a bedprotection with stones in the 10-60kg grading.

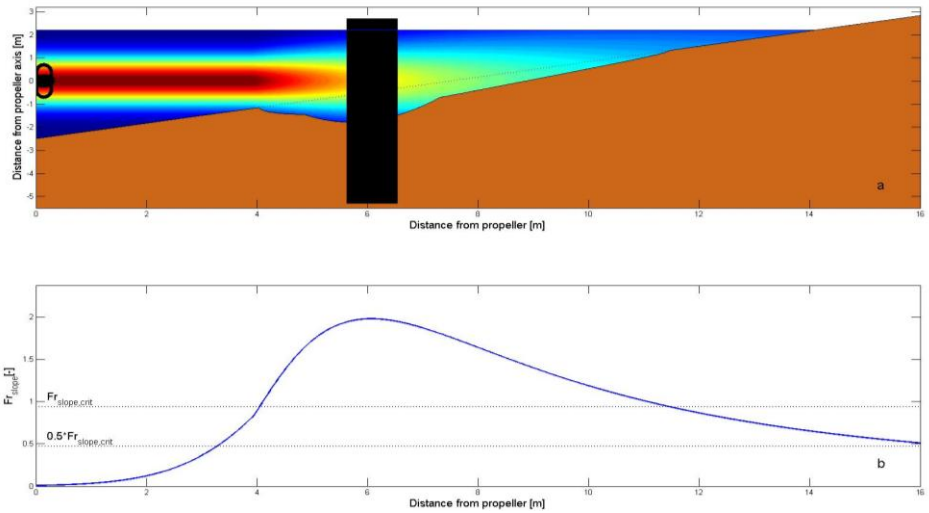

Figure 5-3: Calculated scour case study (d50=0.28m)

5.4 Unprotected slope calculations

When the new method is used to predict the maximum scour depth in case of an unprotected slope, first the size of the bed material has to be determined. In the Rotterdam harbor the bed consists of clay, therefore the newly proposed equation could not be used because it is only valid for non-cohesive bed material. However it is possible to define a stone size which has the same stability as the clay layer. When assuming the maximum velocity of 0.5m/s and filling this in in equation 2.23, the compelling stone diameter for non-cohesive bed material is 0.023m.

When assuming the bed particle diameter of 0.023m as present in the current situation, the maximum equilibrium scour depth during normative conditions, by only assuming the jet diffusion scour mechanism is approximately 2.9m. When adding the pile obstruction mechanism this depth increases to 3.9m (Figure 5-4). The dimensionless scour depth is approximately 3.9/1.4=2.8, which leads to large differences in the flow field over time, making the relation between equilibrium scour depth and initial flow forcing questionable. This approximation is furthermore very questionable because of the clay type of soil and the non-validated approach method that is used.

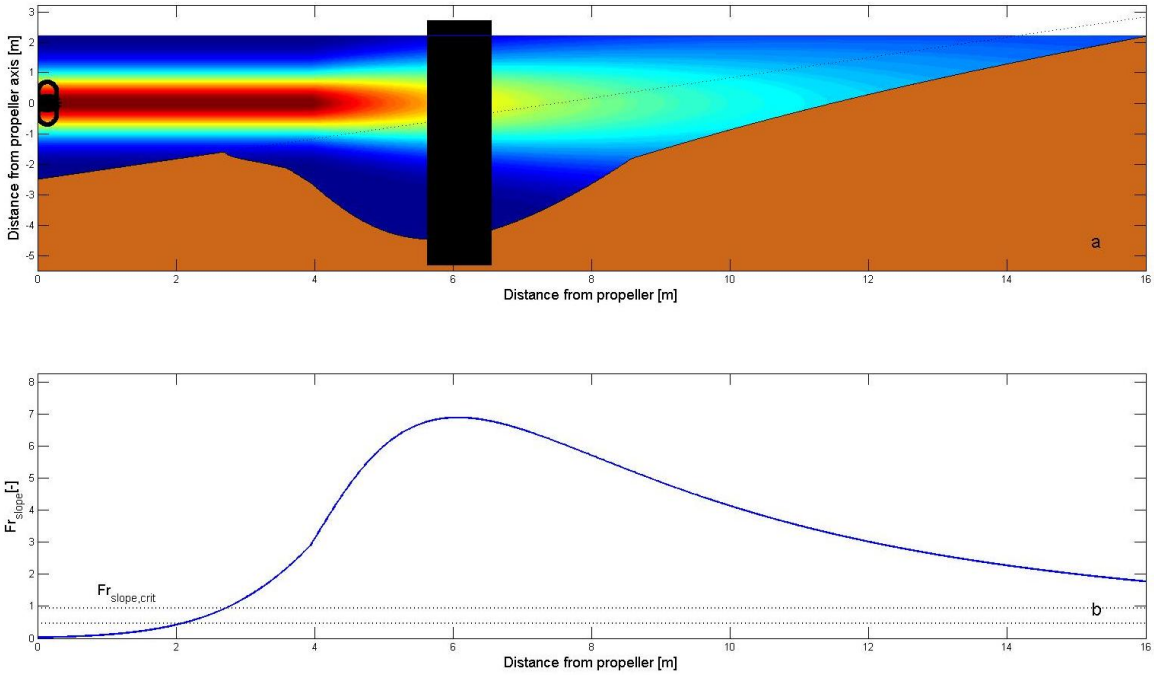

Figure 5-4: Calculated scour case study (d50=0.023m)

5.5 New LCC calculation

With the new scour prediction equation it is possible to redo the LCC calculations for the case of an unprotected slope. By assuming a scour depth of 3.9m and using the Blum method it is possible to define the extra needed pile length and thickness. However because the Blum equation is rather extensive, this method is not completely conducted. In the original calculation the extra pile length needed when scour is allowed is 2m. The assumed scour depth itself is also 2m, therefore it is assumed that for a scour depth of 3.9m the extra pile length is 3.9m as well. The total extra costs of an extra pile length of 2m were $30*10^3$ euro. In case of 3.9 meters extra this will roughly increase up to $60*10^3$ euro. With these extra costs the difference between option 2 (€$554*10^3$) and option 3 ($487*10^3+(60*10^3-30*10^3)$)=€$517*10^3$) is reduced, however option 3 is from economical point of view still the best solution. Though still a large uncertainty in the scour prediction is present.

5.6 Conclusions

During the case study it was noted that in the current design method, very large stone sizes are required to assure stability of the bed material. Therefore in practice often smaller stone sizes are placed, which could result in displacement of bed material during normative conditions. Consequently the bed protection requires frequent monitoring.

In the life cycle cost calculations the extra costs by applying the proposed scour prediction equation are approximately $30*10^3$ euro. Consequently an unprotected slope is from economical point of view still more preferable than the protected slope. However due to uncertainties in the scour prediction, the applied design (option 2) is more reliable.

6 Probabilistic calculation

In both the input parameters and the proposed scour prediction equation there are a lot of uncertain parameters involved. Therefore a probabilistic calculation is conducted to provide insight in the different uncertainties and their possibility of occurrence. In order to define which parameters are important a first order reliability method (FORM) is conducted. FORM is a method to approximate the solutions by means of linearization around a design point. The Z-function and the probability density functions are all described as normal distributions. The probability of failure can be distinguished for a mean value of Z, the standard deviation and the beta value. The design point is the point for which failure probably will occur. It is the point where Z=0 and where the probability density function of the input parameters are at their maximum. When the governing parameters are determined it is possible to include this knowledge in future lab tests.

6.1 Z-function

Failure means that the load at the structure exceeds the strength of the structure. It is possible to express load and strength in a limit state function Z:

Z=S-L

In which S represents the strength of the structure and L represents the load. When Z is smaller than zero, it means that the load exceeds the strength, failure occurs. In order to conduct a probabilistic calculation, a Z-function has to be determined. In this case, the failure probability is defined as the probability that the scour depth is larger than the calculated scour depth:

$$Z = h_{sem,calculated} - h_{sem}$$

The total Z-function for the Steiger 39 case is:

$$Z = 3.9 - \left(C \cdot D_0 \cdot \alpha_2 \cdot \left(Fr^2_{slope,max} - Fr^2_{slope,crit} \right)^{0.50} + \gamma \cdot K \cdot D_{pile} \cdot \tanh\left(\frac{h}{D_{pile}} \right) \right) \qquad (6.1)$$

6.2 Probability density functions

In equation 6.1 a factor C is added because the location of the pile with respect to the jet diffusion induced scour depth is not certain, by adding a factor C the jet diffusion scour mechanism is not totally taken into account. For all independent input parameters a probability function should be entered into the FORM calculation. In this FORM calculation the value of β_2 is taken as a constant (=0.50 in equation 6.1) because α_2 and β_2 are dependent parameters (see appendix D.1). For the other input parameters the following distributions are determined:

Parameter	Parameter	Distribution	Mean value	Standard deviation	Unity	Source
C	Coefficient for the location of the pile	Normal	0.9	0.05	-	Estimation
D_0	Propeller diameter	Normal	1.6	0.1	m	Estimation
ϕ_s	Angle of repose	Normal	35	5	°	(CIRIA, 2007)
α_{slope}	Slope angle	Normal	18.4	2	°	Estimation

α_2	Coefficient	Normal	0.3	0.05	-	Estimated value (Chapter 4)
L	Distance propeller slope	Normal	7.5	0.2	m	Grontmij
ρ_w	Density water	Normal	1015	5	kg/m^3	Grontmij
g	Gravitational acceleration	Deterministic	9.81	-	m/s^2	
d_{50}	Mean grain diameter	Normal	0.023	0.02	m	Estimation
ρ_s	Stone density	Normal	2650	10	kg/m^3	Estimation
γ	Coefficient	Normal	1.2	0.1	-	Chapter 4
D_{pile}	Pile diameter	Deterministic	0.914	-	m	Grontmij
h	Water depth	Normal	2	0.1	m	Estimation
C1	Coefficient in efflux velocity calculation	Normal	1.16	0.02	-	Estimation
P	Thruster power	Normal	705000	20000	W	Grontmij
$\beta_{Iz,crit}$	Critical Izbash coeff.	Normal	3.0	0.3	-	Estimation
Ψ_{cr}	Critical Shields coeff.	Normal	0.055	0.005	-	Estimation

Table 6-1 Used probabilistic density functions in the FORM calculation

6.3 FORM-calculation

The α-values (Table 6-2) computed in the FORM calculation shows the importance of each parameter with respect to the failure of the structure as their contribution to the overall standard deviation. Therefore the FORM method can be used to predict the important parameters during lab tests. The results of the FORM calculation for the steiger 39 case are presented in (Table 6-2), the calculation is described in appendix D.

Parameter	α^2
C	0.13
α_2	0.47
D_0	0.12
d_{50}	0.009
ρ_w	9.5 x 10^{-4}
ρ_s	7.0 x 10^{-4}
F	0.16
α_{slope}	3.6 x 10^{-7}
L	0.03
$\beta_{Iz,crit}$	2.7 x 10^{-5}
ϕ_s	4.7 x 10^{-6}
γ	0.03
D_{pile}	0.01
h	4.5 x 10^{-5}
C1	0.04
P	0.002

Table 6-2: results of the FORM-calculation

The results of the FORM calculation are case dependent. Therefore it is impossible to predict the relative importance of parameters of the proposed equation on the failure mechanism in general. However, it is obvious that the deviation in the α_2-parameter will lead to large uncertainties in the scour prediction during diffusion dominated scouring. The deviation in the γ-parameter is important for pile obstruction dominated scouring. Also the large α^2-value of f is logical because there is still a high uncertainty in the computed slope velocity. When it is possible to predict the maximum slope velocities more accurate, the uncertainty in f is reduced, reducing the failure probability of the entire calculation.

6.4 Conclusions

According to the results of the FORM calculation it can be concluded that the most important parameters are the α_2 and γ parameters, depending on the dominating scour process. When the slope velocity could be predicted more accurate this will also increase the accuracy of the proposed equation. Therefore it is recommended to focus on these three parameters during future lab experiments.

7 Conclusions and recommendations

7.1 Conclusions

In the introduction of this report several research questions are presented. During the research answers on these questions were found. The answers are summarized in this chapter.

How large is the hydraulic load induced by a bow thruster on a slope with piles?
The hydraulic loads caused by a bow thruster consist of both time averaged flow velocities and turbulent flow velocity fluctuations (characterized by turbulence intensities). Time averaged flow velocities can be predicted by using the equation as presented in (van Doorn, 2012), however the proposed values of the correction factor f are not calculated correctly. Therefore it is recommended to recalculate the flow velocities and the turbulence near the slope in the measurements of Van Doorn and to examine the flow velocities and the turbulences near the slope during future tests. Although in reality the turbulence fluctuations near the slope do have a large influence on the scour formation, it is assumed that the maximum scour depth could be calculated given the initial time averaged flow velocities only. This assumption is made because in practice it is very hard to predict the turbulence intensities and their effects on the scour mechanisms. When the hydraulic loads can be determined with more accuracy it is also possible to predict the scour more accurate. Because of the changing flow field characteristics during the scouring process, numerical models could provide more accurate hydraulic load prediction methods.

How do hydraulic loads induced by a thruster current cause scour?
Hydraulic loads could lead to instability of the bed material, which leads to bed material transport. Due to this transport, degradation of the bed occurs and a scour hole is formed. When a pile is located in the flow field, this will induce changes in flow field and therefore induce larger scour depths. Consequently the total scour is caused by two different mechanisms, the first one is the jet diffusion mechanism and the second is the pile obstruction mechanism.

How big is the erosion that occurs on an unprotected or inadequately protected slope with piles due to the hydraulic load of a thruster?
The total equilibrium scour depth is predicted for a calculated initial flow field. In practice the flow field will change due to changes in bed location during the scouring process. This time depended changes in both flow field and bed location are not taken into account during this research. The assumption of predicting the equilibrium scour depth with the initial flow forcing could only be made for relative small changes in bed location, because when large changes in bed location occur, the changes in flow field become also large. The maximum scour depth can be predicted by using the proposed calculation method as described below. This equation is composed of the scour induced by the jet diffusion mechanism and the pile obstruction mechanism. The proposed equation is fitted through data points of lab tests with a horizontal bottom, it is not validated yet for a slope. Future tests should provide this validation.

Summary of the proposed calculation procedure:
1. Calculate the efflux velocity (equation 2.7).
2. Calculate the slope velocities (equation 2.17).
3. Calculate the slope Froude numbers (equation 3.2).
4. Calculate the critical slope Froude number (equation 3.3).
5. Calculate the jet diffusion induced scour (equation 3.4).
6. Add the pile obstruction induced scour (equation 3.5).

The total scour depth prediction formula is given by equation 4.6:

$$\frac{h_{se}}{D_0} = 0.3 \cdot \left(Fr^2_{slope} - Fr^2_{slope,crit}\right)^{0.5} + 1.2 \cdot K \cdot \frac{D_{pile}}{D_0} \cdot \tanh\left(\frac{h}{D_{pile}}\right) \quad (4.6)$$

7.2 Recommendations

The proposed method still contains some uncertainties and inaccuracies, future research should reduce these inaccuracies. In this paragraph the recommendations for future research are described.

7.2.1 Lab experiments

It is recommended to validate the proposed equation by conducting lab tests. During the lab tests the values of the coefficients of the proposed equation (equation 3.8) $\alpha_2, \beta_2, \gamma$ should be found. A possible lab experiment set-up is given in appendix C. It is recommended to measure the development of both the bed location and the flow field in time during the tests. These measurements could help to define a more accurate flow field prediction. Extensive measurements of both flow field and bed location could also help to define an upper limit for the proposed equation (e.g. for which scour depth range is the proposed scour prediction method valid?).

7.2.2 Use more accurate flow field prediction methods

Hydraulic forces are responsible for the scour formation. In order to give a more accurate scour prediction method, the flow velocities and turbulence intensities should be calculated more precisely. In this thesis the method as presented by (van Doorn, 2012) is used to calculate the hydraulic forcing. In this method a correction factor is defined. This correction factor is slope configuration dependent, so only applicable for a limited number of slope configurations. It is recommended to use for future research a more sophisticated method, which is applicable for all slope configurations.

7.2.3 Conduct research in the development of the scour hole

When a scour hole is formed the flow field also changes. The new flow field causes again differences in scouring, etcetera. It is recommended to conduct research concerning this development of the scour hole in time in combination with the flow velocity development. These iterative calculations could be made by using computer modeling.

7.2.4 Validate the extrapolation into the gravel or stone range

The proposed equation is validated by test data from lab experiments with bed material within the sand range. It is assumed that the equation could also be used in the gravel or stone range, because in that case the critical slope Froude number changes. It is recommended to validate this extrapolation by conducting lab tests with bed material in the gravel or stone range.

7.2.5 Validate the proposed equation in the clay range

During the case study an open quay structure with a bed consisting of clay is examined. In order to use the proposed equation (which is applicable for non-cohesive bed materials), an equivalent stone

diameter is defined which has the same critical velocity as the clay bed. Lab experiments with a clay bed should provide the validation of this assumption.

7.2.6 Use data from monitoring procedures

Not only lab experiments could provide data for the validation of the proposed equation, also monitoring of existing open quay structures could provide data. However, in practice the equilibrium scour depth may not be reached. Therefore it is important to have data available concerning ship berthing locations and the number of ships that have used the berthing facilities. Equilibrium scour could only be approached after multiple ship moorings at the same location at the quay structure.

References

Albertson, M., Dai, Y., Jensen, R., & Rouse, H. (1948). Diffusion of submerged jets. *ASCE Transactions* , 648-697.

Blaauw, H., & Van de Kaa, E. (1978). *Erosion of bottom and sloping banks caused by the screwrace of maneuvering ships, publication 202.* Delft: Delft Hydraulics laboratory.

Chiew, Y., & Lim, S. (1996). Local scour by a deeply submerged horizontal circular jet. *J. Hydraulic Eng.* , 529-532.

Chiew, Y., Hong, J., Susanto, I., & Cheng, N. (2012). International Congres on Scour and Erosion. *Local scour by offset and propeller jets*, (pp. 949-956). Paris.

Chin, C., Chiew, Y., Lim, S., & Lim, F. (1996). Jet scour around vertical pile. *J.l of waterway, port, coastal, and ocean eng.* (2), 59-67.

CIRIA, CUR, CETMEF. (2007). *The rock manual.* London: CIRIA.

Drewes, U., Römisch, K., & Schmidt, E. (1995). *Propellerstrahlbedingte Erosionen im Hafenbau und Möglichkeiten zum Sohlschutz fur den Ausbau des Burchardkais im Hafen Hamburg.* TU Braunschweig. Braunschweig: TU Braunschweig.

Fuehrer, Römisch, & Engelke. (1977). Effects of modern ship traffic on islands and ocean waterways and their structures. *Proceedings 24th PIANC Congress,* (pp. 187-198). Leningrad: PIANC.

FWHA. (2001). *Evaluating scour at bridges.* National Highway Institute. Springfield: National technical information service.

Gemeentelijk Havenbedrijf Rotterdam. (1997). *Informatiebulletin (info 7).* Rotterdam: Gemeentelijk havenbedrijf Rotterdam.

Hamill, G. (1987). *Characteristics of the screw wash of a manoeuvring ship and the resulting bed scour.* Belfast: The Queen's University of Belfast.

Hoan, N. (2008). *Stone stability under non-uniform flow (PhD Thesis).* Delft: Delft University.

Hoffmans, G., & Verheij, H. (1997). *Scour Manual.* Rotterdam: Balkema Publishers.

Hofland, B. (2005). *Rock & Roll, turbulence-induced damage to granular bed protections (PhD thesis).* Delft: Delft University.

Hong, J.-H., Chiew, Y.-M., Susanto, I., & Cheng, N.-S. (2012). International Conference on scour and erosion. *Evolution of scour induced by propeller wash*, (pp. 831-838). Paris.

Jongeling, T., & Blom, A. (2003). *Project steenstabiliteit WBKI2003, verslag studie (in Dutch).* Delft: Delft Hydraulics.

Karki, M., Faruque, M., & Balachandar, R. (2007). Local scour by submerged offset jets. *Proceedings of the institution of Civil Engineers (paper 14567)* , 169-179.

Melville, B., & Chiew, Y.-M. (1999). Time scale for local scour at bridges. *Journal of hydraulic eng. , 1999* (1), 59-65.

Olthof, J. (2002). *PAO cursus belastingen door scheepvaart (in Dutch).* Delft: Stichting postacademisch onderwijs.

PIANC. (2013). *guidelines for scour at berthing structures, related to thrusters (Draft).* Brussels: PIANC.

PIANC. (1997). *guidelines for the design of armoured slopes.* Brussels.

Römisch, K. (2012). *Durch Schifspropeller verursachte Kolkbildung (In German).* HANSA, no.9.

Römisch, K. (2006, November). Erosion potential of bow thrusters on canal banks (In German). *Binnenschifffahrt* , 8-12.

Roubos, A. (2006). *Omgaan met onzekerheden bij het ontwerpen van bodembescherming nabij kademuren (MSc thesis, in Dutch).* Delft: Delft University.

Schiereck, G. (2007). *Concise overview of scale rules in coastal engineering.* Hanoi.

Schiereck, G. (2004). *Introduction to bed, bank and shor protection, engineering the interface of soil and water.* Delft: Delft University Press.

Schokking, L. (2002). *Bowthruster-induced damage (MSc thesis).* Delft: Delft University.

Shields, A. (1936). *Anwendung der Aehnlichkeitsmechanik und der turbulenzforschung auf die Geschibebewegung.* Berlin: Preussischen Versuchsanhalt fur Wasserbau und Schiffbau.

Van Doorn, R. (2012). *Bow thruster currents at open quay constructions on piles (MSc thesis).* Delft: Delft University.

Van Velzen, G. (2012). *Flexibel scour protection around cylindrical piles (MSc thesis).* Delft: TU Delft.

Verheij, H. (1985). *Aantasting van dwarsprofielen in vaarwegen, schroefstralen en de stabiliteit van bodem en oevers onder invloed van de stroomshelheden van de schroefstraal. (in Dutch).* Delft: Delft Hydraulics.

Yüksel, A., Celicoglu, Y., Cevik, E., & Yüksel, Y. (2005). Jet scour around vertical piles and pile groups. *Ocean Engineering 32* , 349-362.

List of figures

List of symbols

A	Coefficient (=2.8) in equation2.17	[-]
b	Coefficient (=15.43) in equation 2.17	[-]
B	Cross section width	[m]
B_s	Ships beam	[m]
C	Chezy coefficient	[$m^{0.5}$/s]
C_{ad}	Correction factor (in equation 2.45)	[-]
C_{mr}	Rudder angle and maneuvering correction factor (in equation 2.45)	[-]
C_2	Coefficient (in equation 2.12)	[-]
C_5	Coefficient for spreading of the jet (=0.3) in equation 2.15	[-]
d	Characteristic stone diameter	[m]
d_{50}	Diameter of the stone that exceeds the 50% value of the sieve curve	[m]
d_{85}	Diameter of the stone that exceeds the 85% value of the sieve curve	[m]
d_{n50}	Median nominal stone diameter	[m]
D	Deposition rate	[m/s]
D_P	Propeller diameter	[m]
D_{pile}	Pile diameter	[m]
$D_{thruster}$	Bow thruster diameter	[m]
E	Entrainment rate	[m/s]
f	Factor for slope configuration	[-]
f_p	Used percentage of installed engine power	[-]
Fr	Froude number	[-]
Fr_0	Densimetric Froude number (efflux velocity)	[-]
Fr_{slope}	Densimetric Froude number (slope velocity)	[-]
g	Gravitational acceleration	[m/s^2]
h_0	Water depth	[m]
h_{pb}	Distance between propeller axis and bed	[m]
h_{sem}	Maximum equilibrium scour depth	[m]
H	Turbulence influence region	[m]
k	Kinetic turbulence energy	[m^2/s^2]
k_h	Velocity profile factor	[-]
k_r	Equivalent roughness	[m]
k_{sl}	Slope factor	[-]
k_t	Turbulence factor	[-]
K_g	Pile group correction factor	[-]
K_{gr}	Sediment graiding correction factor	[-]
K_i	Correction factor	[-]
K_u	Velocity correction factor	[-]
K_s	Pier shape correction factor	[-]
K_T	Propeller thrust coefficient	[-]
l	Entrainment length	[m]
L	Axial distance between slope and the propeller plane	[m]
Lm	Bakhmetev mixing length	[m]
L_s	Length ship	[m]
m_h	Slope stability factor	[-]

n	Number of particles	[-]
n_p	Rotation speed of propeller	[s^{-1}]
p	Turbulence multiplication factor	[-]
P	Engine power	[kW]
$P_{thruster}$	Bow thruster power	[kW]
q_s	Bed load transport per section width	[m^2/s]
r	Distance from propeller axis	[m]
r_u	Relative turbulence	[-]
R	Hydraulic radius	[m]
T	Time step	[s]
T_s	Draught ship	[m]
U_0	Efflux velocity	[m/s]
U'	Turbulent velocity fluctuation	[m/s]
$\overline{U}$	Mean flow velocity	[m/s]
U_*	Shear velocity	[m/s]
$U_{b,max}$	Maximum bed velocity (horizontal bed)	[m/s]
U_c	Critical flow velocity	[m/s]
$U_{slope,max}$	Maximum bed velocity (sloping bed)	[m/s]
$U_{x,max}$	Maximum axial flow velocity	[m/s]
x	Distance from propeller plane in axial direction	[m]
$x_{jd,min}$	Axial distance to the location of the start of the jet diffusion zone	[m]
$x_{jd,max}$	Axial distance to the location of the end of the jet diffusion zone	[m]
x_{pile}	Axial distance between the pile and the propeller plane	[m]
$x_{u,max}$	Axial distance location of maximum flow velocity	[m]
z_b	Distance from bed	[m]
Δz_b	Bed degradation	[m]

List of Greek symbols:

α	Slope angle	[°]
α_1	Coefficient (in equation3.1)	[-]
α_2	Coefficient (in equation 3.4)	[-]
β_1	Coefficient (in equation 3.1)	[-]
β_2	Coefficient (in equation 3.4)	[-]
$\beta_{Iz,crit}$	Critical Izbash coefficient	[-]
γ	Coefficient (in equation 3.5)	[-]
Δ	Relative density	[-]
ϵ	Porosity	[-]
κ	Von Karman constant	[-]
ν	Kinematic viscosity	[m^2/s]
τ_b	Bed shear stress	[N/m^2]
ϕ	Stability correction factor	[-]
ϕ_s	Angle of repose	[°]
Φ	Transport parameter	[-]
ρ_w	Water density	[kg/m^3]
ρ_s	Stone density	[kg/m^3]
σ	Standard deviation	[-]

Θ_u	Angle of velocity component	[°]
Ψ	Mobility parameter	[-]
Ψ_{cr}	Critical mobility parameter or stability parameter	[-]

Appendices

Appendix A Extension of the slope velocity equation to the horizontal bed

In the master thesis of Rory van Doorn (2012) an equation is proposed to define the maximum velocity at the slope, this equation is derived from the flow distribution as given by (Blaauw & Van de Kaa, 1978). Van Doorn validated this flow distribution for a limited number of slopes. Therefore it is questionable whether or not the equation as given by van Doorn is applicable in practice and if it is applicable for all slope angles. In this appendix the applicability for the van Doorn equation is investigated.

A.1 Flow distribution

In literature a method to define the flow distribution behind a propeller jet in the zone of established flow ($\frac{x}{D_0} > 2.8$) is determined by (Blaauw & Van de Kaa, 1978)

$$U_{x,r} = U_{x,max} \cdot \exp\left[-15.43 \cdot \left(\frac{r}{x}\right)^2\right] \tag{2.14}$$

By assuming this distribution it is possible to determine the horizontal velocity at every point within the zone of established flow. Figure A-1 shows the flow distribution that follows from this equation. In this figure the lines with equal velocities are calculated, the values in the lines give the proportion of the efflux velocity, so a line with 0.1 means that at this line the flow velocity is 0.1*U_0.

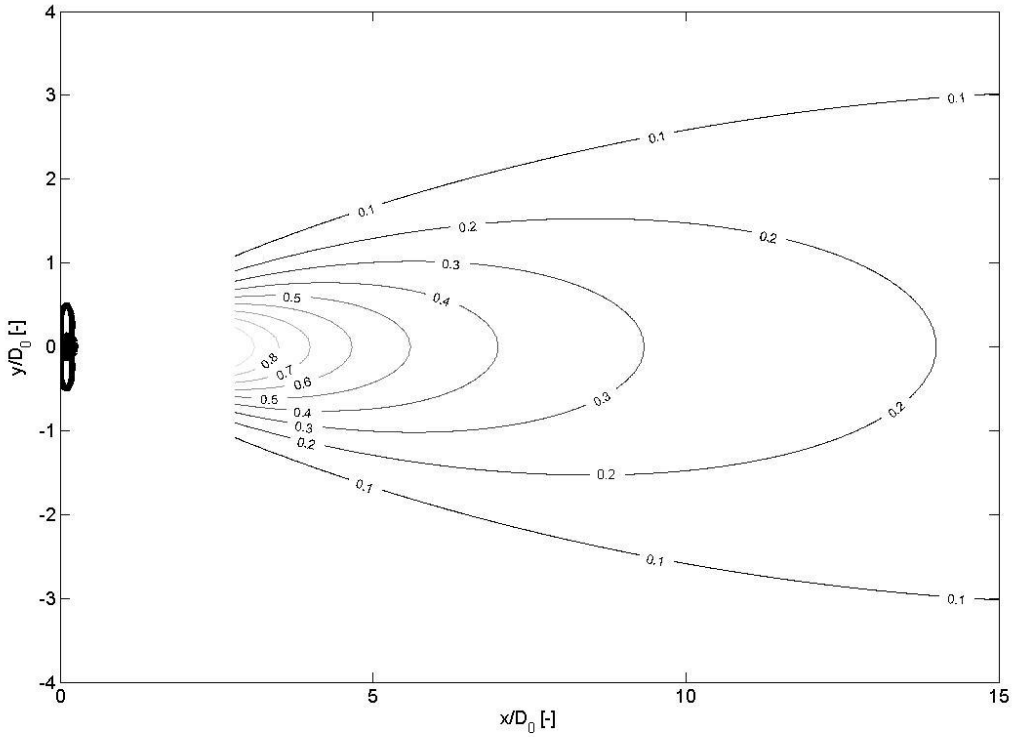

Figure A-1: Established flow field according to Blaauw & van de Kaa, 1978

A.2 Maximum bed velocity at a horizontal bed

When assuming a horizontal bed at a distance h_{pb} from the a propeller (for example the upper plot in Figure A-3, with $h_{pb} = 2 \cdot D_0$), the flowfield distribution as given by (Blaauw & Van de Kaa, 1978) provides a method to determine the flow distribution at the bed (Figure A-3 bottom plot), by filling in $r = h_{pb}$ in equation (2.14). When differentiating the bed velocity, it is possible to define the maximum horizontal velocity near the bed:

$$U_{x,r} = 2.8 \cdot U_0 \cdot \left(\frac{x}{D_0}\right)^{-1.0} \cdot \exp\left(-15.4 \cdot \left(\frac{r}{x}\right)^2\right) \quad \text{for } x > 2.8 \cdot D_0$$

$$U_{x,r} = a \cdot U_0 \cdot \left(\frac{D_0}{x}\right)^{m} \cdot \exp\left(-b \cdot \left(\frac{r}{x}\right)^2\right) \quad \text{for } x > 2.8 \cdot D_0$$

$$\left.\frac{\partial U}{\partial x}\right|_{r=h_{pb}} = 0 \Rightarrow -m \cdot \left(\frac{D_0}{x}\right)^{m} \cdot \frac{1}{x} \cdot \exp\left(-b \cdot \left(\frac{h_{pb}}{x}\right)^2\right) - \left(\frac{D_0}{x}\right)^{m} \exp\left(-b \cdot \left(\frac{h_{pb}}{x}\right)^2\right) \cdot (-2) \cdot (-b) \cdot \left(\frac{h_{pb}}{x}\right)^2 \cdot \frac{1}{x} = 0$$

$$\Rightarrow 2b \cdot \left(\frac{h_{pb}}{x}\right)^2 = m \Rightarrow x = \sqrt{\frac{2b}{m}} \cdot h_{pb}$$

$$\frac{U_{b,max}}{U_0} = \underbrace{a \cdot \left(\frac{1}{\sqrt{2b/m}}\right)^{m} \cdot \exp\left(\frac{-m}{2}\right)}_{=C_5} \cdot \left(\frac{D_0}{h_{pb}}\right)^{m}$$

$$C_5 = a \cdot \left(\frac{m}{2 \cdot e \cdot b}\right)^{m/2} \approx a \cdot \left(\frac{m}{5.43 \cdot b}\right)^{m/2}$$

If: m=1 ; b=15.4 , then $x = 5.55 \cdot h_{pb}$
and a = 2.8 , then $C_5 = 0.306$

Figure A-2: Calculation of the maximum bed velocity, (Van Doorn, 2012)

The maximum bed velocity is now given by:

$$U_{b,max} = f_p \cdot C_5 \cdot \frac{U_0 \cdot D_0}{h_{pb}}$$

For f_p=1:

$$U_{b,max} = 0.3 \cdot \frac{U_0 \cdot D_0}{h_{pb}} \qquad (2.15)$$

The differentiation shows that the location of maximum velocity is located at $x = 5.55 \cdot h_{pb}$. The red circle in Figure A-3 marks the location of maximum bed velocity. Free water jets have a less diffusive character compared with a propeller jet. Therefore the coefficients a and b as presented in Figure A-2 are different for a free jet. (Albertson *et al.,* 1948) suggests for a free jet: a=6.5 and b=69. In case of a free water jet with these coefficients, the location of maximum velocity is at $x = 11.7 \cdot h_{pb}$. The maximum bed velocity is a bit larger compared with the propeller maximum bed velocity ($C_5 = 0.32$ instead of 0.306).

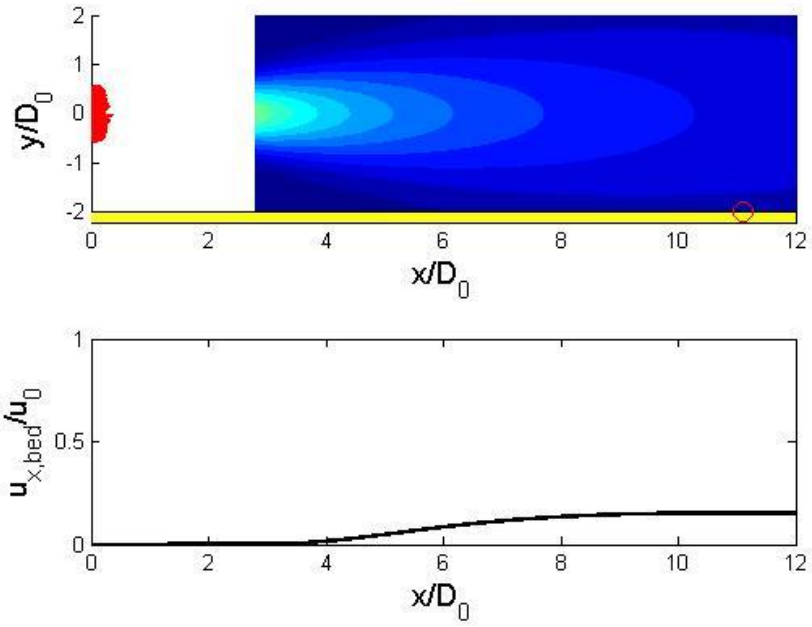

Figure A-3: flow distribution at horizontal bed

The calculated values of the maximum location of the bed velocity and the maximum bed velocity are calculated by the matlab script (appendix D) are listed in Table A-1. The calculated values confirm the validity of equation 2.15 for the horizontal bed case.

Slope	X,bed,max [m]	xmax/hpb [-]	ubedmax/u0 [-]
Horizontal bed	11,1	5,55	0,153006

Table A-1: calculated values for hpb=2*D0 and D0=1m

A.3 Maximum bed velocity at a slope

As in the case of a horizontal bed, it is also possible to define the flow distribution at sloping bed by using equation 2.17. When differentiating the velocity at the slope the maximum velocity can be determined:

$$z = \frac{1}{\alpha_m}(L - x) = \frac{L}{\alpha_m}\left(1 - \frac{x}{L}\right)$$

$$\Rightarrow \quad \frac{z}{L} = \frac{1}{\alpha_m} \cdot \left(1 - \frac{x}{L}\right)$$

and $\frac{z}{x} = \frac{1}{\alpha_m} \cdot \left(\frac{L}{x} - 1\right)$

$$U_{x,z} = \quad a \cdot U_0 \cdot \left(\frac{D_0}{L} \cdot \frac{L}{x}\right)^m \cdot \exp\left(-\frac{b}{\alpha_m^2} \cdot \left(\frac{L}{x} - 1\right)^2\right)$$

$$\left.\frac{\partial U}{\partial x}\right|_{r=z} = 0 \quad \Rightarrow \quad -m \cdot x^{-m-1} + x^{-m} \cdot (-2) \cdot \frac{b}{\alpha_m^2} \cdot \left(\frac{L}{x} - 1\right) \cdot \frac{-L}{x^2} = 0$$

$$\Rightarrow \quad +2 \cdot \frac{b}{\alpha_m^2} \cdot (L - x) \cdot \frac{L}{x^2} = m \quad \Leftrightarrow \quad \frac{1}{2} \cdot \frac{m \cdot \alpha_m^2}{b} \cdot \left(\frac{x}{L}\right)^2 = 1 - \frac{x}{L}$$

$$\Rightarrow \quad \frac{x_{max}}{L} = K \cdot \left(\sqrt{1 + 2/k} - 1\right) \quad \text{with} \quad K = \frac{b}{m \cdot \alpha_m^2}$$

If: b = 15.4 ; m = 1 ; α_m = 1.5 ; K = 6.844 ; $\frac{x_{max}}{L} = 0.936$;

$\frac{z}{L} = 0.0427$; $\frac{z}{x_{max}} = 0.0456$; a = 2.8

Then: $U_{b,max} = a \cdot \frac{U_0 \cdot D_0}{L} \cdot \frac{0.9685}{0.9360} = 1.035 \cdot a \cdot \frac{U_0 D_0}{L}$

$$U_{b,max} = 2.897 \cdot \frac{U_0 \cdot D_0}{L} \quad \text{if a = 2.8}$$

Figure A-4: Calculation of the maximum slope velocity, (Van Doorn, 2012)

In lab tests conducted by (Van Doorn, 2012) the applicability of the method as described in Figure A-4 is examined. Van Doorn concluded that the values of the maximum velocity are higher in practice than as calculated by this method. Therefore he added a correction factor (f) to this equation. Different values of the correction factor are defined for the test set-up as used in the lab tests by van Doorn. The value of f depends on the slope angle, the pile alignment and the slope roughness. Because van Doorn used only a limited number of test set-ups the values of f as calculated by van Doorn are also only applicable on a limited range of calculations.

$$U_{slope,max} = \mathrm{f} \cdot A \cdot \left(\frac{D_0}{L} \cdot \frac{L}{x_{U,max}}\right)^a \cdot U_0 \cdot \exp\left[-b \cdot \left(\frac{\frac{L}{x_{U,max}} - 1}{cot(\alpha)}\right)^2\right] \tag{2.17}$$

By examination of the data of van Doorn it is discovered that in the data processing van Doorn made a calculation mistake. Consequently the values of f should be smaller than given in PIANC(2013).

Due to the limited range of the correction factors defined by van Doorn, combined with the errors made in the determination, it is recommended to not use these values. Therefore in the calculation in this report the value of f=1 is assumed. More research into the flow field at a slope with piles, should give a more accurate method to define the f-factor for the entire range of slopes and pile alignments.

Figure A-5 to Figure A-9 show the numerical calculation of the velocity distribution at different slopes ($h_{pb} = 2 \cdot D_0$). Where h_{pb} is the distance between the propeller axis and the bed at the location of the propeller plane (x=0). For all figures the location of the maximum bed velocity is marked with a red circle. The calculated values are listed in Table A-2.

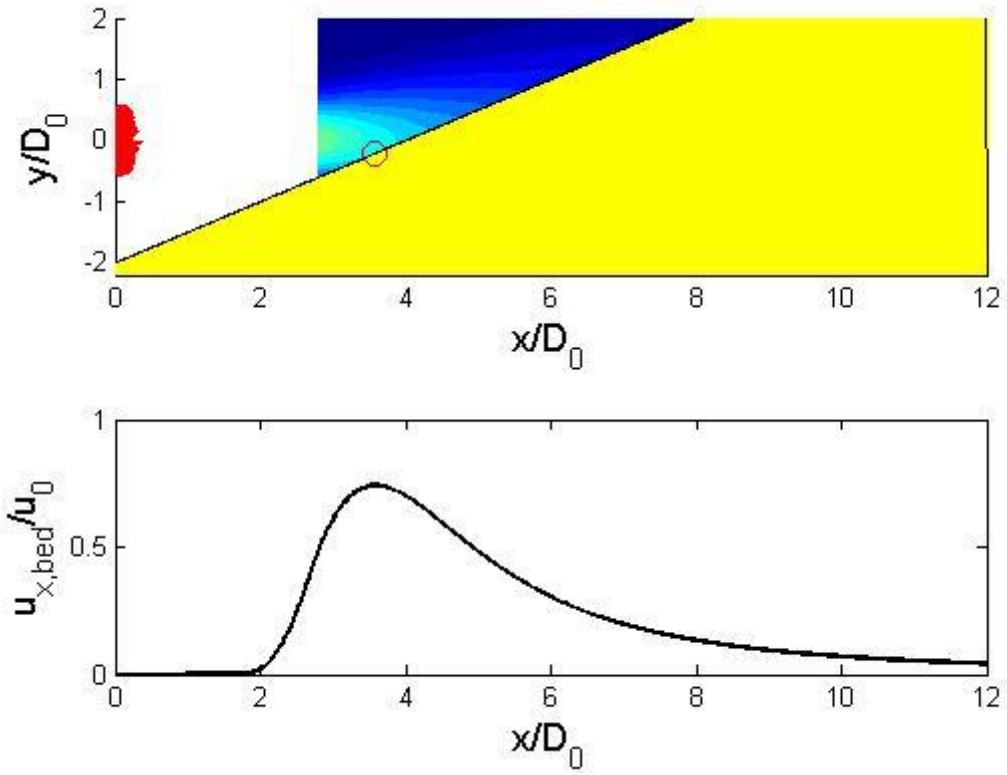

Figure A-5: Flow distribution at a 1:2 slope

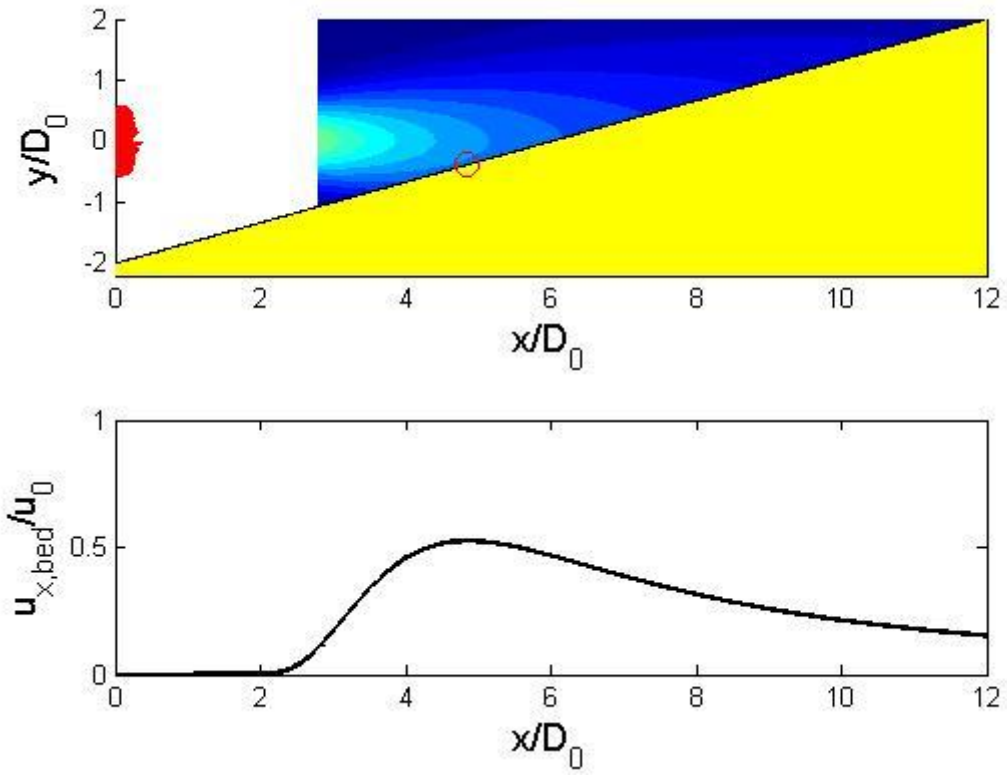

Figure A-6: flow distribution at a 1:3 slope

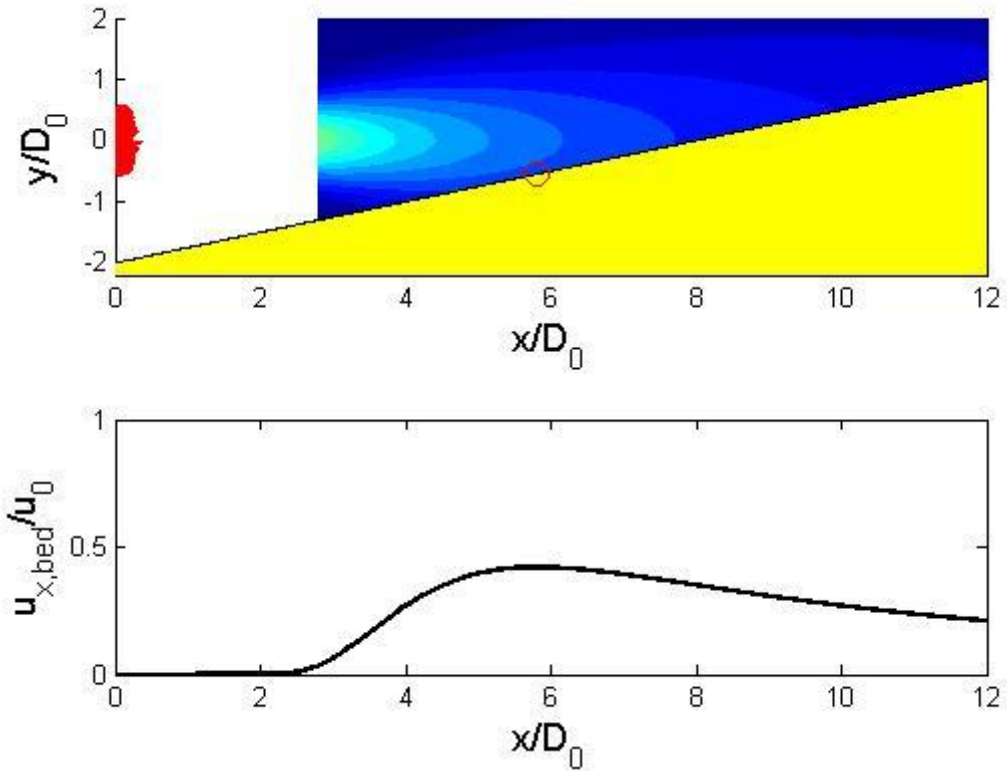

Figure A-7: Flow distribution at a 1:4 slope

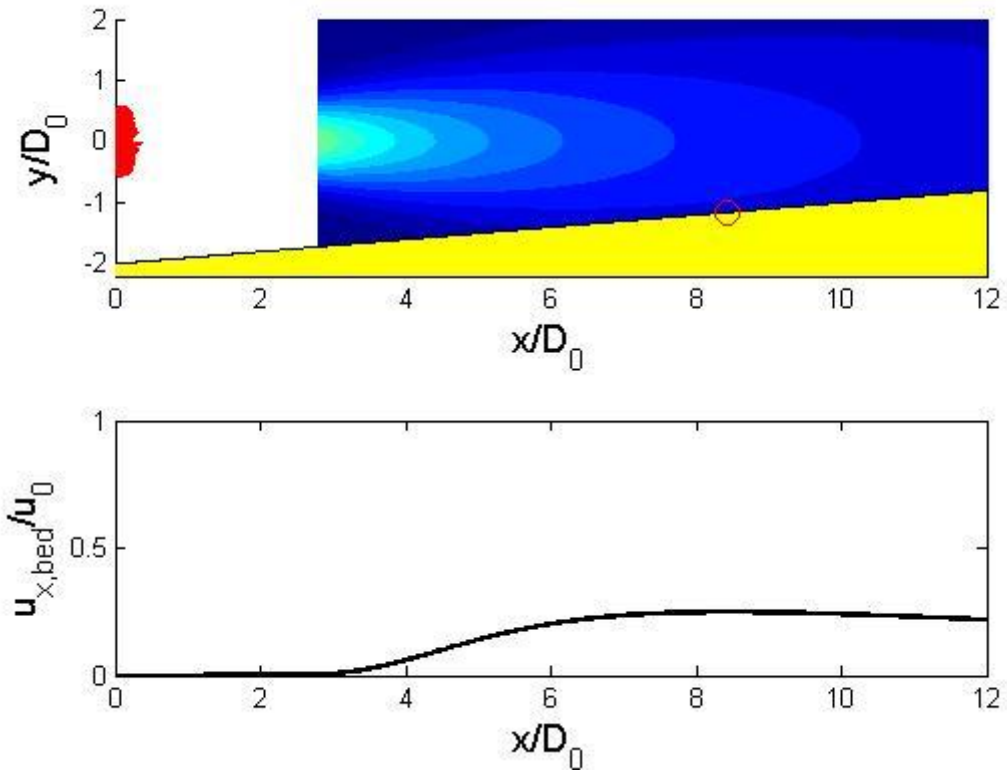

Figure A-8: flow distribution at a 1:10 slope

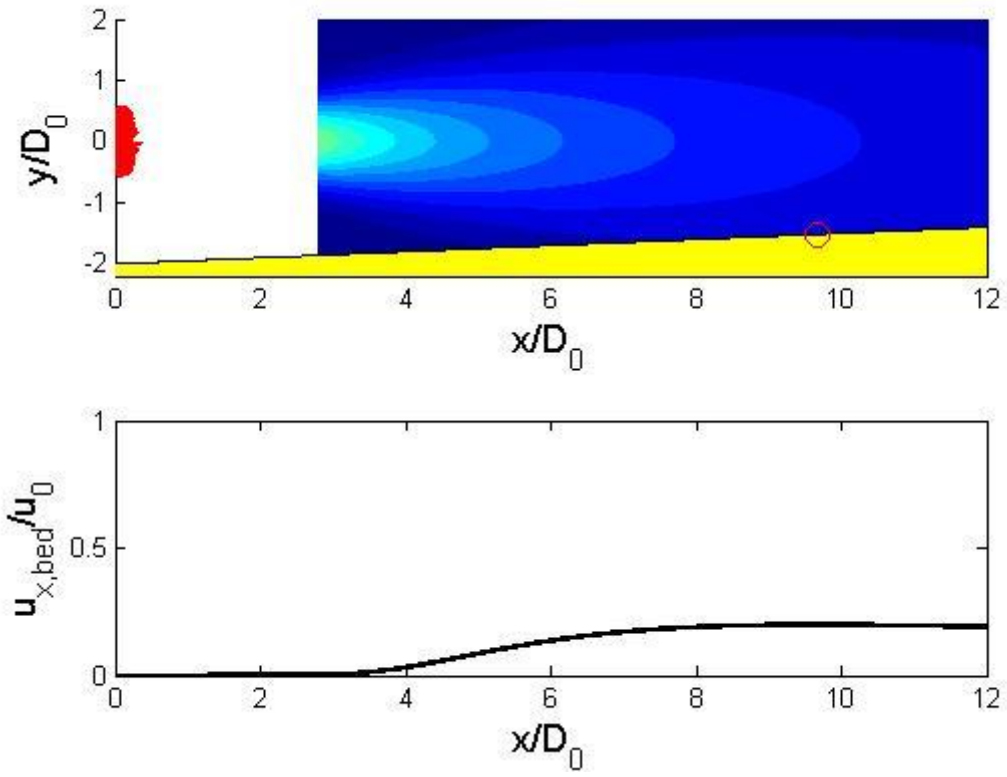

Figure A-9: flow distribution at a 1:20 slope

Slope (1:α_m)	$x_{slope,max}$	$\frac{x_{slope,max}}{h_{pb}}$	$\frac{u_{slope,max}}{u_0}$	$\frac{u_{b,max}}{u_{slope,max}}$
2	3,58	1,79	0,741757	0.21
3	4,85	2,425	0,524367	0.29
4	5,81	2,905	0,42033	0.36
10	8,44	4,22	0,248512	0.62
20	9,67	4,835	0,198263	0.77

Table A-2: Combining calculated data from figures 1-5 to 1-9

The values of $\frac{x_{slope,max}}{h_{pb}}$ show an increasing trend for a decreasing slope steepness. For a slope approaching a horizontal bed (for example slope 1:100) the horizontal location of maximum slope velocity approaches the location as computed for the horizontal bed (x_{max} =5.55h_{pb})(Figure A-10). In the last column of Table A-2 the calculated maximum velocity near the bed is calculated with the method for a horizontal bed (equation 2.15) and divided by the method for the sloping bed (equation 2.17). There is still a large difference between the two methods for a mild slope (for example 1:10).

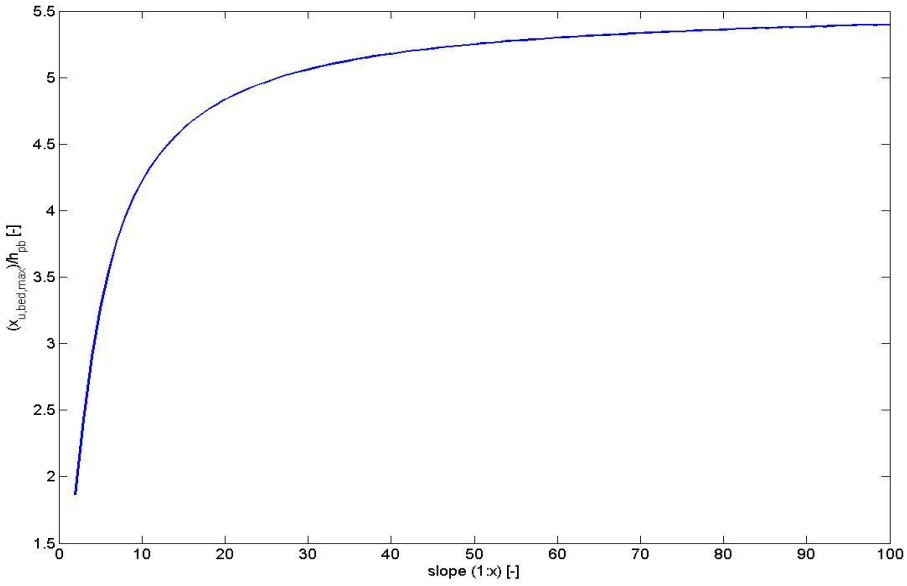

Figure A-10: relative distance from propeller plane to the location of maximum bed velocity for different slopes

A.4 Conclusion

It can be shown that the location of maximum bed velocity depends on the slope angle. For a very gentle slope (approaching a horizontal bed) the maximum bed velocity occurs at a distance of 5.55 times the offset distance. Figure A-10 shows that the value of 5.55 is an asymptotic value and that it is approached only for very small angles. When assuming a horizontal bed in case of a mild slope (for example 1:10), the maximum bed velocity will be underestimated. Therefore it is recommended to use the equation for a slope to calculate the maximum bed velocity even for very mild slopes, instead of the horizontal bed calculation. Van Doorn uses a correction factor f for the maximum slope velocity, the values calculated by van Doorn should not be used in practice because of errors during the calculations of these values. When in the calculation the distance between the propeller plane and the slope is unknown this value can be estimated by: $L = \alpha_m \cdot h_{pb,0}$.

Appendix B Data sets

The hypothesis formula is set up for a tunnel bow thruster. The seven data sets available are not conducted with tunneled propellers. In some cases a free propeller is used, in other tests a jet is used. These differences in jets can cause differences in scour formation and consequently lead to scatter in the data. Other varying boundary conditions in data sets compared to the hypothesis equation are described in this paragraph, also the applicability of different datasets in the hypothesis validation is described. All available data are stored in the table at the end of this appendix. During lab tests, scaling effects could occur (appendix C). The scaling effects should be negligible, therefore $Re_{jet-flow}$ should be larger than 3000 and Re_{bed} should be larger than 600.

B.1 Karki et al. (2007)

(Karki *et al.,* 2007) conducted scour tests with a squared offset jet, with height and width (b_0) of 26.6mm. In order to compare the measurements with the hypothesis, a D_0 has to be determined. This is done by equalizing the surface of the jet with the surface of an imaginary circular jet.

$$b_0^2 = \frac{1}{4} \cdot \pi \cdot D_0^2 \rightarrow D_0 = \sqrt{\frac{4}{\pi} \cdot b_0^2} \approx 30mm$$

The densimetric Froude number (Fr_0) was 10.0 and the offset height varied from 13.3 to 53.2mm (0.5-2 times the square jet height). The sand used had a d_{50} of 0.71mm. During the tests at different time steps the scour depth was measured. These measurements can be found in Figure B-. It is assumed that the equilibrium scour depth was reached after approximately 96 hours, these measurements are shown in most right located data points in Figure B-. The data points showed in the figure are also provided by Dr. Faruque and are presented in Table B-. In the tests the offset height is given as the distance from the initial bed to the underside of the jet. Therefore for the offset height till the axis of the jet, 0.5 times the jet diameter has to be added to this value. This will give dimensionless offset heights h_{pb}/b_0 of 0.5, 1, 1.5 and 2.0. Because of the square shape of the jet, different turbulence intensities occur compared to a propeller jet, which could lead to differences in scour formation.

The jet was only 26.6mmx26.6mm, because of these small dimensions it is questionable whether these data can be uses to examine the real case with potential jet diameters in the order of meters. The Reynolds number in the jet flow is in this case 25.000, therefore the scalingfactors in the jet flow are negligible. The bed Reynolds number is however in the order of 500, therefore the scale effects near the bed are not fully negligible.

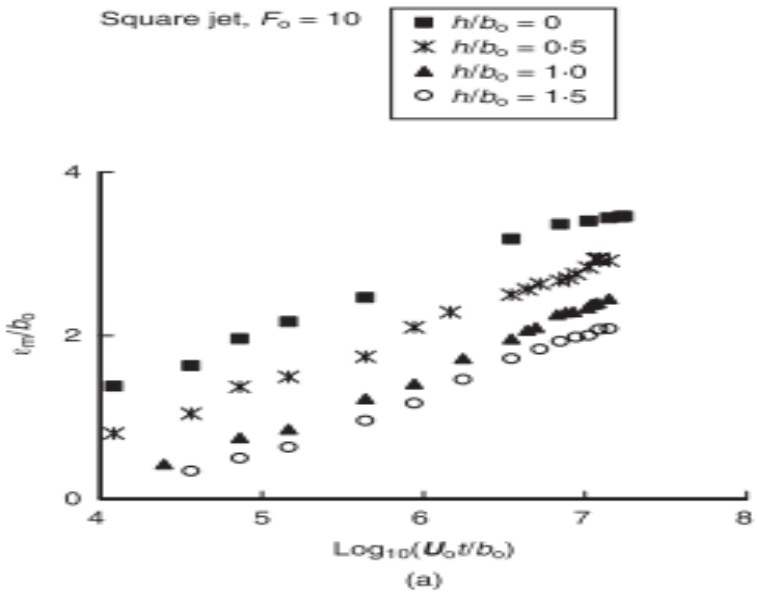

Figure B-1: scour measurements for different dimensionless runtimes and offset heights. Karki et al. (2007)

h_{pb}/b_0	h_{pb}/D_0	h_{sem}/b_0	h_{sem}/D_0
0.5	0.44	3.46	3.08
1	0.89	2.45	2.60
1.5	1.33	2.92	2.18
2	1.77	2.08	1.85

Table B-1: equilibrium scour depths (personal communication Dr. Faruque)

B.2 Drewes et al. (1995)

In data from (Drewes *et al.,* 1995) measurements do not give the scour as a function of the densimetric Froude number but as a function of B/B_{crit} . This quantity can be rewritten to the densimetric Froude number but some assumptions are needed. B is defined as:

$$B = \frac{U_{bed}}{\sqrt{d_{85} \cdot g \cdot \Delta}}$$

Where the bed velocity can be calculated by using the German approach (eq. 2.16):

$$U_{bed} = E \cdot \frac{D_0}{h_{pb}} \cdot U_0.$$

When assuming that E=0.4 (vessel without a rudder) and $d_{85} = 1.3 \cdot d_{50}$, it follows that (given the relative offset=0.72): $B \approx 0.48 Fr_0$. And assuming $B_{crit} = 1.25$: $\frac{B}{Bcrit} \approx 0.38 \cdot Fr_0$. In the lab tests d_{85}=1.6mm, the propeller diameter was 180mm and the offset distance is 130mm. The red data points in Figure B-2 where used in this data analysis, the red points are given for a stationary ship with a rudder angle of 0°.

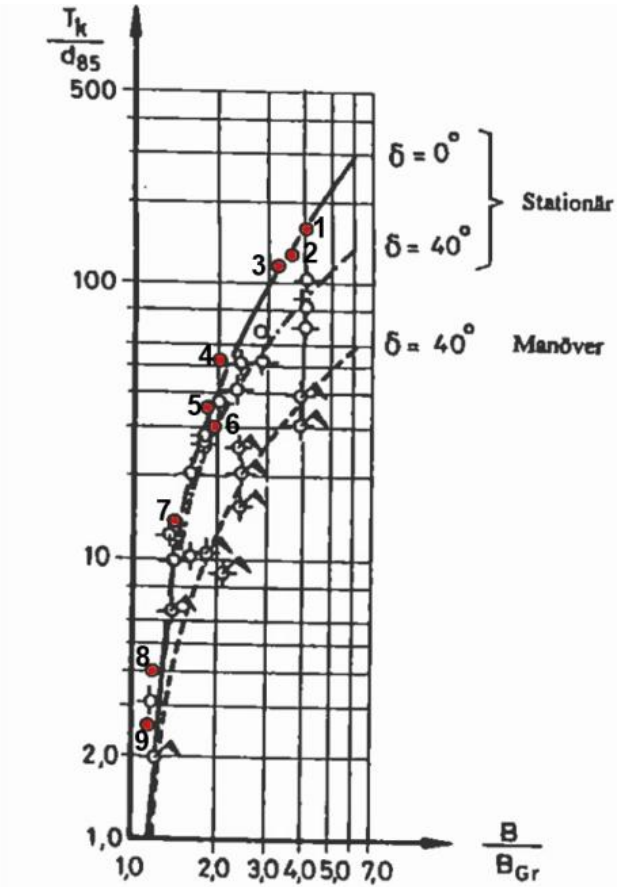

Figure B-2: Scour measurements from Drewes et al. (1995)

In the test by (Drewes *et al.,* 1995), a model of a container vessel was used with a propeller with a diameter of 180mm. Due to the relative large scale model, the scaling effects are negligible. In the translation from B/B_{crit} to the densimetric Froude number, a lot of sensitive assumptions have to be taken. Especially the assumption of a E-value is very sensitive in (Drewes *et al.,* 1995) values for E differ from 0.25 to 0.71. Also when the sieve curves are not known, the derivation from d_{85} to d_{50} can cause relative large uncertainties. Furthermore it is hard to define accurate data from Figure B- because of the indistinct axes.

B.3 Hong et al. (2012)

In (Hong *et al.*, 2012) measurements with a non-ducted propeller and a Froude number of approximately 9 are conducted. Two different propellers were used, one with a 100mm diameter and the other had a diameter of 210mm. Also different sand sizes where used (d_{50} of 0.24mm and 0.34mm) and different offset heights (0.5-1.5 times the propeller diameter). The triangular points in Figure B- show the propeller jet measurements.

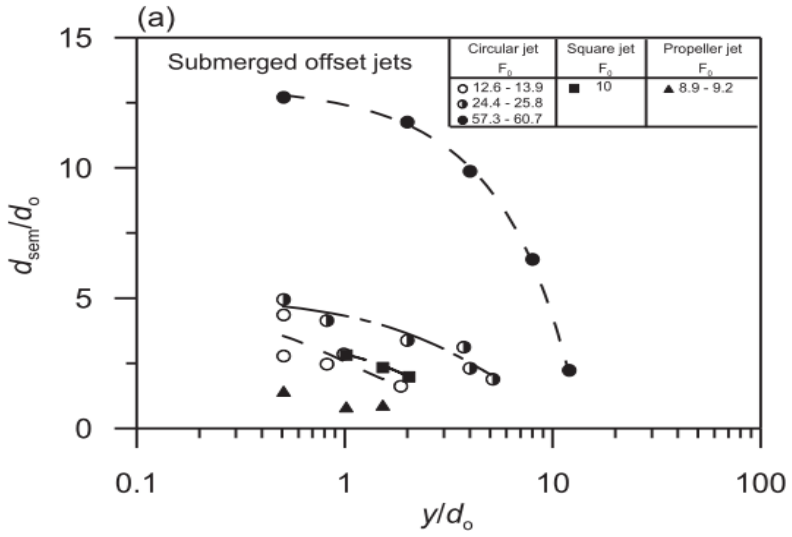

Figure B-3: Scour measurements for different researches. Hong et al. (2012)

In this research the propeller diameters are large enough to neglect the scaling effects. However just a few data points are present (triangular markers given in Figure B-). The square data points in Figure B- are the data points as found by (Karki *et al.*, 2007), the circles are data from the measurements found by (Chiew & Lim, 1995).

B.4 Chiew and Lim (1995)

In this research different scour depths where measured for different offset heights and different Froude numbers both for water and air jets. During the validation calculations of the proposed new equation only the data of the water tests are used. The data with a Froude number of around 25 and around 13 are used because these values are in the range of Froude numbers in practice. The jet diameter was 12.7mm and dimensionless offset heights varied from 0.5 to 6. Given the small diameter of the jet, scaling problems could occur when using these data points. In this test the sand had a d_{50} of 0.25mm. In Figure B- the open triangles ($Fr_0 \approx 13$) and open circles ($Fr_0 \approx 25$) are used to distract data points.

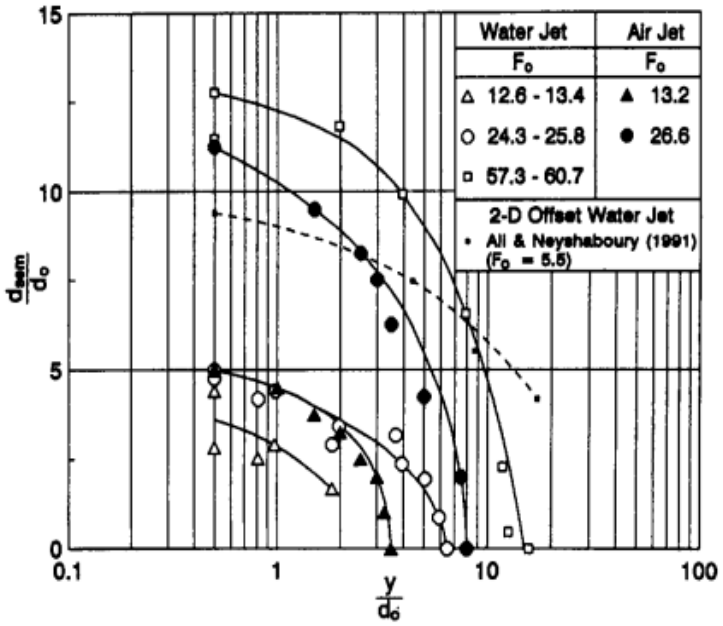

Figure B-4: scour measurements. Chiew and Lim (1995)

B.5 Chin et al. (1996)

In these tests both the jet diffusion scour mechanism and the pile obstruction mechanism where involved. However (Chin *et al*, 1996) described that the obstruction mechanism was negligible. The data used from these tests for the hypothesis validation are those of scour type II and type IV and the measurements without piles. In scour type II and IV the pile was outside the scour zone (Figure B-5 and Figure B-6), therefore the scour induced by the obstruction mechanism is negligible. The data are taken from Figure B-7, the open triangular points and the open circular points. In the lab tests different jet diameters were used(12.7mm-50.8mm) and different sand sizes (0.25mm-1.65mm), but it is unknown which jet diameter and sand size belongs to the points in the figure. Due to the small jet diameters, scale effects could occur, but this cannot be validated because the combination of flow velocities, jet diameters and sand size are not known.

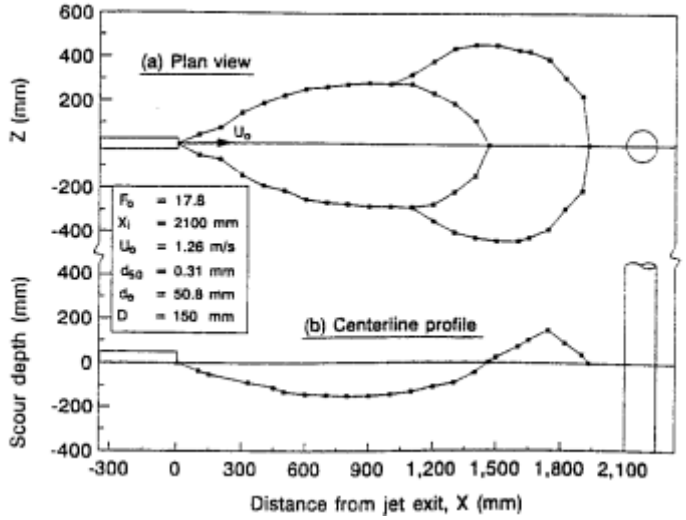

Figure B-5: Scour profile for type II scour. Chin et al. (1996)

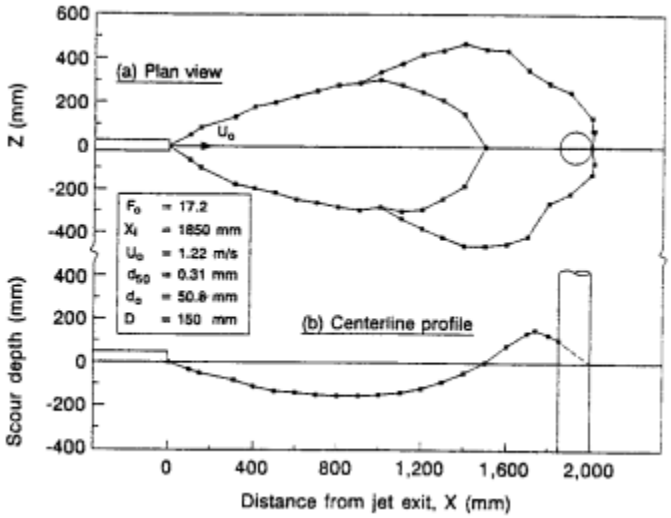

Figure B-6: Scour profile for type IV scour. Chin et al. (1996)

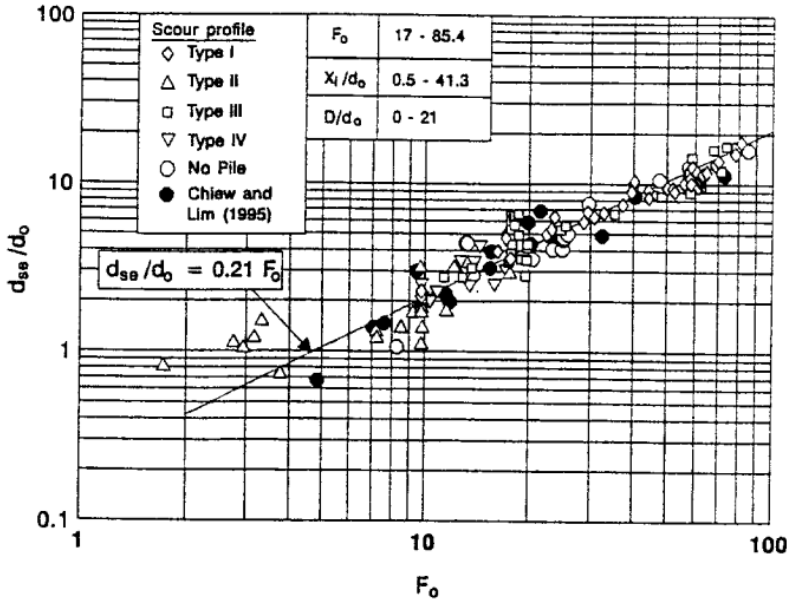

Figure B-7: scour measurements. Chin et al. (1996)

B.6 Yüksel et al. (2005)

Also (Yüksel *et al.*,2005) conducted research into scour on a horizontal bed with piles, the conclusion of this research was that the pile obstruction mechanism was negligible. In these tests different offset heights were used. The circular jet nozzle had a diameter of only 22mm and the dimensionless offset distances varied from 0.5 to 11.5. In Figure B-8 the measurements are plotted, the densimetric Froude number was 18.3, the bed had a d_{50} of 1.2mm.

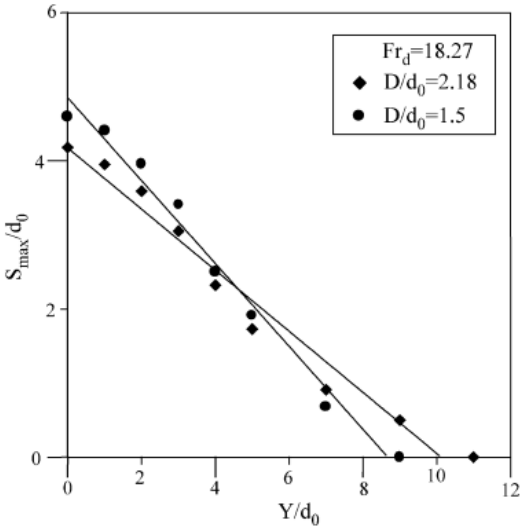

Figure B-8: Scour measurements. Yüksel et al. (2004)

Because of the small nozzle width it is possible that scaling effects occur when translating the results to practical cases.

B.7 Conclusion

Only three tests were conducted with propellers (Drewes, Hong and Hamill), the other tests are conducted with very small jets. Although the tests conducted with small jet diameters do not predict scaling effects, it is assumed that these tests could lead to an inaccurate comparison with bow thrusters in practice. In the data sets very high Froude numbers are present, in practice very high slope Froude numbers will probably not occur because this could lead to very large scour holes. Therefore in the validation of the hypothesis formula, it is recommended to focus on the low values of the slope Froude numbers.

B.8 Table datasets

	Research	Fr_0	propeller or jet diameter (D_0) [mm]	Offset height (h_{pb}) [mm]	d_{85}[mm]	d_{50} [mm]	Relative offset ($\frac{h_{pb}}{d_{85}}$) [-]	Relative offset ($\frac{h_{pb}}{d_{50}}$) [-]	Relative offset ($\frac{h_{pb}}{D_0}$) [-]	Relative scour depth ($\frac{h_{sem}}{d_{85}}$)[-]	Absolute scour depth (h_{sem}) [mm]	Relative scour depth ($\frac{h_{sem}}{D_0}$) [-]	Pile Diameter (D_{pile})[mm]
1	Karki2007 (squared jet) Fig.4a (from source)	10	30	13,3		0,71		18,73239437	0,443333333		92,382	3,0794	0
1	Karki2007 (squared jet) Fig.4a (from source)	10	30	26,6		0,71		37,46478873	0,886666667		77,964	2,5988	0
1	Karki2007 (squared jet) Fig.4a (from source)	10	30	39,9		0,71		56,1971831	1,33		65,415	2,1805	0
1	Karki2007 (squared jet) Fig.4a (from source)	10	30	53,2		0,71		74,92957746	1,773333333		55,536	1,8512	0
2	Drewes (TU Braunschweig) Fig.24 #1	10,526	153	130	1,6	1,230769231	81,25	105,625	0,849673203	170	272	1,777777778	0
2	Drewes (TU Braunschweig) Fig.24 #2	9,4737	153	130	1,6	1,230769231	81,25	105,625	0,849673203	130	208	1,359477124	0
2	Drewes (TU Braunschweig) Fig.24 #3	8,4211	153	130	1,6	1,230769231	81,25	105,625	0,849673203	120	192	1,254901961	0
2	Drewes (TU Braunschweig) Fig.24 #4	5,2632	153	130	1,6	1,230769231	81,25	105,625	0,849673203	52	83,2	0,54379085	0
2	Drewes (TU Braunschweig) Fig.24 #5	5	153	130	1,6	1,230769231	81,25	105,625	0,849673203	37	59,2	0,386928105	0
2	Drewes (TU Braunschweig) Fig.24 #6	4,7368	153	130	1,6	1,230769231	81,25	105,625	0,849673203	30	48	0,31372549	0
2	Drewes (TU Braunschweig) Fig.24 #7	3,9474	153	130	1,6	1,230769231	81,25	105,625	0,849673203	15	24	0,156862745	0
2	Drewes (TU Braunschweig) Fig.24 #8	3,4211	153	130	1,6	1,230769231	81,25	105,625	0,849673203	4	6,4	0,041830065	0
2	Drewes (TU Braunschweig) Fig.24 #9	3,1579	153	130	1,6	1,230769231	81,25	105,625	0,849673203	2,6	4,16	0,027189542	0
3	Hong(propeller) (Hong 2012 fig. 3a circle)	6,08	210	105		0,24		437,5	0,5		200	0,952380952	0
3	Hong(propeller) (Hong 2012 fig. 3a triangle)	7,73	210	105		0,24		437,5	0,5		230	1,095238095	0
3	Hong(propeller) (Hong 2012 fig. 3a diamond)	8,94	210	105		0,24		437,5	0,5		300	1,428571429	0
3	Hong(propeller) (Hong 2012 fig. 3b circle)	6,08	210	210		0,24		875	1		100	0,476190476	0
3	Hong(propeller) (Hong 2012 fig. 3b triangle)	7,73	210	210		0,24		875	1		120	0,571428571	0
3	Hong(propeller) (Hong 2012 fig. 3b diamond)	8,94	210	210		0,24		875	1		120	0,571428571	0
3	Hong(propeller) (Chiew 2012 fig. 6 triangle)	9,19	100	150		0,34		441,1764706	1,5		80	0,8	0
4	Chiew and lim (1996) fig. 5 (open triangle)	13	12,7	6,35		0,25		25,4	0,5		16,51	2,6	0
4	Chiew and lim (1996) fig. 5 (open triangle)	13	12,7	6,35		0,25		25,4	0,5		25,4	4	0
4	Chiew and lim (1996) fig. 5 (open triangle)	13	12,7	10,16		0,25		40,64	0,8		25,4	2,5	0
4	Chiew and lim (1996) fig. 5 (open triangle)	13	12,7	12,7		0,25		50,8	1		34,29	2,7	0
4	Chiew and lim (1996) fig. 5 (open triangle)	13	12,7	22,86		0,25		91,44	1,8		45,72	2	0
4	Chiew and lim (1996) fig. 5 (open circle)	25	12,7	6,35		0,25		25,4	0,5		30,48	4,8	0
4	Chiew and lim (1996) fig. 5 (open circle)	25	12,7	6,35		0,25		25,4	0,5		31,75	5	0
4	Chiew and lim (1996) fig. 5 (open circle)	25	12,7	10,16		0,25		40,64	0,8		38,608	3,8	0
4	Chiew and lim (1996) fig. 5 (open circle)	25	12,7	12,7		0,25		50,8	1		50,8	4	0
4	Chiew and lim (1996) fig. 5 (open circle)	25	12,7	22,86		0,25		91,44	1,8		64,008	2,8	0
4	Chiew and lim (1996) fig. 5 (open circle)	25	12,7	25,4		0,25		101,6	2		91,44	3,6	0
4	Chiew and lim (1996) fig. 5 (open circle)	25	12,7	48,26		0,25		193,04	3,8		159,258	3,3	0
4	Chiew and lim (1996) fig. 5 (open circle)	25	12,7	50,8		0,25		203,2	4		127	2,5	0
4	Chiew and lim (1996) fig. 5 (open circle)	25	12,7	63,5		0,25		254	5		139,7	2,2	0

4	Chiew and lim (1996) fig. 5 (open circle)	25	12,7	76,2		0,25		304,8	6		91,44	1,2	0
5	Chin (1996) fig. 15 (no pile)	8,3							0,5			1,1	0
5	Chin (1996) fig. 15 (no pile)	14,8							0,5			4,5	0
5	Chin (1996) fig. 15 (no pile)	15							0,5			2,9	0
5	Chin (1996) fig. 15 (no pile)	20							0,5			3,8	0
5	Chin (1996) fig. 15 (no pile)	23							0,5			4	0
5	Chin (1996) fig. 15 (no pile)	25							0,5			4	0
5	Chin (1996) fig. 15 (no pile)	25							0,5			4,8	0
5	Chin (1996) fig. 15 (no pile)	26							0,5			5	0
5	Chin (1996) fig. 15 (no pile)	30							0,5			7,5	0
6	Chin (1996) fig. 15 (with pile, type II)	1,8							0,5			0,8	
6	Chin (1996) fig. 15 (with pile, type II)	2,8							0,5			1,2	
6	Chin (1996) fig. 15 (with pile, type II)	2,9							0,5			1,1	
6	Chin (1996) fig. 15 (with pile, type II)	3,2							0,5			1,3	
6	Chin (1996) fig. 15 (with pile, type II)	3,3							0,5			1,7	
6	Chin (1996) fig. 15 (with pile, type II)	3,8							0,5			0,75	
6	Chin (1996) fig. 15 (with pile, type II)	7,2							0,5			1,3	
6	Chin (1996) fig. 15 (with pile, type II)	7,2							0,5			1,4	
6	Chin (1996) fig. 15 (with pile, type II)	8,6							0,5			1,5	
6	Chin (1996) fig. 15 (with pile, type II)	9,2							0,5			1,8	
6	Chin (1996) fig. 15 (with pile, type II)	9,8							0,5			1,2	
6	Chin (1996) fig. 15 (with pile, type II)	9,8							0,5			1,5	
6	Chin (1996) fig. 15 (with pile, type II)	9,8							0,5			1,8	
6	Chin (1996) fig. 15 (with pile, type II)	9,8							0,5			3,2	
6	Chin (1996) fig. 15 (with pile, type II)	12							0,5			1,8	
6	Chin (1996) fig. 15 (with pile, type II)	13							0,5			3,2	
6	Chin (1996) fig. 15 (with pile, type II)	18							0,5			3	
6	Chin (1996) fig. 15 (with pile, type IV)	9,8							0,5			2,7	
6	Chin (1996) fig. 15 (with pile, type IV)	10,5							0,5			2	
6	Chin (1996) fig. 15 (with pile, type IV)	11							0,5			2,4	
6	Chin (1996) fig. 15 (with pile, type IV)	14							0,5			3,6	
6	Chin (1996) fig. 15 (with pile, type IV)	15							0,5			2,6	
6	Chin (1996) fig. 15 (with pile, type IV)	15							0,5			3,5	
6	Chin (1996) fig. 15 (with pile, type IV)	16							0,5			4,3	
6	Chin (1996) fig. 15 (with pile, type IV)	17							0,5			2,6	
7	Chin (1996) fig. 15 (with pile,type III)	12							0,5			2,8	

7	Chin (1996) fig. 15 (with pile,type III)	18							0,5			5	
7	Chin (1996) fig. 15 (with pile,type III)	19							0,5			2,9	
7	Chin (1996) fig. 15 (with pile,type III)	20							0,5			3,6	
7	Chin (1996) fig. 15 (with pile,type III)	20							0,5			4,5	
7	Chin (1996) fig. 15 (with pile,type III)	26							0,5			5,7	
7	Chin (1996) fig. 15 (with pile,type III)	35							0,5			6,5	
7	Chin (1996) fig. 15 (with pile,type III)	58							0,5			9	
7	Chin (1996) fig. 15 (with pile,type III)	58							0,5			15	
8	Yuksel (2004) figure 10 circles	18,27	22	11		1,28		8,59375	0,5		103,4	4,7	33
8	Yuksel (2004) figure 10 circles	18,27	22	33		1,28		25,78125	1,5		99	4,5	33
8	Yuksel (2004) figure 10 circles	18,27	22	55		1,28		42,96875	2,5		88	4	33
8	Yuksel (2004) figure 10 circles	18,27	22	77		1,28		60,15625	3,5		77	3,5	33
8	Yuksel (2004) figure 10 circles	18,27	22	99		1,28		77,34375	4,5		55	2,5	33
8	Yuksel (2004) figure 10 circles	18,27	22	121		1,28		94,53125	5,5		44	2	33
8	Yuksel (2004) figure 10 circles	18,27	22	165		1,28		128,90625	7,5		17,6	0,8	33
8	Yuksel (2004) figure 10 squares	18,27	22	11		1,28		8,59375	0,5		90,2	4,1	48
8	Yuksel (2004) figure 10 squares	18,27	22	33		1,28		25,78125	1,5		88	4	48
8	Yuksel (2004) figure 10 squares	18,27	22	55		1,28		42,96875	2,5		81,4	3,7	48
8	Yuksel (2004) figure 10 squares	18,27	22	77		1,28		60,15625	3,5		66	3	48
8	Yuksel (2004) figure 10 squares	18,27	22	99		1,28		77,34375	4,5		50,6	2,3	48
8	Yuksel (2004) figure 10 squares	18,27	22	121		1,28		94,53125	5,5		37,4	1,7	48
8	Yuksel (2004) figure 10 squares	18,27	22	165		1,28		128,90625	7,5		22	1	48
8	Yuksel (2004) figure 10 squares	18,27	22	209		1,28		163,28125	9,5		17,6	0,8	48
9	Hamill	8,43	131	74,5		1,46		89,7260274	0,56870229		150	1,145038168	0

Appendix C Model tests set-up

The proposed equation is not validated yet for sloping beds. The validation can examined by conducting lab experiments. During this master thesis it was not possible to conduct these tests. However a possible model set-up is given in this chapter, this set-up can be used as a guideline during further researches.

C.1 Scaling

According to (Schiereck G. , 2007) 'scale' simply means the relation between the value of some parameter in prototype and model, usually indicated by N. N_L(length scale)=10, means that lengths in the model are 10 times smaller than in prototype. A limitation in the use of scale models is given by the fact that, while reducing the geometrical dimensions, the material properties do not change. We cannot change the properties of water, like density, viscosity and surface tension, unless we use other fluids, which is often very expensive.

Scale rules can be expressed with dimensionless numbers, stating that the number should be the same in model and prototype. If the dimensionless number of the prototype and the model are not the same, scale effects occur. According to Schiereck the Froude number and the Reynolds number are main criteria in fluid motions combined with a flow around a structure. The Froude number is defined as the ratio between inertia and gravity:

$$Fr = \frac{u^2}{g \cdot L} \tag{C.1}$$

The Reynolds number is defined as the ratio between inertia and viscosity and is given by:

$$Re = \frac{u \cdot L}{\nu} \tag{C.2}$$

Since gravity is the same in the model as in the prototype, when using the length scaling and assuming the same Froude number in the prototype as in the model, it is possible to determine the scaling factor for velocity:

$$\frac{u_{prototype}^2}{g \cdot L_{prototype}} = \frac{u_{model}^2}{g \cdot L_{model}}$$

$$\frac{u_{prototype}^2}{N_L \cdot L_{model}} = \frac{u_{model}^2}{L_{model}}$$

$$U_{prototype} = \sqrt{N_L} \cdot U_{model}$$

$$N_u = \sqrt{N_L}$$

When the same is done for the Reynolds number it follows that:

$$N_u = \frac{1}{N_L}$$

These two criteria show conflicting criteria. So it is impossible to apply the same Reynolds number and Froude number in both the prototype and the model. This means that scaling effects will occur.

According to (Verheij, 1985) the scaling effects due to viscosity are negligible if the Reynolds number of the propeller flow is greater than 70,000. With:

$$Re_{prop} = \frac{n_p \cdot D_p \cdot L_{smb}}{\nu} \quad \text{(C.3)}$$

With L_{smb} is the length term dependent on the blade area ratio:

$$L_{smb} = \beta_p \cdot D_p \cdot \pi \cdot \left(2 \cdot N\left(1 - \frac{D_h}{D_p}\right)\right)^{-1}$$

For near-bed flow the scaling effects are negligible when the Reynolds number of the near-bed flow is larger than 600. With:

$$Re_{bed} = \frac{u_{bed} \cdot d_{50}}{\nu} \quad \text{(C.4)}$$

With:

n_p	Rotational speed of the propeller	[s^{-1}]
D_p	Propeller diameter	[m]
ν	Kinematic viscosity	[m^2/s]
β	Blade area ratio	[-]
N	Number of blades	[-]
D_h	Diameter of hub	[m]
u_{bed}	Velocity near the bed	[m/s]
d_{50}	Stone diameter	[m]

C.2 Scenarios

In order to validate the proposed equation different scenarios should be examined. Depending on the available time for lab tests, extra scenarios could be added. When more scenarios are examined, more data points are created which will lead to a more reliable result. It is recommended to carry out at least the following 3 scenarios:

C.2.1 Scenario 1: validating the critical densimetric slope Froude number

In this scenario the objective is to define the critical densimetric slope Froude number. This can be done by using a propeller and a slope with sand or gravel at a fixed location. During the tests the efflux velocity is increased by increasing the propeller speed. When the slope material starts to move, the critical densimetric Froude number is reached. The following research questions should be answered:

Is the value of the densimetric Froude number equal to $\sqrt{\frac{\Psi_{cr}}{0.055}\frac{2}{3 \cdot m_h}}$?

Is the location where the erosion start equal to the location as predicted in equation2.17 ($x_{u,max}$)?

C.2.2 Scenario 2: validating the values of α_2 and β_2.

During this scenario the same set-up as scenario 1 is used, but now the efflux velocity is even further increased, so that values of the densimetric slope Froude number above the critical value occur. For these tests different efflux velocities should be used during a long time, so that the equilibrium scour hole is reached. Now it is possible to define the values of α_2 and β_2. Do the values as computed in this report $\alpha_2 = 0.32$ and $\beta_2 = 0.53$ match the measured values of the lab experiments?

C.2.3 Scenario 3: validating the pile obstruction mechanism

Use the same slope as used in the first two scenarios, but add a pile at the location of maximum scour as found in scenario 2. By keeping the densimetric slope Froude number below the critical value it is possible to examine the pile obstruction scour mechanism. Now it is possible to define the value of γ.

When this scenario is conducted with densimetric slope Froude numbers above the critical value, both the jet diffusion mechanism and the pile obstruction mechanism will occur.

Could the two mechanisms be added as described in the hypothesis equation?

In order to examine the influence of the pile diameter, both sub scenarios should be conducted with varying pile diameters.

C.2.4 Scenario 4 (optional): validating the pile group factor

In the proposed equation only a single pile is used. It is however possible to introduce a pile group and examine the effects on the scour development. Is it possible to define the pile group factor as described in the scour manual?

C.3 Equipment

The flow field development is a very important characteristic for the scour prediction method. Therefore it is recommended to measure the flow field during the lab experiments. Although in this master thesis only the equilibrium scour depth is examined it is recommended to measure the scour hole development during the lab tests. The scour development in time could provide extra knowledge in the physical processes that occur during the scour processes.

C.3.1 Velocity and turbulence measurements

There are different ways to measure the flow velocities in the modeltests. One possible way is to use an Electromagnetic Velocity Sensor (EMS). This is also used by (Schokking, 2002) in his tests. However there are some disadvantages of the EMS. The EMS disturbs the flow, and the measuring volume is rather large. And because of its size it is impossible to measure the velocity close to the bed. These equipment characteristics cause deviations in the measurements, especially in case of measuring velocity fluctuations. According to Schokking, the EMS can only detect vortices of about 1cm large. This means that smaller vortices are not taken into account. (Hofland, 2005) found that the most important vortices concerning particle stability have a diameter of 1.5 respectively 2 times the diameter of the particle. It is recommended to use particles in the gravel size or the sand size, the EMS is not able to measure the most important vortices for these particle sizes and therefore the EMS should not be used during the research.

The velocities and turbulence intensities close to the bed have a larger effect on the stability of bed material than velocities and turbulences at a larger distance from the bed, as can be seen by the weighting function in the Hoan stability parameter (Equation 2.33). Therefore it seems better to use equipment that can measure the flow velocities and turbulence close to the bed like an Acoustic Doppler Velocimeter (ADV) or a Laser Doppler Velocimeter (LDV). Van Doorn decided not to use a LDV because of safety considerations (shield off light). A disadvantage of the ADV is that it measures only at a single location, because of this characteristic it is difficult to measure the flow field development around the scour hole.

C.3.2 Scour measurements

Also for the scour measurements different methods can be used. The most simple method to measure the scour depth is probably the point gauge measurements, as used by (Yüksel *et al.*, 2005). A second method is to count the displaced stones. This method is used by (Schokking, 2002) and (Hoan, 2008). In this method first the stones are painted in different colors so it is possible to determine where the displaced particle come from. This method is not applicable when sand or small pebbles are used during the experiments. (Van Velzen, 2012) used digital stereo photography (DSP) in her research. With DSP it is possible to give 3d-information of the model bathymetry.

Because the information of the DSP measurements is generated by a computer, it is probably the most quick way to assess scour. The method of stone-counting is the most time consuming. When using point gauge measurements an interpolation is needed to come up with a 3d picture of the scour hole. Therefore it is recommended to use the DSP method. A fourth possible way of measuring the scour hole is by laser line scanning, this method is also used in measuring bottom roughness of the seabed. But it is unknown whether or not can be used in model tests.

C.4 Model set-up lay out

In this paragraph a possible model set-up is given. According to van Doorn a length of the model basin of 10 meters is sufficient to avoid a large influence of the recirculation flow. Therefore it is recommended to use a basin with a length of at least 10m. A basin width of 3m (Figure C-1) should be enough to place a 1:3 slope, in that case there is still enough space for the placement of the ship.

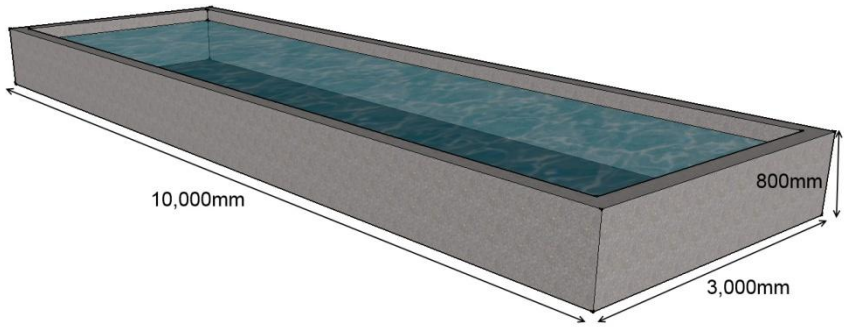

Figure C-1: Basin model

For the ship model, it is recommended to use the same model set up as given in van Doorn. The ship has a rectangular shape as showed in Figure C-, with a length of 2500mm and a width of 300mm. The bow thruster is modeled by a propeller with a diameter of 110mm (Vetus 2512C) in a tunnel of approximately 120mm.

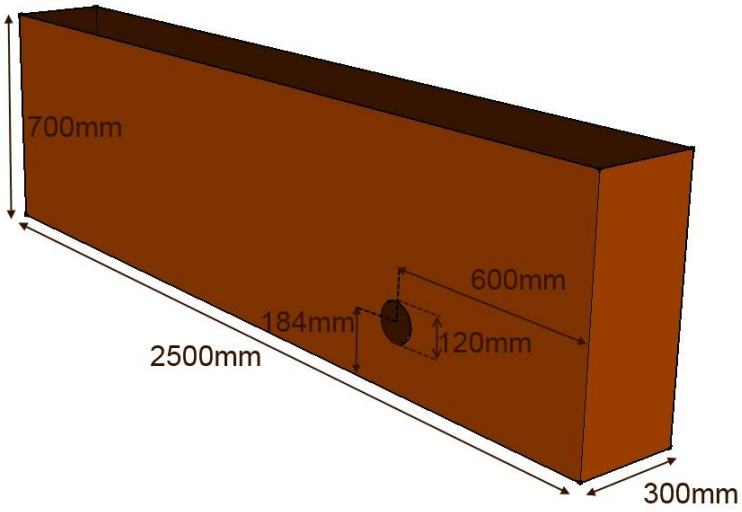

Figure C-2: Ship model

The scour pit is constructed by two triangular boards, at a distance of 2.5 meters. This pit will be filled with sand or gravel, during tests. At the inside of the triangular plates, bar attachment points are constructed. In these attachment points bars could be placed with single pile or multiple piles.

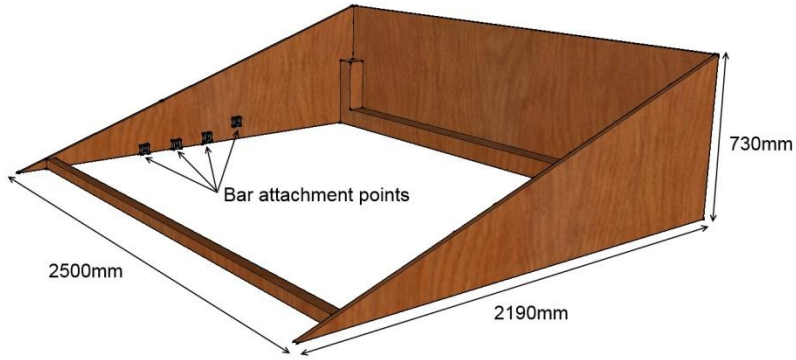

Figure C-3: Scour pit set-up

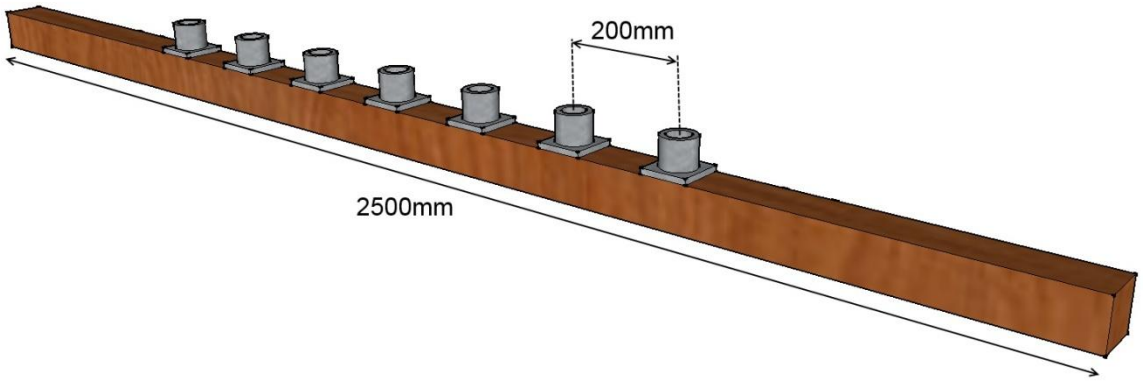

Figure C-4: Possible set-up of bar with pile attachment points

Appendix D Matlab calculations

During this research most calculations are conducted with Matlab. In this appendix the different matlab codes are presented. First the code of the α_2 and β_2 calculations is shown, followed by the code of the γ calculation and the code with the final scour calculation is presented. This code also generates the pictures as showed in this report. Finally the comparison between the different methods and the code of the FORM calculations are presented. All codes are available at the CD added in this report.

D.1 α_2 and β_2 calculations

```
clc; clear all; close;
g=9.81; nu=1e-6; delta=1.65;
```

Show a scatterplot

```
[Qdata, Qtext, Qalldata]=xlsread('interpeteddata');          %open data table
%Qdata=Qdata(find(Qdata(:,11)<1),:);                         % Delete all data with dimensionless offset
larger than x
Qdata=Qdata(find(Qdata(:,3)<24.9),:);                        % Deltete all data with a Fr0 larger than x
betaizcrit=3;                                                % Critical Izbash coefficient [-]
for t=[7 8]                                                  % Do not take in account these researches
Qdata=Qdata(find(Qdata(:,1)~=t),:);
end


Fr0=Qdata(:,3);                                              % Find the Fr0 [-]
offset=Qdata(:,11);                                          % Find the relative offset hpb/D0 [-]
d50=Qdata(:,7)/1000;                                         % Find d50 [m]


dstar=d50.*((g*delta/nu^2)^(1/3)); % non dimensional stone diameter (Rock manual) [-]
% approximation for the Shields parameter for the calculated non dimensional stone diameter:
A=[];
B=[];
for i=1:length(dstar)
Dstar=dstar(i);
Dstar(isnan(Dstar))=0;
if Dstar>1 & Dstar<4;
    a=0.24;
    b=-1;
elseif Dstar>4 & Dstar<10;
    a=0.14;
    b=-0.64;
elseif Dstar>10 & Dstar<20;
    a=0.04;
    b=-0.1;
elseif Dstar>20 & Dstar<150;
    a=0.013;
    b=0.29;
elseif Dstar>150;
    a=0.055;
    b=0;
elseif Dstar==0;
    a=1;
    b=1;
end
A=[A; a];   %for every measurement the value of A
B=[B; b];   %for every measurement the value of B
end
```

```
dstar(isnan(dstar))=0;
psicrit=A.*dstar.^B; %approximated value of the Shields parameter [-]
psicrit(find(psicrit==0))=0.03; %if psicrit is zero, this means no grain size is available...
...therefore we assume psicrit=0.03 because in all tests sand is used.
Frbedcrit=sqrt((psicrit/0.055)*2/(betaizcrit)); %Critical bed Froude number
Frbed=0.306.*offset.^-1.*Fr0;                   %Maximum bed Froude number

% in the datasets 2 3 & 9  a propeller is used, therefore other bed Froude
% numbers are defined compared with the free jet tests:
Frbed(find(Qdata(:,1)==2))=Frbed(find(Qdata(:,1)==2)).*(0.32/0.306);
Frbed(find(Qdata(:,1)==3))=Frbed(find(Qdata(:,1)==3)).*(0.32/0.306);
Frbed(find(Qdata(:,1)==9))=Frbed(find(Qdata(:,1)==9)).*(0.32/0.306);

j=find(Frbed>Frbedcrit);    % Do only take into account data with higher bed Froude numbers than the...
...critical value
Fr0=Qdata(j,3);             % Only measurements with Frbed>Frbedcrit
offset=Qdata(j,11);         % Offset with Frbed>Frbedcrit

Frbed=0.306.*offset.^-1.*Fr0;
Frbed(find(Qdata(j,1)==2))=Frbed(find(Qdata(j,1)==2)).*(0.32/0.306);
Frbed(find(Qdata(j,1)==3))=Frbed(find(Qdata(j,1)==3)).*(0.32/0.306);
Frbed(find(Qdata(j,1)==9))=Frbed(find(Qdata(j,1)==9)).*(0.32/0.306);

x=Frbed.^2-Frbedcrit(j).^2;
scour=Qdata(j,15);          % Find the scour depth hs/D0[-]
research=Qdata(j,1);        % Define different researches [-]

gscatter(x,scour,research,[],'*',14)    % plot datapoints
%'Karki','Drewes','Hong','Chiew and Lim','Chin without piles','Chin with piles (type II & IV)','Hamill'
legend('Drewes','Hong','Hamill','Location','NorthWest') %Change legend with changing input researches
xlabel('Fr_b_e_d^2-Fr_b_e_d_,_c_r_i_t^2 [-]','fontsize',14)
ylabel('h_s_e_m/D_0 [-]','fontsize',14)
hold on
```

Find the best powerlaw fit through the datapoints

the datapoints of the scatterplot as defined above are added in the curvefitting tool (cftool), for this application the curvefitting toolbox has to be installed in matlab. The used equation is a powerlaw: scour=alpha*x^beta

```
alpha=0.28; %best fit alpha  (Changes for changing input researches!)
beta=0.50;  %best fit beta   (Changes for changing input researches!)

f=fit(x,scour,'power1'); % (curvefitting toolbox command)
p11=predint(f,x,0.95); % defines the 95% confidence bounds
lower=p11(:,1);        % these datapoints are used to fit the upper confidence bound (in cftool)
upper=p11(:,2);        % these datapoints are used to fit the lower cinfidence bound (in cftool)

j=0:0.01:200;
equation=alpha.*j.^beta; % equation of the best fit power function through the datapoints
uppera=0.21;             % upperbound a
upperb=0.58;             % upperbound b
upperc=0.71;             % upperbound c
equationhigh=uppera.*j.^upperb+upperc; %equation of the upper bound
lowera=0.36;             % lowerbound a
lowerb=0.43;             % lowerbound b
lowerc=-0.74;            % lowerbound c
equationlow=lowera.*j.^lowerb+lowerc;   %equation of the lower bound
plot(j,equation,'LineWidth',2,'Color','k')      % plot the best fit
hold on
plot(j,equationhigh,':');                       % plot the 95% upper bound
plot(j,equationlow,':');                        % plot the 95% lower bound
```

```
axis([0 200 0 8])
```

compare the calculated values with the measured values

```
scourprediction=alpha.*x.^beta;     % calculate the predicted scour depth

SSE=sum(abs((scour-scourprediction)).^2);
TSS=sum(abs((scour-mean(scour)).^2));
R=1-SSE/TSS;                        % calculate R-squared

text(20,1.3,{[num2str(alpha) ,'*(Fr_b_e_d^2-Fr_b_e_d_,_c_r_i_t^2)^' ,(num2str(beta)), '   (R^2=',
num2str(R) ')'];['\downarrow']})

figure
plot(scour,scourprediction,'.')     % Plot calculated scour and measured scour in one plot
hold on
plot([0 5],[0 5]);
axis([0 5 0 5]);
xlabel('scour measurements','fontsize',14)
ylabel('scour prediction','fontsize',14)
Z=scourprediction-scour;
Pf=length(find(Z<0))/length(Z);     % Percentage of predicted scour smaller than real scour
title({'P_f=' num2str(Pf)},'fontsize',14)
```

D.2 γ calculation

```
clc; clear all; close;
[Qdata, Qtext, Qalldata]=xlsread('interpeteddata');
%Qdata=Qdata(find(Qdata(:,11)<8),:);                    %Delete all data with dimensionless offset larger
than x
%Qdata=Qdata(find(Qdata(:,3)<25),:);
betaizcrit=3;
for t=8                                                 % only take into account research 8
Qdata=Qdata(find(Qdata(:,1)==t),:);
end

Fr0=Qdata(:,3);
offset=Qdata(:,11);
Frbedcrit=sqrt(2/betaizcrit);
Frbed=0.3.*offset.^-1.*Fr0;
Qdata=Qdata(find(Frbed>Frbedcrit),:);
Fr0=Qdata(:,3);
offset=Qdata(:,11);
Frbed=0.3.*offset.^-1.*Fr0;
x=Frbed.^2-Frbedcrit.^2;
scour=Qdata(:,15);
research=Qdata(:,1);

alpha=0.32;
beta=0.53;
j=0:0.01:350;
equation=alpha.*j.^beta;

scourpredictionjetdiffusion=alpha.*x.^beta;             % calculate the jet diffusion data points [-]

Dpile=Qdata(:,16);                                      % find the pile diameter [mm]
D0=Qdata(:,4);                                          % find the jet diameter [mm]
h0=Qdata(:,17);                                         % find the water depth [mm]
gamma=(scour-scourpredictionjetdiffusion)./(Dpile./D0.*tanh(h0./Dpile)); % calculate the value of gamma for
all data points [-]
```

```
meangamma=mean(gamma);                                  % calculate the mean value of gamma [-]

scourprediction=alpha.*x.^beta+meangamma*(Dpile./D0).*tanh(h0./Dpile); %calculate the total scour depth
```

plotting

```
gscatter(x,scour,research,[],'*',10)                    % plot the datapoints
xlabel('Fr_b_e_d^2-Fr_b_e_d_,_c_r_i_t^2 [-]','fontsize',14)
ylabel('h_s_e_m/D_0 [-]','fontsize',14)
hold on
plot(j,equation,'LineWidth',2,'Color','k')              % plot the jet diffusion line
axis([0 350 0 8])
plot(x,scourprediction,'d');                            % plot the calculated scour
str={['\alpha=' num2str(alpha)],['\beta=' num2str(beta)],['\gamma=' num2str(meangamma)]};
annotation('textbox',[.6 0.15 .1 .1],'String',str);
```

D.3 Scour calculation

```
clear all; clc; close all;
```

input of the script

```
% PARAMETER INPUT
Dp=1.5; %propeller diameter [m]
d50=0.05; % d50 bed material [m]
u0=5; %efflux velocity [m/s]
hpb=4; %distance between propeller axis and bed at the location of the propeller plain [m]
slope=3; %slope 1:x [-]
xbreak=0; %x coordinate for the beginning of the slope [-]
waterlevel=4; %waterlevel above jet axis [m]
Dpile=0.2; %pile diameter [m]
xpile=[4:2:14]; % pile x-locations [m]

phis=40; %angle of repose of the slope material [degree]
thetau=0; %angle of attack of the flow forcing [degree]
betaizcrit=3; %critical izbash coeffient (usually 2.5 to 3) [-]
rhowater=1025; %density water [kg/m3]
rhostones=2650; %density stone [kg/m3]
g=9.81; %gravitational constant [m/s2]
nu=1e-6; % kinematic viscosity of water [m2/s]
coeff1=2.8; %Coefficient (= 2.8 for propeller jet (Blaauw&vd Kaa)
coeff2=15.4; %Coefficient (= 15.43 for propeller jet (Blaauw&vd Kaa)
Ks=1; % Pier shape factor (=1 for cylindrical piles)
Komega=1; %Angle of attack factor (=1 for cylindrical piles)

deltax=0.01; %grid size of x [m]
deltay=0.01; %grid size of y [m]
xmax=16; % location where the calculations stop [m]
extrabed=1; % in meter below hpb and above waterlevel[m] only essential for plots

alpha=0.3; % alpha value for jet diffusion scour [-] 0.3 ->requires validation
beta=0.5;  % beta value for jet diffusion scour [-] 0.5 -> requires validation
gamma=1.2; % gamma value for the pile obstruction scour [-] 1.2 -> requires validation

% PLOT INPUT
spbelow=2;  % number of subplots below each other
spnext=1;  % number of subplots next to each other
%(1=flow field, 2=initial bed, 3=end bed 4=waterlevel
% 5=propeller 6=piles 7=maximumscourdepth 8=location of maximum flowvel.)
plots=[1 2 3 4 5 6 7 8 9];
```

```
u=[1 2]; % 1 for established flow field, 2 for zone of flow establishment
```

calculated input values

```
D0=Dp;   %jet diameter at the location of the efflux velocity (percentage of the propeller diameter)
delta=(rhostones-rhowater)/rhowater; %relative density [-]
phis=phis*(pi/180); %angle of repose in radian [-]
thetau=thetau*(pi/180); %angle of attack in radian [-]
alphaslope=atan(1/slope); %slope angle in radian [-]
mh=tan(phis)/(cos(thetau)*sin(alphaslope)+...
sqrt(cos(alphaslope)^2*tan(phis)^2-sin(thetau)^2*sin(alphaslope)^2)); %slope factor (Soulsby 1997) [-]
L=xbreak+slope*hpb; % Distance from propeller to slope [m]
dstar=d50*((g*delta/nu^2)^(1/3)); % non dimensional stone diameter (Rock manual) [-]

% approximation for the Shields parameter for the calculated non dimensional stone diameter:
if dstar>1 & dstar<4;
    A=0.24;
    B=-1;
elseif dstar>4 & dstar<10;
    A=0.14;
    B=-0.64;
elseif dstar>10 & dstar<20;
    A=0.04;
    B=-0.1;
elseif dstar>20 & dstar<150;
    A=0.013;
    B=0.29;
elseif dstar>150;
    A=0.055;
    B=0;
end
psicrit=A*dstar^B; %approximated value of the Shields parameter [-]

Frcrit=sqrt((psicrit/0.055)*2/(betaizcrit*mh)); %critical Froude number [-]
```

bed location calculation and plot

```
[xbed,rbed]=bedloc(hpb,slope,xbreak,xmax,deltax);   %calculates the coordinates of the bed location
```

calculation bed velocity

```
ubedinitial=ubed(xbed,rbed,D0,u0,coeff1,coeff2); %calculates the initial bed velocity (before scour
process)
```

Froude number calculation

```
Frbed=ubedinitial/sqrt(g*d50*delta); % calculates the densimetric froude number near the slope
```

jet diffusion (jd) scour calculation

```
t=Frbed.^2-Frcrit^2;
t(find(t(:,1)<0),:)=0;          % Erase values with t smaller than 0 (if this value is smaller than 0 no
scour occurs)
hsemjd=(alpha.*(t).^beta)*D0;   % absolute jet diffusion scour [m]
rbednewjd=rbed-hsemjd;          % Calculate the new bed position after jet diffusion scouring
```

pile obstruction (po) scour calculation

```
hsempototal=zeros(size(xbed)); %initial matrix
for i=xpile                    % creates a loop that calculates all pile seperately
xpilegrid=i/deltax;            % find location of piles in matrix [-]
xpilegrid=round(xpilegrid);    % round the grid number to avoid errors
if i>5*waterlevel
```

```
   h0=waterlevel-rbed(xpilegrid);  % Find the depth of jet that will induce the scour [m]
else
   h0=0.2*i-rbed(xpilegrid);
end
if h0<0;
    h0=0;
end
Frbedpile=Frbed(xpilegrid);     % Find the Froude number at the location of the pile [-]
Ku=2*(Frbedpile/Frcrit)-1;      % Calculate the velocity factor [-]
if Ku>1;
    Ku=1;
elseif Ku<0
    Ku=0;
end
Kd=0.57*log10(2.24*Dpile/d50);  % Correction factor for the relative stonecoarseness (Melville&Chiew
1999)[-]
if Kd>1;
    Kd=1;
end;
hsempomax=gamma*Ks*Komega*Kd*Ku*Dpile*tanh(h0/Dpile);        % Calculate the maximum pile obstruction scour
depth [m]
scourlength=(2*hsempomax)/(tan(phis)*Dpile);    % Calculate the length of the scour hole [m], in this
calculation it is assumed that the maximum...
...slope angle is equal to the angle of internal friction, calculated for a horizontal bed. It is assumed
that the scour hole has a parabolic form with the...
... with the maximum depth at the centre of the pile.

if scourlength==0;                              % If no pile obstruction scour occurs, there has to be a
scour length
    scourlength=1e-3;                           % for further calculations
end
hsempo=-((hsempomax)/((scourlength*Dpile)^2))*(xbed-i).^2+hsempomax;    %Calculate the scour hole induced
by the pile obstr mechanism [m]
hsempo(find(hsempo<0),:)=0;                     % hsempo could be negative for values beyond scourlength,
these values are erased
hsempototal=hsempototal+hsempo;                 % updates the pile obstruction scour in the loop
end
rbednewpo=rbed-hsempototal;                     % total scour caused by all piles
```

combined scour (jet diffusion and pile obstruction)

```
rbednew=rbed-hsemjd-hsempototal;    % calculate the new bed location
totalscour=rbed-rbednew;            % calculate the total scour
maxscour=max(totalscour);           % calculate the maximum scour depth [m]
gridmaxscour=find(totalscour==maxscour); % find the location in the grid for the maximum scour depth
xmaxscour=xbed(gridmaxscour);       % find the location x for maximum scour [m]
if length(xmaxscour)>1;             % if no scour occurs xmaxscour is at every location zero
    xmaxscour=NaN;
end
```

bed velocity new bed

in this calculation still the original flow field is assumed, however in reality a recirculation zone will occur.

```
ubednew=ubed(xbed,rbednew,D0,u0,coeff1,coeff2);
Frbednew=ubednew/sqrt(g*d50*delta);
```

plots

```
figure
subplot(spbelow,spnext,1)                       % generate a subplot (2,1,1) for the figure
for i=plots %generates the plots as defined in the input section
```

```
    if i==1;
flowfield(D0,deltax,xmax,hpb,waterlevel,u0,u,coeff1,coeff2)%plot flowfield
    elseif i==2
plot(xbed,rbed,':k'); %plot initial bed with a dotted line
    elseif i==3
 area(xbed,rbednew,-hpb-extrabed-2,'FaceColor',[0.8  0.4  0.1])   %plot area below the new bed
    elseif i==4
waterlevelplot=plot([0 xbreak+slope*(hpb+waterlevel)],[waterlevel waterlevel]);          %plot waterlevel
    elseif i==5
        propeller(D0)                                          %plot propeller
    elseif i==6                                                %plot the piles
for i=xpile;
area([i-0.5*Dpile i+0.5*Dpile],[waterlevel+0.5*extrabed waterlevel+0.5*extrabed],-hpb-0.8*extrabed-
2,'FaceColor','k');
end
    elseif i==7
      plot([xmaxscour xmaxscour],[rbed(gridmaxscour) rbednew(gridmaxscour)],'.-w') %plots the maximum scour
depth with a white line
    elseif i==8;

plot(xbed(find(ubedinitial==max(ubedinitial))),rbed(find(ubedinitial==max(ubedinitial))),'.r','MarkerSize',
25);
    end
    axis([0 xmax -hpb-extrabed-1 waterlevel+extrabed])
    xlabel('Distance from propeller [m]','FontSize',14)
    ylabel('Distance from propeller axis [m]','FontSize',14)
    text(0.95,0.15,'a','FontSize',18,'Units', 'Normalized', 'VerticalAlignment', 'Top')
    hold on
end
% annotation('textbox',[0.75 0.62 0.08 0.125],'String',{['u_0=' num2str(u0) ' m/s']...
%    ;['L=' num2str(L) ' m'];['d_5_0=' num2str(d50) ' m'];['h_s_e_m=' num2str(maxscour) '
m'];['x_m_a_x_s_c_o_u_r=' num2str(xmaxscour) ' m']},'color','w','FontSize',8)

subplot(spbelow,spnext,2)
plot(xbed,Frbed,'LineWidth',2)      % generate a subplot (2,1,2) for the Froude distribution plot
hold on
%plot(xbed,Frbednew,'r','LineWidth',2) %adds the new Froude distribution
plot([0 xmax],[0.5*Frcrit 0.5*Frcrit],':k','LineWidth',2)   % plot the line of 0.5 times the critical
Froude number
plot([0 xmax],[1*Frcrit 1*Frcrit],':k','LineWidth',2)       % plot the line of 1 times the critical Froude
number
axis([0 xmax 0 1.2*max([max(Frbed) Frcrit])])
text([0.2 0.2],[0.6*Frcrit 1.1*Frcrit],{['0.5*Fr_s_l_o_p_e_,_c_r_i_t'] ['Fr_s_l_o_p_e_,_c_r_i_t']},...
  'FontSize',14)
xlabel('Distance from propeller [m]','FontSize',14)
ylabel('Fr_s_l_o_p_e[-]','FontSize',14)
text(0.95,0.15,'b','FontSize',18,'Units', 'Normalized', 'VerticalAlignment', 'Top')
subplot(spbelow,spnext,3)
plot(xbed,totalscour)
```

warnings;

shows a warning when the angle of the scour hole is larger than the angle of internal repose

```
slopeangle=abs(diff(rbednew)/deltax);
maximumslopeangle=atan(max(slopeangle))/(pi/180);
if max(slopeangle)>tan(phis)
    display(['WARNING: maximum slope angle=' num2str(maximumslopeangle) ' > ' num2str(phis/(pi/180))])
end
% shows a warning when the maximum scour depth is only 10 times the d50 or
% less
relativedepth=maxscour/d50;
```

```
if relativedepth<10
    display(['WARNING: hsem/d50=' num2str(relativedepth) '=> displacement instead of scour'])
end
if (maxscour/D0)>3
    display(['WARNING: hsem/D0=' num2str(maxscour/D0) '=> large scour depth! probably large changes in
flowfield'])
end
```

D.4 Comparison proposed method, German method and Chiew method

```
clc; clear all; close;
g=9.81; nu=1e-6; delta=1.65;
[Qdata, Qtext, Qalldata]=xlsread('interpeteddata');   %open data table
%Qdata=Qdata(find(Qdata(:,11)<1),:);                        % Delete all data with dimensionless offset
larger than x
Qdata=Qdata(find(Qdata(:,3)<24.9),:);                       % Deltete all data with a Fr0 larger than x
betaizcrit=3;                   % Critical Izbash coefficient [-]
for t=[1 4 5 6 7 8]                                          % Do not take in account these researches
Qdata=Qdata(find(Qdata(:,1)~=t),:);
end


Fr0=Qdata(:,3);                                             % Find the Fr0 [-]
offset=Qdata(:,11);                                         % Find the relative offset hpb/D0 [-]
d50=Qdata(:,7);


dstar=d50.*((g*delta/nu^2)^(1/3)); % non dimensional stone diameter (Rock manual) [-]
% approximation for the Shields parameter for the calculated non dimensional stone diameter:
A=[];
B=[];
for i=1:length(dstar)
Dstar=dstar(i);
Dstar(isnan(Dstar))=0;
if Dstar>1 & Dstar<4;
    a=0.24;
    b=-1;
elseif Dstar>4 & Dstar<10;
    a=0.14;
    b=-0.64;
elseif Dstar>10 & Dstar<20;
    a=0.04;
    b=-0.1;
elseif Dstar>20 & Dstar<150;
    a=0.013;
    b=0.29;
elseif Dstar>150;
    a=0.055;
    b=0;
elseif Dstar==0;
    a=1;
    b=1;
end
A=[A; a];
B=[B; b];
end
dstar(isnan(dstar))=0;
psicrit=A.*dstar.^B; %approximated value of the Shields parameter [-]
psicrit(find(psicrit==0))=0.03;
```

```
%psicrit=0.03;                                          % Give the critical Shields parameter (not for
all data this quantity is known...
...however all tests use sand, and therefore a psicrit of 0.03 assumed.
Frbedcrit=sqrt((psicrit/0.055)*2/(betaizcrit));
Frbed=0.306.*offset.^-1.*Fr0;
Frbed(find(Qdata(:,1)==2))=Frbed(find(Qdata(:,1)==2)).*(0.32/0.306);
Frbed(find(Qdata(:,1)==3))=Frbed(find(Qdata(:,1)==3)).*(0.32/0.306);
Frbed(find(Qdata(:,1)==9))=Frbed(find(Qdata(:,1)==9)).*(0.32/0.306);

j=find(Frbed>Frbedcrit);                        % Do only take into account data with higher bed Froude
numbers than the...
...critical value
Fr0=Qdata(j,3);
offset=Qdata(j,11);

Frbed=0.306.*offset.^-1.*Fr0;
Frbed(find(Qdata(j,1)==2))=Frbed(find(Qdata(j,1)==2)).*(0.32/0.306);
Frbed(find(Qdata(j,1)==3))=Frbed(find(Qdata(j,1)==3)).*(0.32/0.306);
Frbed(find(Qdata(j,1)==9))=Frbed(find(Qdata(j,1)==9)).*(0.32/0.306);

x=Frbed.^2-Frbedcrit(j).^2;
scour=Qdata(j,15);%./(sqrt(9.81*1.65.*d50(j)));                                    % Find the scour
depth [m]
research=Qdata(j,1);                                    % Define different researches [-]
```

Addapted German method (using d50)

```
measuredscour=Qdata(:,13);
hpboverd50=Qdata(:,10);
Cad=1;
Cmr=1;
alphaa=0.65;
Bcrit=0.9;

german=hpboverd50.*Cad*Cmr.*(alphaa*(Frbed./Bcrit)-1).*d50;
german(find(german<0))=0;
figure
%x=Frbed./Bcrit;
x=x;
%plot((x),german./Qdata(:,4),'.r');
hold on
plot((x),measuredscour./Qdata(:,4),'+k');
hold on
```

Roelse

```
D0=Qdata(:,4);
roelse=(0.3*x.^0.5).*D0;
plot((x),roelse./D0,'*g');
```

Chiew

```
t=Fr0-(4.114.*offset);
t(find(t<0))=0;
chiew=0.265.*D0.*(t.^0.955).*offset.^-0.022;
plot((x),chiew./D0,'db')
```

all scour

```
allscour=[german roelse chiew measuredscour];
figure
bar(allscour); legend('German Prediction','Roelse Prediction','Chiew Prediction','Measured Scour')
absolutedifference=[german-measuredscour roelse-measuredscour chiew-measuredscour];
```

```
relativedifference=[absolutedifference(:,1)./measuredscour absolutedifference(:,2)./measuredscour
absolutedifference(:,3)./measuredscour]*100;
figure
bar(absolutedifference); legend('german', 'roelse', 'chiew')
figure
bar(relativedifference([1:7 10:17],:)); legend('german', 'roelse', 'chiew')
```

Rsquared calculation

```
SSEgerman=sum(abs((measuredscour-german)).^2);
TSSgerman=sum(abs((measuredscour-mean(measuredscour)).^2));
Rgerman=1-SSEgerman/TSSgerman

SSEroelse=sum(abs((measuredscour-roelse)).^2);
TSSroelse=sum(abs((measuredscour-mean(measuredscour)).^2));
Rroelse=1-SSEroelse/TSSroelse

SSEchiew=sum(abs((measuredscour-chiew)).^2);
TSSchiew=sum(abs((measuredscour-mean(measuredscour)).^2));
Rchiew=1-SSEchiew/TSSchiew
```

D.5 Form calculation

For the first order reliability method calculations, the FORM script in the open earth tools (open source by Deltares) is used. In this script, first the input parameters are defined. Later the Z-function was defined. The script shows the results as presented in chapter 6.

D.5.1 Input parameters

create a structure with fields 'Name', 'Distr', 'Params' and 'propertyName'

```
stochast = struct(...
    'Name', { % define the stochastic variable names:
    'C'...              % 1: pile location coefficient [-]
    'alpha2'...         % 2: alpha2 coefficient [-]
    'D0'...             % 3: jet diameter [m]
    'd50'...            % 4: bed material diameter [m]
    'rhow'...           % 5: water denisty [kg/m3]
    'rhos'...           % 6: stone density [kg/m3]
    'f'...              % 7: velocity correction factor [-]
    'alphaslope'...     % 8: slope angle [degree]
    'L'...              % 9: distance propeller plane to slope [m]
    'betaizcrit'...     % 10: critical Izbash coefficient [-]
    'phis'...           % 11: angle of repose [degree]
    'gamma'...          % 12: gamma coefficient [-]
    'Dpile'...          % 13: pile diameter [m]
    'h'...              % 14: water depth [m]
    'C1'...             % 15: coeficient[-]
    'P'...              % 16: bow thruster power [W]
    },...
    'Distr', { % define the probability distribution functions
    @unif_inv...       % 1: pile location coefficient [-]
    @norm_inv...       % 2: alpha2 coefficient [-]
    @norm_inv...       % 3: jet diameter [m]
    @norm_inv...       % 4: bed material diameter [m]
    @norm_inv...       % 5: water denisty [kg/m3]
    @norm_inv...       % 6: stone density [kg/m3]
    @norm_inv...       % 7: velocity correction factor [-]
```

```
@norm_inv...        % 8: slope angle [degree]
@norm_inv...        % 9: distance propeller plane to slope [m]
@norm_inv...        % 10: critical Izbash coefficient [-]
@norm_inv...        % 11: angle of repose [degree]
@norm_inv...        % 12: gamma coefficient [-]
@norm_inv...        % 13: pile diameter [m]
@norm_inv...        % 14: water depth [m]
@norm_inv...        % 15: coeficient[-]
@norm_inv...        % 16: bow thruster power [W]
},...
'Params', { % define the parameters of the probability distribution functions
{0.8 1}...           % 1: pile location coefficient [-]
{0.3 0.05}...        % 2: alpha2 coefficient [-]
{1.6 0.1}...         % 3: jet diameter [m]
{0.023 0.001}...     % 4: bed material diameter [m]
{1000 15}...         % 5: water denisty [kg/m3]
{2650 20}...         % 6: stone density [kg/m3]
{1.1 0.1}...         % 7: velocity correction factor [-]
{18*(pi/180) 3*(pi/180)}...   % 8: slope angle [degree]
{8 0.3}...           % 9: distance propeller plane to slope [m]
{2.8 0.4}...         % 10: critical Izbash coefficient [-]
{35*(pi/180) 5*(pi/180)}...   % 11: angle of repose [degree]
{1.2 0.2}...         % 12: gamma coefficient [-]
{0.8 0.08}...        % 13: pile diameter [m]
{2 0.2}...           % 14: water depth [m]
{1.16 0.05}...       % 15: coeficient[-]
{705000 20000}...    % 16: bow thruster power [W]
},...
'propertyName', { % specify here to call the z-function with propertyname-propertyvalue pairs
true...        % 1: pile location coefficient [-]
true...        % 2: alpha2 coefficient [-]
true...        % 3: jet diameter [m]
true...        % 4: bed material diameter [m]
true...        % 5: water denisty [kg/m3]
true...        % 6: stone density [kg/m3]
true...        % 7: velocity correction factor [-]
true...        % 8: slope angle [degree]
true...        % 9: distance propeller plane to slope [m]
true...        % 10: critical Izbash coefficient [-]
true...        % 11: angle of repose [degree]
true...        % 12: gamma coefficient [-]
true...        % 13: pile diameter [m]
true...        % 14: water depth [m]
true...        % 15: coeficient[-]
true...        % 16: bow thruster power [W]
} ...
```

D.5.2 Z-function

```
samples = struct(...
    'C', [],...             % 1: pile location coefficient [-]
    'alpha2', [],...        % 2: alpha2 coefficient [-]
    'D0', [],...            % 3: jet diameter [m]
    'd50', [],...           % 4: bed material diameter [m]
    'rhow', [],...          % 5: water denisty [kg/m3]
    'rhos', [],...          % 6: stone density [kg/m3]
    'f', [],...             % 7: velocity correction factor [-]
    'alphaslope', [],...    % 8: slope angle [degree]
    'L', [],...             % 9: distance propeller plane to slope [m]
    'betaizcrit', [],...    % 10: critical Izbash coefficient [-]
    'phis', [],...          % 11: angle of repose [degree]
    'gamma', [],...         % 12: gamma coefficient [-]
    'Dpile', [],...         % 13: pile diameter [m]
    'h', [],...             % 14: water depth [m]
    'C1', [],...            % 15: coeficient[-]
    'P', []);               % 16: bow thruster power [W]

samples = setproperty(samples, varargin{:});
z = nan(size(samples.C));
% loop through all samples and derive z-values
for i = 1:length(samples.C)
    g=9.81;
    sigmacrit=0.055;
    u0=samples.C1(i)*((samples.P(i))/(samples.rhow(i)*samples.D0(i)^2))^(1/3);
    delta=(samples.rhos(i)-samples.rhow(i))/samples.rhow(i);
    mh=sin(samples.phis(i))/(sin(samples.phis(i)+samples.alphaslope(i)));
    Frcrit=sqrt((sigmacrit/0.055)*(2/(mh*samples.betaizcrit(i))));
    K=15.43/(atan(samples.alphaslope(i))^2);
    xumax=K*samples.L(i)*(sqrt(1+2/K)-1);
    uslopemax=samples.f(i)*2.8*(samples.D0(i)/xumax)*u0*exp(-15.43*((samples.L(i)/xumax-
1)/atan(samples.alphaslope(i)))^2);
    Frmax=uslopemax/sqrt(delta*g*samples.d50(i));
    hsemjd=samples.C(i)*samples.alpha2(i)*samples.D0(i)*(Frmax^2-Frcrit^2)^0.53;
    hsempo=samples.gamma(i)*samples.Dpile(i)*tanh(samples.h(i)/samples.Dpile(i));
    z(i,:) = 4.5-(hsemjd+hsempo);
end
```

Appendix E Steiger 39 drawings